Effects of the inflammatory mediator bradykinin on intestinal functions

Lisa Katharina Würner

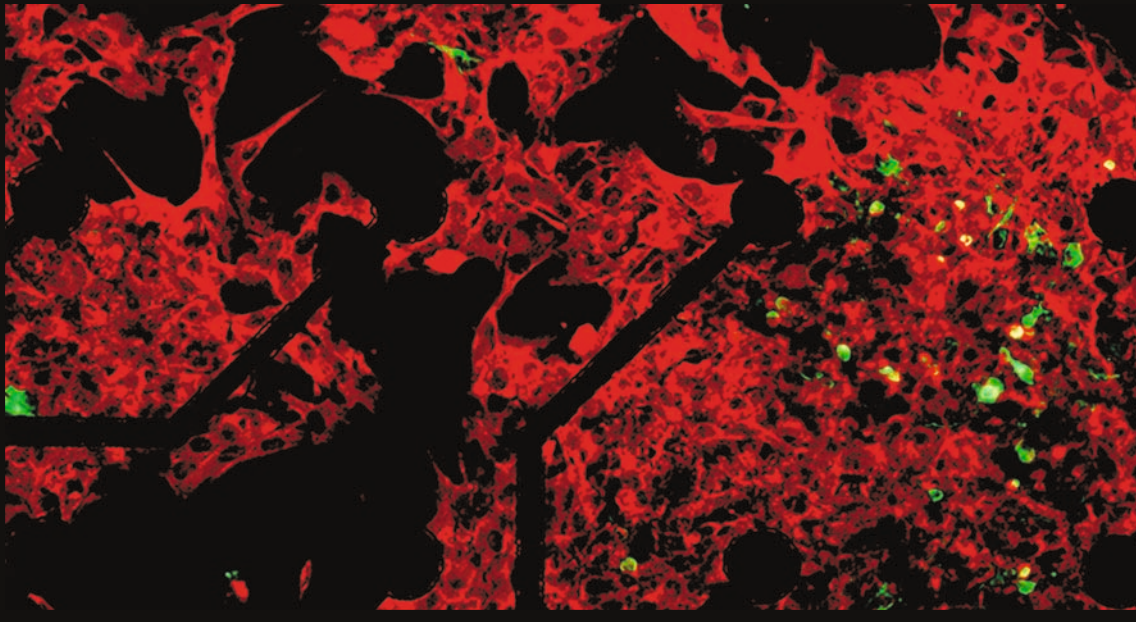

INAUGURAL DISSERTATION
submitted to the Faculty of Veterinary Medicine
in partial fulfilment of the requirements
for the PhD-degree
of the Faculties of Veterinary Medicine and Medicine
of the Justus Liebig University Giessen, Germany

édition scientifique
VVB LAUFERSWEILER VERLAG

1. Auflage 2013

1st Edition 2013

Printed in Germany

édition scientifique
VVB LAUFERSWEILER VERLAG

STAUFENBERGRING 15, D-35396 GIESSEN
Tel: 0641-5599888 Fax: 0641-5599890
email: redaktion@doktorverlag.de

www.doktorverlag.de

Effects of the inflammatory mediator bradykinin on intestinal functions

Inaugural Disseration

submitted to the

Faculty of Veterinary Medicine

in partial fulfilment of the requirements

for the PhD-Degree

of the Faculties of Veterinary Medicine and Medicine

of the Justus Liebig University Giessen

by

Würner, Lisa Katharina

from

Rüsselsheim, Germany

Giessen, 2013

From the Institute for Veterinary Physiology and Biochemistry
of the Faculty of Veterinary Medicine of the Justus Liebig University Giessen

First Supervisor and Referee: Prof. Dr. Martin Diener
Second Supervisor: Prof. Dr. Wolfgang Kummer
Second Referee: Prof. Dr. Henrik Sjövall
Examiner: Prof. Dr. Holger Hackstein
Head of the examination board: Prof. Dr. Heinz-Jürgen Thiel,

Date of Doctoral Defence: August 7th, 2013

Table of contents

List of abbreviations

ADP	adenosine diphosphate
AM	acetoxymethyl ester
ATP	adenosine triphosphate
B_1 and B_2 receptor	bradykinin B_1 and bradykinin B_2 receptor
BK	bradykinin
BSA	bovine serum albumin
C	capacitance
cAMP	cyclic adenosine monophosphate
cDNA	complementary deoxyribonucleic acid
C_e	epithelial capacitance
CFTR	cystic fibrosis transmembrane conductance regulator
cGMP	cyclic guanosine monophsphate
CGRP	calcitonin gene-related peptide
DAB	Des-arg^9-bradykinin
DAG	diacylglycerol
DAMP	damage-associated molecular pattern molecules
DAPI	4´,6-diamidino-2-phenylindol dilactate
DEPC	diethylpyrocarbonat
DMEM/F12	advanced Dulbecco´s modified eagle medium/Ham´s F12
DNA	deoxyribonucleic acid
dNTP	deoxyribonucleotide
DTT	dithiothreitol
EDTA	ethylenediaminetetraacetic acid
ENaC	epithelial sodium channels
ENS	enteric nervous system
F_{ab}	fragment antigen binding
F_c	fragment crystalisable
FCS	fetal calve serum
FET	field-effect transistor

FRET	fluorescence resonance energy transfer
G_t	tissue conductivity
HBSS	Hank´s balanced salt solution
HEPES	N-(2-hydroxyethyl)piperazine-N´-2-ethanesulfonic acid
I	current
IBD	inflammatory bowel disease
ICC	immunocytochemistry
IgG	immunglobulin G
IHC	immunohistochemistry
IL	interleukin
IPAN	intrinsic primary afferent neuron
I_{sc}	short-circuit current
Kd	dissociation constant
MAP2	microtubule-associated protein 2
MEA	microelectrode array
mRNA	messenger ribonucleic acid
PB	phosphate buffer
PBS	phosphate buffered saline
PBS-T	phosphate buffer with Triton-X
PCR	polymerase-chain-reaction
PD	potential difference
PFA	paraformaldehyde
PGP9.5	protein gene product 9.5
qPCR	quantitative real time PCR
R	resistance
R_e	epithelial resistance
RNA	ribonucleic acid
ROI	region of interest
RQ	relative quantity
R_s	subepithelial resistance
R_t	transcellular resistance

RT-PCR	reverse transcription polymerase-chain-reaction
SCFA	short-chain fatty acid
t	time
TAE	tris-acetate EDTA buffer
TNFα	tumor necrosis factor α
V	volt
v/v	volume per total volume
VIP	vasoactive intestinal peptide
w/v	weight per total volume

1 Introduction

1.1 The enteric nervous system

1.1.1 Anatomy

The Enteric Nervous System (ENS) is, besides the sympathetic and the parasympathetic system, part of the autonomous nervous system. The ENS plays a crucial role in the regulation of gastrointestinal functions, such as motility, secretion and blood flow. In 1899, Bayliss and Starling (Bayliss & Starling 1899) described the characteristic of the ENS to be able to control the motility of the gut without involvement of the central nervous system. This feature as well as the enormous number of neurons in the ENS (2 – 1000 million, depending on species and animal size; Furness 2006) highlights the importance of the ENS for the regulation of gastrointestinal functions.

The enteric nervous system consists of two main plexuses located within the intestinal wall (Figure 1.1). The myenteric or Auerbach´s plexus can be found throughout the whole gastrointestinal tract and is located between the circular and the longitudinal muscle layer. It consists of a network of ganglia, connected via interganglionic fibers (Auerbach 1864). The submucosal or Meissner´s plexus is located in the submucosa, i.e. between the circular muscle layer and the mucosa and can be found exclusively in the intestine (Schemann 2000; Hansen 2003a). It also consists of ganglia connected via interganglionic fibers, but the ganglia are smaller and contain less neurons (Furness 2006).

There are also aganglionic plexuses within the intestinal wall; one of these is the mucosal plexus, which either consists of fibres from the submucosal plexus or can contain neuronal somata in some intestinal segments (Mestres *et al.* 1992a, 1992b). If present, its neurons are associated with the muscularis mucosa and the intestinal glands (Kramer *et al.* 2011; Figure 1.1).

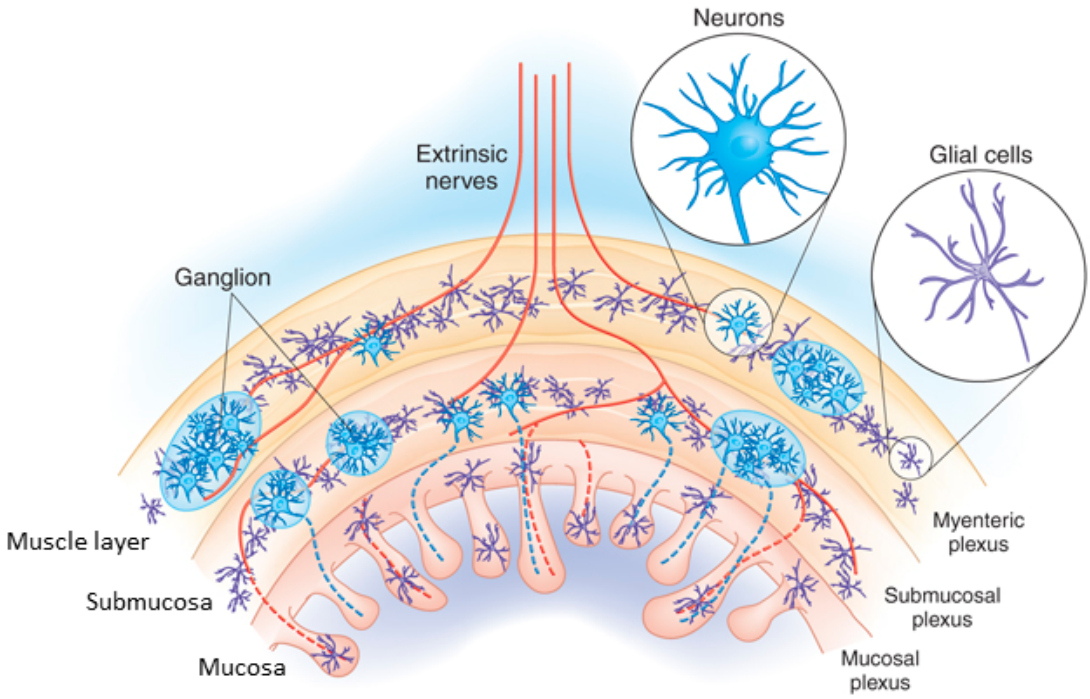

Figure 1.1: Schematic picture of the location of the myenteric, the submucosal and the mucosal plexus within the intestinal wall.
Modified from Rescigno (2008).

1.1.2 Physiology

1.1.2.1 Classification of neurons

Since the first description of the enteric nervous system by Bayliss and Starling (Bayliss & Starling 1899), different classifications of the enteric neurons have been introduced. As first author, Dogiel (Dogiel 1899) categorised neurons according to their shape. Depending on their size, their surface and the number of their processes, the neurons were defined as Dogiel type I, II or III neurons. However, this classification does not provide information about the functions of the neurons. Nevertheless, it is still widely used for categorising enteric neurons from all species.

Another way of classification is according to their electrical properties. Hirst and McKirdy (Hirst & McKirdy 1974) initially proposed to classify enteric neurons as S (synaptical)- and AH (after-hyperpolarisation)-neurons. S-neurons are characterised by a fast action potential followed by a short after-hyperpolarisation, whereas AH-neurons exhibit an action potential with a longer duration and two phases of after-hyperpolarisation, an early and a late one.

The third classification can be made according to the function of the neurons: motor and secreto-/vasomotor neurons, interneurons and intrinsic primary afferent neurons (Lomax & Furness 2000; Michel *et al.* 2000; Pfannkuche *et al.* 1998; Schemann *et al.* 1995).

Motor neurons innervate muscular tissue, most importantly the circular and longitudinal muscle layers of the muscularis propria and the muscularis mucosae (Schemann 2000). Most of the motor neurons projecting to the muscularis propria originate from the myenteric plexus, although it is known for the circular muscle of the rat that some of the innervating neurons originate from the submucosal plexus as well (Furness 2006). The secreto- and vasomotor neurons project from the submucosal plexus to the mucosa and control the blood flow within the intestinal wall and the secretion of the intestinal epithelium. But also the myenteric plexus takes part in the control of the secretion of electrolytes. Jodal et al. (Jodal *et al.* 1993) and See and Bass (See & Bass 1993) showed an involvement of the myenteric plexus in the fluid secretion induced by cholera-toxin and glucose, respectively. The mucosal plexus has inhibitory effects on the electrolyte secretion as well (Bridges *et al.* 1986).

The motor neurons can be subdivided into neurons with excitatory or inhibitory effects on the target cells. In the myenteric plexus, approximately half of the myenteric neurons release inhibitory neurotransmitters, the other half excitatory (Furness 2006; Table 1.1). However, there is a functional dominance of inhibitory motor neurons in the myenteric plexus, as the overall, predominant action of the enteric nervous system on gastrointestinal motility is an inhibitory one (Hansen 2003b), demonstrated e.g. by the increase in intestinal motility after blockade of neuronal activity with tetrodotoxin (Diener & Gabato 1994). Intrinsic primary afferent neurons (IPANs) are responding to stimuli, such as distension, luminal chemistry and mechanical stimulation (Furness 2006, Hansen 2003a). The third class of enteric neurons are the interneurons. These neurons are involved in secretomotor and motility reflexes (Schemann 2000, Furness 2006) and represent the connection between the sensory information gathered by the intrinsic primary afferent neurons and the effects caused by the motor and secreto- and vasomotor neurons in response to the sensory stimuli. This reflex circuitry enables the ENS to work independently from the central nervous system (Schemann 2000). However, there is a considerable modulating influence by the central nervous system

via the classical autonomous nervous system. It has been shown by Lister (Lister 1858) that noradrenergic fibers ramify between myenteric neurons, but are very rarely found in the muscle itself. Paton and Zar (Paton & Zar 1968) demonstrated that the stimulation of sympathetic nerves as well as the exposure of the intestine to noradrenaline reduces the acetylcholine release from enteric neurons. Hirst and McKirdy (Hirst & McKirdy 1974) showed that this effect of adrenergic neurons is mediated via presynaptic inhibition. A similar effect can be seen on the secretion. The sympathetic nerves have an inhibitory effect on the secretion, by innervating the submucosal plexus (Wright *et al.* 1940; Sjövall 1984)

An overview of the neuronal types, their functions and the neurotransmitters involved is presented in Table 1.1.

Type of neurons	Main transmitters	Functions
Intrinsic primary afferent neurons (IPANs)	Substance P, calcitonin gene-related peptide (CGRP), acetylcholine, serotonin	Detection of stimuli, such as distension, luminal chemistry, and mechanical stimulation
Interneurons	Acetylcholine, somatostatin, serotonin, substance P, dopamine	Activation of inhibitory and excitatory neurones via nicotinic (and partially muscarinic) receptors
Excitatory motor neurons	Acetylcholine, substance P	Contraction in myocytes via muscarinic receptors
Inhibitory motor neurons	Nitric oxide (NO), vasoactive intestinal peptide (VIP), ATP	Relaxation in myocytes
Excitatory secretomotor neurons	Acetylcholine, vasoactive intestinal peptide (VIP)	Activation of secretory cells in the mucosa
Inhibitory secretomotor neurons	Neuropeptide Y, somatostatin	Inhibition of secretory cells in the mucosa
Vasomotor neurons	Vasoactive intestinal peptide (VIP), acetylcholine, NO	Relaxation of blood vessels

Table 1.1: Overview of the subclasses of neurons, their neurotransmitters and the effects on the intestine. Modified from Schemann 2000.

1.1.3 The myenteric plexus and the regulation of intestinal motility

Although the general excitability of intestinal smooth muscle cells is generated by the interstitial cells of Cajal (see 1.5.2), the enteric nervous system plays a crucial role in regulating and adjusting the contractions in order to achieve a target-oriented peristalsis (Schemann 2000). There are three stimuli, which can induce the reflex responses necessary to cause peristalsis: distension, mechanical distortion of the mucosa and changes in the chemical composition of the luminal content (Kunze & Furness 1999). The bowel reacts to these stimuli with a contraction of the circular muscle orally to the bolus and a relaxation at the aboral side of the bolus. This effect is caused by excitatory and inhibitory myenteric neurons, which are activated by interneurons via the reflex circuitry described above. These motor neurons have a direct impact on the smooth muscle cells, but also influence the interstitial cells of Cajal (Kunze & Furness 1999). Since the smooth muscle cells are electrically coupled to each other, it is obvious that the motor neurons always influence the cells as a group forming a motor unit with a size of approximately 2 - 3 mm. These motor units are innervated by roughly 600 - 900 excitatory and 800 – 1200 inhibitory motor neurons (Kunze & Furness 1999).

Since the myenteric plexus primarily projects to the intestinal muscle, we aimed to investigate the effect of bradykinin on the intestinal motility. We particularly focused on the question if bradykinin has effects on the electrical activity of myenteric neurons, and how this stimulation influences the contractility of the intestinal muscle in comparison to a direct effect of bradykinin on the muscle cells (see 1.5.3). Furthermore, we aimed to find out if the stimulation of myenteric neurons with bradykinin might also mediate changes in the intestinal ion secretion, as the myenteric plexus has also been found to be involved in the regulation of secretion (Jodal *et al.* 1993; See & Bass 1993).

1.2 Bradykinin

1.2.1 Production and degradation

Bradykinin is a nonapeptide, which is produced after tisssue injury and inflammation in the blood plasma as well as in tissues. In the plasma bradykinin is produced from high-molecular-weight kininogen, whereas the tissue-originated bradykinin is produced from low-molecular-weight kininogen. The latter is transformed to kallidin and then converted to bradykinin by an aminopeptidase (Regoli & Barabe 1980) (Figure 1.2). The transformation of kininogen to kallidin (10 amino acids) and bradykinin (9 amino acids), respectively, is carried out by the enzyme kallikrein, which is activated by tissue injury, inflammation, toxins, but also by the blood coagulation system (Farmer & Burch 1992). Bradykinin and kallidin both are degraded by a carboxypeptidase to des-arg^{9}-bradykinin and des-arg^{10} kallidin, respectively (Regoli & Barabe 1980).

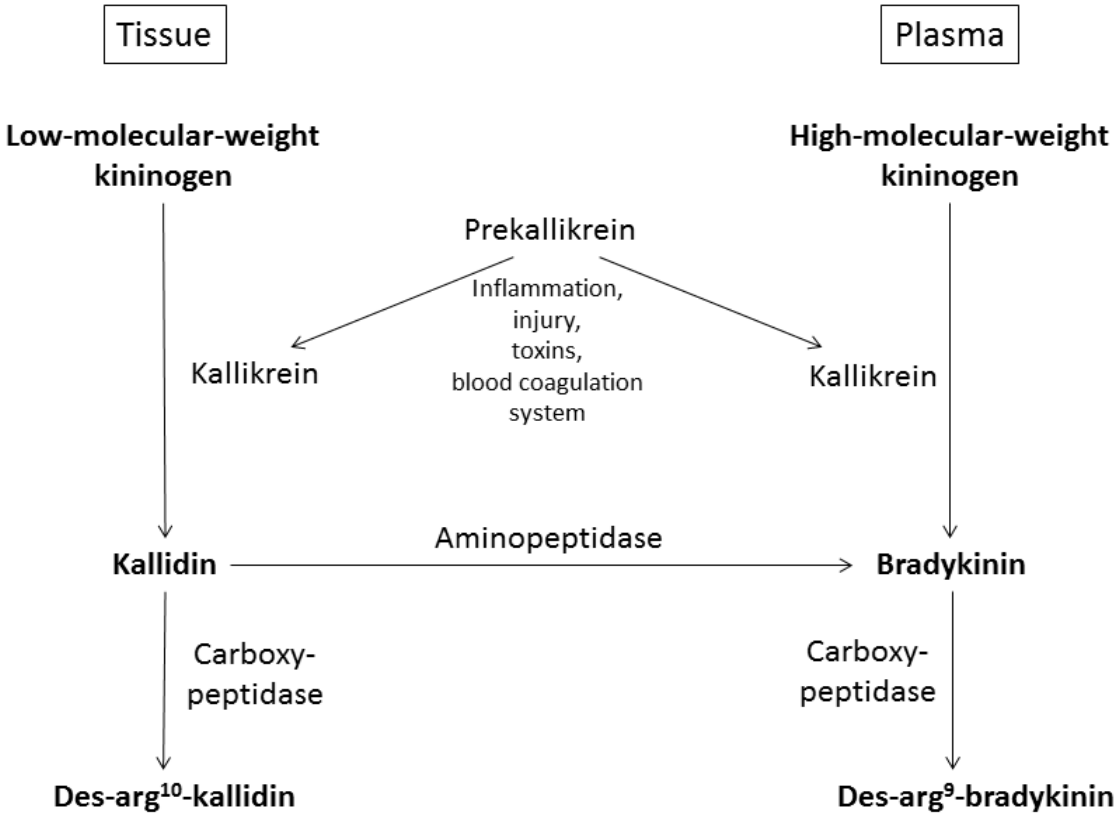

Figure 1.2: The production and metabolism of bradykinin.
The enzymes are written next to the arrows. Adapted from Avemary 2010.

1.2.2 Functions and receptors

Bradykinin has various functions in the body, most of them being related to inflammatory processes: it is involved in the development of pain, dilates blood vessels and enhances their permeability (Farmer & Burch 1992; Regoli & Barabe 1980). This holds also true for the intestine. Additionally, bradykinin induces ion secretion in the intestine, by directly stimulating epithelial cells or by activating neurons, primarily submucosal neurons (Diener *et al.* 1988). This can disturb the balance between secretion and absorption and thus lead to a secretory diarrhoea. Bradykinin also induces contraction and/or relaxation in the intestinal muscle and stimulates myenteric neurons, which might lead to changes in motility and to diarrhea as well (Murakami *et al.* 2007). It can be speculated that this is a helpful effect for the organism during inflammation, since an increased motility causes a quick elimination of potentially hazardous agents. However, the loss of water and electrolytes during diarrhea can harm the organism due to dehydration. Bradykinin has also been found to be involved in inflammatory bowel diseases (Devani *et al.* 2005*;* Stadnicki *et al.* 2003a), which is described in more detail in 1.4.

Two different bradykinin-receptors have been described: the highly regulated B_1 receptor and the constitutively expressed B_2 receptor (Farmer & Burch 1992; Regoli & Barabe 1980). Although the B_1 receptor is constitutively expressed in some tissues, e.g. rat dorsal root ganglia (Wotherspoon & Winter 2000), in the majority of cells an upregulation is necessary. In vivo, this usually occurs after tissue injury and/or inflammation, and in vitro after tissue dissection or incubation (for review see Farmer & Burch 1992; Leeb-Lundberg 2005). This upregulation can be inhibited by blockers of the protein synthesis (Bouthillier *et al.* 1987), demonstrating a de-novo protein formation. The B_1 receptor has a high affinity for the carboxypeptidase metabolites des-arg^{10}-kallidin and des-arg^{9}-bradykinin (Farmer & Burch 1992; Leeb-Lundberg 2005; Figure 1.2), therefore the latter was used as a B_1 agonist in my experiments.

The B_2 receptor is constitutively expressed and can be found throughout the organism, emphasising the importance of bradykinin in physiological and pathophysiological processes. This receptor has – in contrast to the B_1 receptor - a high affinity for hyp^{3}-bradykinin (Leeb-Lundberg 2005), which was used as a B_2 agonist in the present study.

In most tissues the activation of bradykinin receptors leads to a stimulation of the enzyme phospholipase C, resulting in the formation of inositol-1,4,5-trisphosphate (IP_3) and diacylglycerol (DAG) (Farmer & Burch 1992; Leeb-Lundberg 2005). The subsequent increase in the cytosolic Ca^{2+} concentration can either be induced by a release of Ca^{2+} from intracellular stores after binding of IP_3 to its receptor or by an influx of Ca^{2+} from the extracellular space. In rat submucosal neurons the increase in the cytosolic Ca^{2+} concentration evoked by bradykinin is mediated by voltage-dependent Ca^{2+} channels, activated after depolarisation, which is a result of a closure of K^+ channels (Avemary & Diener 2010a). In the cell type investigated in the present study - rat myenteric neurons - it was proposed that both voltage-dependent Ca^{2+} channels as well as non-selective cation channels mediate the rise in cytosolic Ca^{2+} concentration after receptor activation by bradykinin (Murakami *et al.* 2007). Another characteristic of bradykinin receptors is the activation of the enzyme phospholipase A_2. Arachidonic acid produced from membrane phospholipids by this phospholipase is rapidly converted to eicosanoids such as prostaglandins (Farmer & Burch 1992). An involvement of prostaglandins in the bradykinin effect has been shown for myenteric neurons as well (Gelperin *et al.* 1994; Murakami *et al.* 2007).

Another difference between B_1 and B_2 receptors is their desensitisation behaviour. Whereas the B_1 receptor is desensitised only to a small degree, the B_2 receptor rapidly loses sensitivity after agonist stimulation (Leeb-Lundberg 2005).

1.3 Absorption and secretion at the colonic epithelium

1.3.1 The colonic epithelium

The colon is part of the large intestine and can be divided into the proximal colon, the transversal colon and the distal colon. The function of the colon consists in the transport of ingesta, in hosting bacteria fermenting structure carbohydrates for which mammals do not express digestive enzymes, in immune defence, in the secretion of isotonic fluid containing K^+, HCO_3^-, and mucus, and – most importantly – in the absorption of water and electrolytes. Approximately 90 % of the water entering the large intestine is absorbed in the colon; that is ~1.5 l electrolyte-rich fluid per day in humans (Cooke 1991; Kunzelmann & Mall 2002). However, this system of absorption and secretion represents a highly-controlled equilibrium, which can, if getting out of balance, induce severe diarrhoea or constipation (Binder *et al.* 1991; Field & Semrad 1993; Binder & Sandle 1994).

The colonic wall consists of the mucosa, the submucosa, the muscularis propria, and the serosa. The mucosa is composed of the epithelium, the lamina propria, and the lamina muscularis mucosae. The epithelium builds intestinal glands (Potten *et al.* 1997), which are covered by the columnar enterocytes with their surface-magnifying microvilli and, in a smaller amount, by the mucus-producing goblet cells, which together represent 95 % of all colonic epithelial cells. The other 5 % are the enteroendocrine cells, which produce hormones, such as glucagon, serotonin, somatostatin, and vasoactive intestinal peptide (VIP) (Specht 1977; Turnberg 1984).

The epithelial cells of the intestinal tract are constantly replaced by new cells. The average length of survival time of an enterocyte is approximately three days. New enterocytes are built in the ground of the intestinal glands, moving to the surface while maturating (Barrett & Keely 2000). Although both secretion and absorption occur in the surface epithelium as well as in the crypts, it is hypothesised that young enterocytes in the base of the crypt have primarily secreting functions, whereas the mature surface enterocytes are mostly involved in absorptive processes (Kockerling & Fromm 1993; Kunzelmann & Mall 2002).

1.3.2 Absorption

The colon plays an important role in the absorption of water and ions, such as Na^+, K^+ and Cl^-. Sodium and chloride ions are absorbed via electroneutral processes in the rat colon (Figure 1.3). This differs from e.g. the human or rabbit colon, where the electrogenic Na^+ absorption via epithelial Na^+ channels (ENaC-channels) plays an important role as well (Kunzelmann & Mall 2002).

The apical membrane is provided with Na^+-H^+-exchangers and Cl^--HCO_3^--exchangers, which allow to absorb Na^+ and Cl^- ions and at the same time secret H^+ ions and HCO_3^- ions into the gut lumen (Figure 1.3). Via Na^+-K^+-ATPases and Cl^- channels on the basolateral side, the ions are transported out of the cell (Diener *et al.* 1992; Kunzelmann & Mall 2002; Ikuma *et al.* 2003).

The absorption of K^+ ions is an ATP-dependent process and occurs via K^+-H^+-ATPases. Basolateral K^+ channels enable a transport of the absorbed K^+ out of the cell, (Kunzelmann & Mall 2002).

Water is absorbed by different pathways: it follows paracellularly the gradient produced by the ion absorption or transcellularly by diffusion via water channels (aquaporines) (Barrett & Keely 2000; Kunzelmann & Mall 2002).

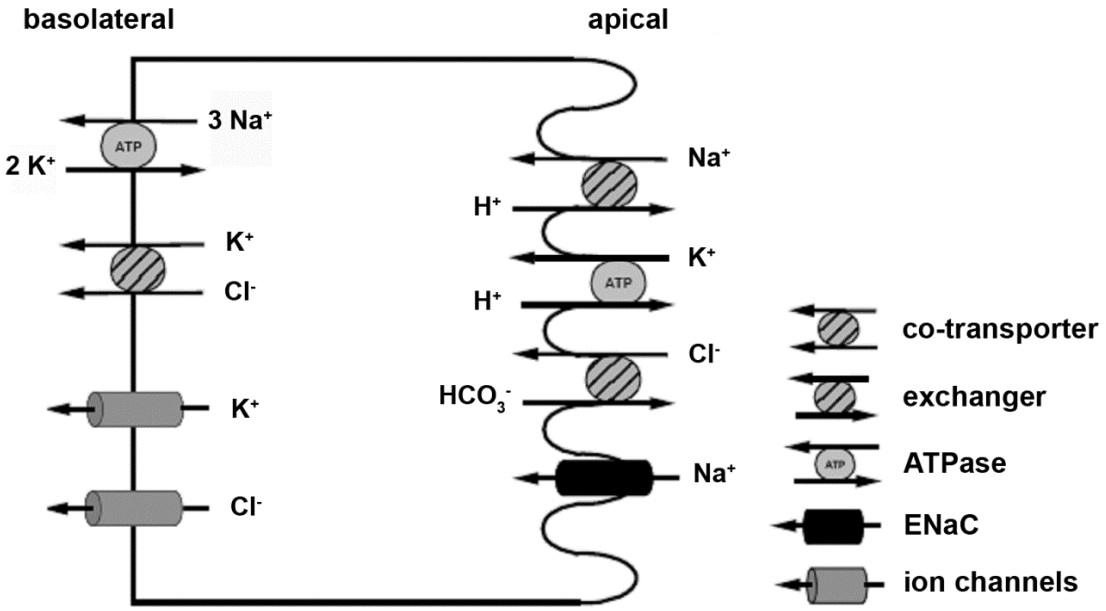

Figure 1.3: Mechanisms of Na^+, Cl^- and K^+ absorption.
By courtesy of M. Diener.

1.3.3 Secretion

Colonic secretion and absorption is a balanced system. The purpose of the secretion is the hydration and transport of the mucus out of the crypt (Kunzelmann & Mall 2002); consequently the mucus secretion and ion secretion are activated in parallel (Halm *et al.* 1995).

The colon is able to secrete ions, primarily Cl^-. A basolaterally located Na^+-K^+-ATPase generates a high concentration of K^+ and a low concentration of Na^+ in the cell (Figure 1.4). This gradient enables the Na^+-K^+-$2Cl^-$-cotransporter to accumulate Cl^- inside the cytosol. Potassium ions are transported out of the cell via K^+ channels. When the chloride channels, which are predominantly CFTR-channels (cystic fibrosis transmembrane conductance regulator channels), in the apical membrane are opened, chloride follows the electrochemical gradient and moves into the colonic lumen (Figure 1.4). A paracellular flux of Na^+ balances the charge transfer (Kunzelmann & Mall 2002).

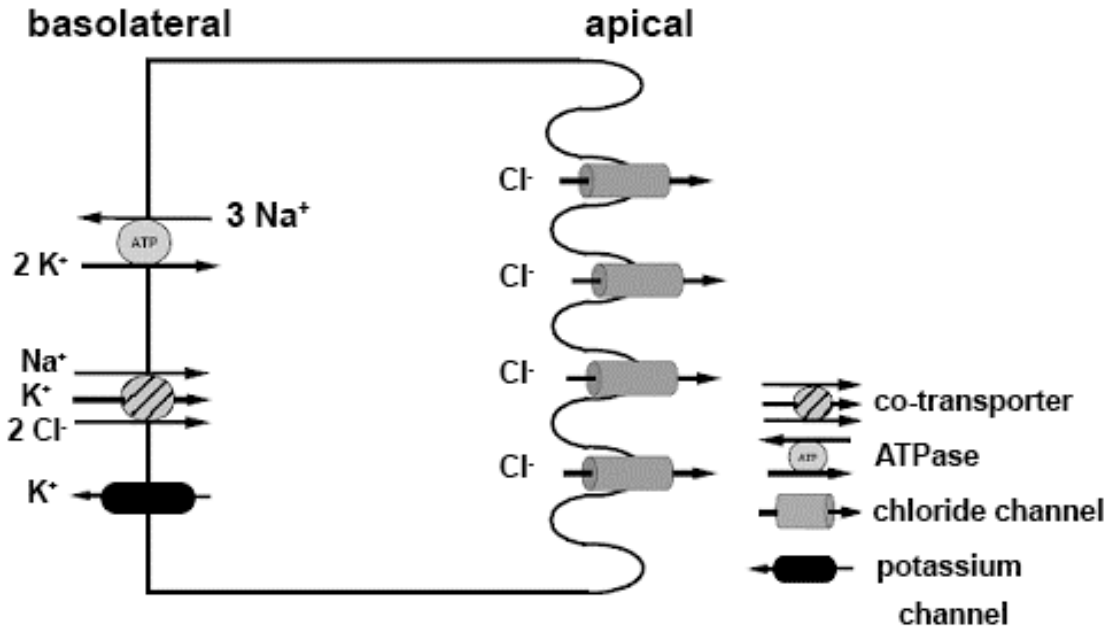

Figure 1.4: Mechanisms of Cl^- secretion.
By courtesy of M. Diener.

The colon is also capable of secreting HCO_3^-. Bicarbonate is either absorbed from the basolateral side of the cell via Na^+-dependent, electroneutral processes or is produced in the cell by carboanhydrase(s). The secretion occurs via CFTR-channels, apical Cl^--HCO_3^--exchanger or $SCFA^-$(short-chain fatty acid)-HCO_3^- exchanger. The transport is paralleled with the Na^+-H^+-exchanger (Poulsen *et al.* 1994; Kunzelmann & Mall 2002).

1.3.4 Regulation of ion transport

The regulation of the absorption and secretion is dependent on a large variety of substances. Hormones, neurotransmitters, food components, biliary acids, or viral and microbial toxins play an important role. But also the distension of the colonic wall can induce secretion (Kunzelmann & Mall 2002).

To the group of secretagogues belongs e.g. VIP, acetylcholine or prostaglandins, which activate the cell after receptor binding (Kunzelmann & Mall 2002). This occurs either via the formation of cyclic adenosine monophosphate (cAMP) catalysed by adenylate cyclase(s) or via the production of cyclic guanosine monophosphate (cGMP) by guanylate cyclase(s). These intracellular messengers change the driving forces for ions and thus induce secretion.

Another second messenger system involved in the secretion is the IP_3-pathway (Abdel-Latif 1986; Lindqvist *et al.* 1998). After receptor activation of a G-protein coupled receptor, the formation of IP_3 and subsequent binding to its receptor on the endoplasmic reticulum leads to a release of intracellular Ca^{2+} from this compartment (more detailed description in 1.2.2). Ca^{2+} influx from the extracellular space can be induced as well (Spassova *et al.* 2004). This increase in the cytosolic Ca^{2+} concentration leads to the activation of Ca^{2+}-dependent K^+ channels and thereby indirectly induces Cl^- secretion via hyperpolarisation of the cell (Kunzelmann & Mall 2002).

Another part of the intestine is crucial for the regulation of absorption and secretion: the enteric nervous system. Especially the submucosal plexus is provided with multiple processes innervating the mucosa (Furness 2006). But also the myenteric plexus is known to be involved in the regulation of absorption and secretion (Jodal *et al.* 1993; See & Bass 1993) (see 1.1.2.1).

1.3.5 Bradykinin and ion secretion

Bradykinin causes a chloride secretion in the intestinal tract, a finding that has been described in rat colon, guinea pig ileum, rabbit ileum and colon and also human colon (Musch *et al.* 1983; Cuthbert *et al.* 1984a, 1984b; Perkins *et al.* 1988; Phillips & Hoult 1988; Baird *et al.* 2008). All investigators demonstrated that the effect of bradykinin on the ion secretion is dependent on the synthesis of prostaglandins. Warhurst et al. (Warhurst *et al.* 1987) as well as Phillips et al. (Phillips & Hoult 1988) hypothesised that bradykinin induces the chloride secretion via two pathways: firstly, the kinin directly stimulates bradykinin receptors located on the epithelial cells and secondly, bradykinin induces a release of prostaglandins from sub-epithelial cells, which then cause a chloride secretion by binding to prostaglandin receptors on the epithelium.

Diener et al. (Diener *et al.* 1988) showed that bradykinin has direct effects on the epithelial cells causing chloride secretion, but stated that there was also a neuronal component, since the neurotoxin tetrodotoxin reduced the bradykinin effect in a preparation, in which the submucosal plexus was preserved, whereas in a purely mucosal preparation tetrodotoxin did not have an effect on the bradykinin-induced chloride secretion.

Since the myenteric plexus has been shown to be involved in the secretory mechanisms as well (see 1.1.2), I aimed to clarify the question whether bradykinin, by stimulating myenteric neurons, alters the ion secretion in the rat colon.

1.3.6 Mucus secretion

Mucus is an important component of the intestine building an adherent layer, which fulfils a barrier function and thus protects epithelial cells from abrasion and bacterial invasion (Specian & Oliver 1991; Halm & Halm 2000). The mucus is released by goblet cells via exocytosis. Goblet cells originate from progenitor cells in the depth of the crypt and move upwards during maturation, similar as the enterocytes, to the surface epithelium. The life span of a goblet cell is 2 - 3 days (Specian & Oliver 1991). The released mucus consists of a heterogeneous collection of high-molecular-weight glycoproteins: the mucins (Specian & Oliver 1991).

In the intestinal tract there is a basal secretion of mucus (Specian & Oliver 1991), which can be strongly augmented by secretagogues increasing either the cytosolic Ca^{2+}

concentration or the intracellular cAMP level (Kunzelmann & Mall 2002). It is well known that the mucus properties critically depend on the secreted chloride and HCO_3^- (Grubb & Gabriel 1997; Garcia *et al.* 2009).

Whether bradykinin alters the mucus secretion in the intestine has been rarely investigated. Stanley et al. (Stanley & Phillips 1994) demonstrated that bradykinin induced a mucus release in HT29 cells (human colon adenocarcinoma grade II cell line). Akiba et al. found by in vivo experiments that bradykinin increased the mucus gel thickness in the rat duodenum (Akiba *et al.* 2001). In the respiratory tract Nagaki et al. (Nagaki *et al.* 1996) showed that bradykinin caused a mucus release from human isolated submucosal glands. However, no studies have been performed so far investigating the effect of bradykinin on the mucus secretion in human intestinal mucosa, especially in regard to an involvement of this system in inflammatory bowel diseases, for which an altered mucus release has been demonstrated (Gustafsson *et al.* 2012, see 1.4.2).

1.4 Inflammatory bowel diseases

1.4.1 Genesis and symptoms

Two diseases fall into the category of human inflammatory bowel diseases (IBD): Crohn´s disease and ulcerative colitis. Both have similarities in the matter of symptoms and genesis, but differ in location and nature of the pathological changes. In both cases an inflammation of the intestine leads to diarrhoea, abdominal pain and rectal bleeding. However, Crohn´s disease can affect the whole gastrointestinal tract, whereas in ulcerative colitis - the focus of the respective part of my study - exclusively the colon and rectum exhibit inflammatory changes (Strober *et al.* 2007).

During acute inflammation, ulcerative colitis patients have a strongly altered colonic mucosa. Massive infiltrations of immune cells, mucus release by the goblet cells, as well as changes in the crypt architecture dominate the histological examination (Lewis *et al.* 2008). During remission, these histopathological alterations are mostly restored, but 30 % of the patients still suffer from symptoms such as abdominal pain and diarrhoea, despite a histologically inconspicuous mucosa (Isgar *et al.* 1983; Simren *et al.* 2002). Gustafsson et al. (Gustafsson *et al.* 2012) showed that remissional patients have an altered responsiveness to secretagogues in regard to ion (as well as mucus) secretion, which might be involved in the pathogenesis of abdominal symptoms. But also the consistent influence of inflammatory mediators, such as bradykinin, might play a role.

1.4.2 The involvement of bradykinin

Since bradykinin is an important inflammatory mediator, it was hypothesised that this peptide plays a role in the pathophysiology of IBD. It has been shown in two animal models of enterocolitis (indomethacin and proteoglycan polysaccharide-induced colitis) in genetically susceptible Lewis rats that during acute phases of the disease, plasma kallikrein - the enzyme transforming high molecular weight kininogen to bradykinin (see 1.2.1) - is activated (Stadnicki *et al.* 1998a; Stadnicki *et al.* 1998b). Additionally, the application of a plasma kallikrein inhibitor attenuates acute and chronic enterocolitis in rats (Sartor *et al.* 1996; Stadnicki *et al.* 1996). It was also demonstrated that in rats being deficient of high- and low-molecular-weight kininogen,

a gross gut score evaluating intestinal wall thickening, adhesions, mesenteric contractions and serosal nodules was reduced by 60 % (Isordia-Salas *et al.* 2002).

In human inflammatory bowel diseases the kallikrein-kinin system has been found to be involved as well. Stadnicki et al. (Stadnicki *et al.* 2003a) showed that under healthy and diseased conditions intestinal tissue kallikrein is located in the goblet cells. But in colitis patients the amount of kallikrein in the goblet cells was reduced, although the mRNA level was unchanged, indicating a release of kallikrein into the lumen. Additionally, a natural inhibitor of kallikrein, kallistatin, was decreased in intestinal tissue from IBD patients, which led to the assumption that kallistatin binds to kallikrein and thus is no longer detectable (Stadnicki *et al.* 2003a; Devani *et al.* 2005). In a rat model of enterocolitis, intestinal tissue kallikrein was also found in macrophages of granulomas located in the submucosa (Stadnicki *et al.* 1998a). In consistency with that, granulomas in tissue from IBD patients exhibited plasma cells containing high amounts of tissue kallikrein as well (Stadnicki *et al.* 2005).

Another finding supporting the hypothesis of an involvement of the kallikrein-kinin system in IBD is that, in contrary to patients suffering from diverticular disease, the inflamed colonic mucosa from patients with ulcerative colitis contains kininogen, the precursor molecule for bradykinin (Zeitlin & Smith 1973). Furthermore Stadnicki et al. (Stadnicki *et al.* 2005) showed an increased expression of the B_1 receptor in the colonic mucosa of patients suffering from inflammatory bowel disease (Stadnicki *et al.* 2005). In Crohn´s disease they also found a positive staining for the B_1 receptor in macrophages forming granulomas (Stadnicki *et al.* 2005).

These findings strongly suggest an involvement of bradykinin in the genesis and symptoms of IBD. However, these studies concentrated on a morphological proof of the involvement of the kallikrein-kinin system, whereas the functional involvement in human IBD has not been investigated yet, especially in regard to a consistent influence of bradykinin on the symptoms observed in remissive ulcerative colitis patients.

Since there is evidence for alterations in the mucus secretion in ulcerative colitis patients (Gustafsson *et al.* 2012), and as Stadnicki et al. (Stadnicki *et al.* 2003a) demonstrated a kallikrein-release from goblet cells, I was interested if bradykinin induced a mucus release from the human colonic mucosa and whether there are differences between ulcerative colitis patients and control patients. Furthermore, I

investigated whether bradykinin, which is known to induce chloride secretion in the colon of different species (see 1.3.5), causes different responses in ulcerative colitis patients compared to control patients.

I therefore aimed to answer the following questions:

1) Does bradykinin induce ion and mucus secretion in human colonic biopsies?
2) Which receptors are involved in this effect?
3) Are there differences between control and ulcerative colitis patients?
4) Is there a neuronal involvement of the bradykinin-induced effect?

1.5 Intestinal motility

1.5.1 The intestinal smooth muscle

The muscularis propria of the intestine is arranged in two layers, an inner circular and an outer longitudinal layer. The interplay between the vectors of the two forces generated by these perpendicularly arranged muscles enables a coordinated peristaltic movement, which is crucial for the target-oriented transport of ingesta.

Smooth muscle cells are spindle-shaped excitable cells, which contain myosin and actin as contractile elements. Actin is a globular protein, which forms two-stranded helical filaments. Myosin consists of two heavy chains, each forming a head and a helical neck and tail, and two light chains, which are bound to the head region (Figure 1.5). Each head contains a binding site for actin and a magnesium-adenosine triphosphate molecule (Huber 2010).

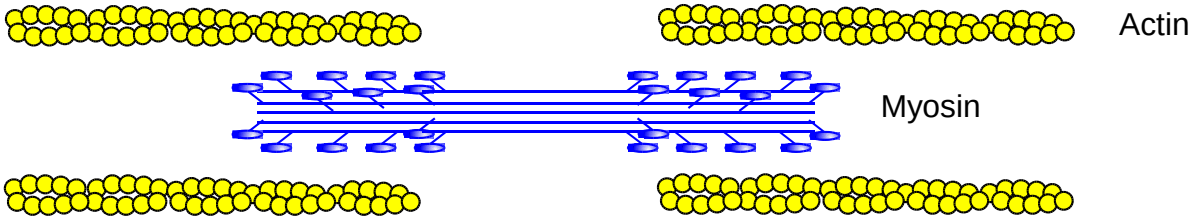

Figure 1.5: The structure of actin and myosin.
By courtesy of M. Diener.

The smooth muscle cells are connected electrically via gap junctions, which facilitate a propagation of excitation and thus induce coordinated contraction. The intestinal muscle possesses interstitial cells of Cajal, which serve as electrical pacemakers by depolarising spontaneously. This depolarisation follows a phasic pattern, which is mirrored by the phasic contractions in the intestinal muscle, called slow waves. Depending on the segment of the gastrointestinal tract, these slow waves occur with a frequency between 3 and 20 times per minute (Bowen 1996) and are essential for the transport of food through the gastrointestinal tract.

Classically, a depolarisation of a smooth muscle cell – either after propagation of a depolarisation from the neighbouring cell or after receptor activation by an agonist – leads to an opening of voltage-dependent Ca^{2+} channels and a subsequent Ca^{2+} influx (Catterall 2005). The calcium ions build a complex with calmodulin, which activates the myosin light-chain kinase (Figure 1.6). This enzyme cleaves ATP and phosphorylates myosin. Furthermore the Ca^{2+}-calmodulin complex activates a protein kinase, which phosphorylates caldesmon – an inhibiting protein blocking the binding site for myosin in its unphosphorylated state – and thus enables the phosphorylated myosin to bind to the actin molecule. After cleavage of the phosphate from the myosin-ADP complex, the myosin head performs a power stroke resulting in a shortening of the muscle cell. There is an additional pathway for contraction: Ca^{2+}-independent kinases can activate the myosin light chain kinase, but they play a minor role in the contraction under physiological conditions (Sanders 2008).

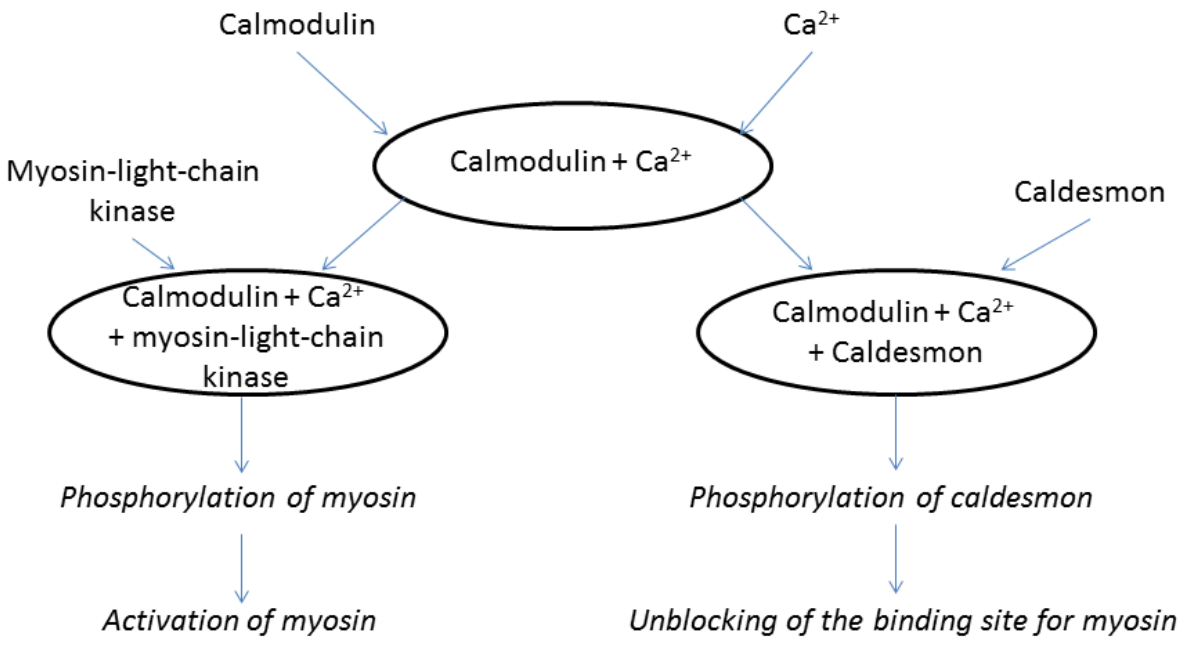

Figure 1.6: Mechanism of contraction induced by Ca^{2+} in the smooth muscle cell.

1.5.2 Regulation of motility

There are three main regulatory systems of the intestinal motility:

1) Interstitial cells of Cajal
2) Enteric motor neurons
3) Hormones, paracrine substances and inflammatory mediators

The basis for the regulation of intestinal motility is formed by the interstitial cells of Cajal. These cells belong to a specialised population of smooth muscle cells. They contain less contractile elements compared to smooth muscle cells, but have more mitochondria and larger endoplasmic reticula. Furthermore, they express a distinct set of ion channels (Mostafa *et al.* 2010).

Interstitial cells of Cajal are not exclusively located in the intestinal tract, although most investigations focused on this organ. They are also important regulators of motility in e.g. the bladder, the uterus or the vas deferens. 5 % of the smooth muscle cells in the intestinal muscularis propria are interstitial cells of Cajal (Mostafa *et al.* 2010).

These cells are responsible for the resting potential, the sensitivity to stretch, the responsiveness to neurotransmitters and, maybe most importantly, they have pacemaker activity (Ehrlein 2010). Interstitial cells produce slow waves, i.e. spontaneous large amplitude transient depolarisations, which are primarily produced by Ca^{2+}-activated Cl^- channels. These depolarisations are conducted to the smooth muscle cells via gap junctions. These cells respond with an activation of voltage-dependent Ca^{2+} channels (Koh *et al.* 2012). This leads to large amplitude propulsive contractions transporting the ingesta through the intestinal tract.

The second regulatory system consists of the enteric motor neurons, most of them having their cell bodies located in the myenteric plexus. They regulate major motor patterns, such as the amplitude or duration of contractions, and are able to respond to stimuli such as distension (Wood 1994). But nevertheless, the general excitability of the smooth muscle cells is produced by the Cajal cells and the ENS only modulates the resulting motor activity (for a detailed description see 1.1.3).

The third factor controlling gastrointestinal motility are hormones and paracrine substances. These substances act mostly via receptor binding, which results in a change in ion conductance. This can occur via an increased Ca^{2+} inward current or Cl^- outward current causing a depolarisation of the cell and a subsequent opening of voltage-dependent Ca^{2+} channels leading to a contraction. A relaxation can evolve via an increased K^+ outward current resulting in a hyperpolarisation and an inactivation of the voltage-dependent Ca^{2+} channels (Sanders 2008). Another possible action of hormones or other mediators is independent from ion conductance and affects the myosin light chain phosphatase. This enzyme dephosphorylates the myosin light chain subunits and therefore prevents a cross bridge cycling. By altering the activity of this enzyme, the sensitivity of the contractile apparatus to Ca^{2+} can be decreased or increased (Sanders 2008).

The excitability of the intestinal tract shows a high variability depending on the intestinal segment. The resting membrane potential varies along the intestine from -85 to -40 mV. This is due to a differential expression of ion channels and their different open probabilities. Especially K^+ channels (there are 20 species known in the intestine) play a crucial role in the development of the resting membrane potential and are known to show a high variability in expression along the intestinal tract (Sanders 2008). This is comprehensible when considering the segment-dependent functions in the intestine: whereas the small intestine is responsible for digestion and absorption of nutrients, the large intestine is essential for the absorption of water and electrolytes and mucus secretion. Therefore, the characteristic of the intestine should always be interpreted with regard to the specific segment.

1.5.3 The effect of bradykinin on smooth muscle cells

Since bradykinin is an inflammatory mediator known to be involved in the development of gastrointestinal diseases, such as inflammatory bowel diseases (see 1.4.2), several studies have been performed investigating the effect of bradykinin on the intestinal muscle. In rat duodenum and colon (Elliott *et al.* 1960; Altinkurt & Ozturk 1990; Feres *et al.* 1992; Ozturk *et al.* 1993; Wassdal *et al.* 1999a; Wassdal *et al.* 1999b), as well as guinea pig ileum and colon (Hall & Bonta 1973; Ozturk *et al.* 1993; Calixto 1995; Zagorodnyuk *et al.* 1998), it was shown that bradykinin induces a biphasic change in intestinal motility, with an initial relaxation followed by a contraction. This characteristic of the kinin response was particularly interesting in terms of the mechanisms. Earlier studies hypothesised that this effect was due to the activation of the two different receptors for bradykinin, the B_1 and the B_2 receptor (Boschcov *et al.* 1984; Paiva *et al.* 1989). But in regard to the expression of the B_1 receptor, there were quite contradictory results (Boschcov *et al.* 1984; Hall & Morton 1991). Later it was proposed that the relaxative part of the kinin response was caused by an opening of Ca^{2+}-activated K^+ channels with a subsequent hyperpolarisation of the cell (Hall & Morton 1991; Griesbacher 1992; Zagorodnyuk *et al.* 1998; Wassdal *et al.* 1999a).

However, in rat tissue most studies concentrated on the duodenum and there is only one scarce description of the changes induced in the rat colon (Elliott *et al.* 1960) and none for the other intestinal segments. Due to this instance and the unsolved questions concerning the mechanisms underlying the biphasic response, I was interested in the effect of bradykinin on the rat intestinal muscle, especially in regard to:

1) The comparison of the different segments of the rat intestine

2) The receptors involved

3) The mechanisms underlying the biphasic response to bradykinin.

1.6 Aim of the study

The following questions I aimed to answer in this study:

1) How does bradykinin influence the excitability of myenteric neurons and which receptors are involved?
2) Is there an impact of the myenteric neurons stimulated by bradykinin on the ion secretion in the rat colon?
3) How does bradykinin alter the ion and mucus secretion in the human colon and is there an involvement of this system in ulcerative colitis?
4) Which effect has bradykinin on the intestinal smooth muscle, in regard to segment-dependency, involvement of the bradykinin receptors, and mediation of the effect? Are myenteric neurons being stimulated by bradykinin involved? Do adjacent non-muscle cells influence the bradykinin response?

2 Material and methods

2.1 Animals

The experiments were carried out with Wistar rats bred at the Institute for Veterinary Physiology and Biochemistry at the Justus-Liebig-University in Giessen. The animals were housed in small groups at stable room temperature of 22.5 °C, air humidity of 50 – 55 % and 12h:12h light dark cycle. They had full access to standard rat diet and water ad libitum.

The preparation of myenteric neurons and isolated muscle cells were carried out with male and female animals with an age of five to nine days. For Ussing chamber and organ bath experiments male and female rats with a weight of 150 - 250 g were used (Schultheiss *et al.* 2002b).

2.2 Human mucosa biopsies

The experiments with human colonic biopsies were approved by the ethical committee of the Sahlgrenska University Hospital. Prior to the colonoscopy (see 2.4.4), the patients were given full information and signed informed consent was taken.

2.3 Chemicals

Chemical	Source
4´,6-diamidino-2-phenylindol dilactate (DAPI)	Sigma-Aldrich (Taufkirchen, Germany)
Agar	Merck (Darmstadt, Germany)
Agarose	Peqlab (Erlangen, Germany)
Bovine serum albumin (BSA)	Sigma-Aldrich (Taufkirchen, Germany)
Bradykinin	Sigma-Aldrich (Taufkirchen, Germany)
Carbachol	Sigma-Aldrich (Taufkirchen, Germany)
Cytosin-β-D-arabinofuranoside	Sigma-Aldrich (Taufkirchen, Germany)
Des(Arg^{10},Leu^{9})-kallidin	Sigma-Aldrich (Taufkirchen, Germany)
Des-Arg^{9}-bradykinin	Sigma-Aldrich (Taufkirchen, Germany)
Donkey serum	Millipore (Billerica, MA, USA)
Fetale calve serum (FCS)	PAA (Pasching, Austria)
Fura-2 AM	Life Technologies (Darmstadt, Germany)
Gelatin solution 1	Merck (Darmstadt, Germany)
Gelatin solution 2	Gelatine for human consumption
Glacial acetic acid	Merck (Darmstadt, Germany)
Goat serum	Dianova (Hamburg, Germany)
HEPES (N-(2-hydroxyethyl)piperazine-N´-2-ethanesulfonic acid)	Sigma-Aldrich (Taufkirchen, Germany)
HOE 140	Sigma-Aldrich (Taufkirchen, Germany)
Hyp^{3}-bradykinin	Sigma-Aldrich (Taufkirchen, Germany)
Kresyl-violet	Merck (Darmstadt, Germany)
Laminin	Sigma-Aldrich (Taufkirchen, Germany)
Manganese chloride	Sigma-Aldrich (Taufkirchen, Germany)
Nifedipine	Sigma-Aldrich (Taufkirchen, Germany)
Paraformaldehyde	Sigma-Aldrich (Taufkirchen, Germany)
Penicillin/Streptomycin	Biochrom (Berlin, Germany)
Pluronic acid	Life Technologies (Darmstadt, Germany)
Poly-D-lysin	Sigma-Aldrich (Taufkirchen, Germany)
Roti®-safe gel stain ready-to-use	Roth (Karlsruhe, Germany)
Tetrodotoxin	Sigma-Aldrich (Taufkirchen, Germany)
Triton-X	Sigma-Aldrich (Taufkirchen, Germany)

Table 2.1: List of chemicals

2.4 Preparation

2.4.1 Solutions

Solution	Source	Purpose	Concentration/supplements
Hank´s balanced salt solution (HBSS) without Ca^{2+}/Mg^{2+}	Life technologies, Darmstadt, Germany	Preparation of myenteric ganglionic cells and intestinal muscle cells	20 mmol·l^{-1} HEPES 10.000 units·ml^{-1} penicillin 10 mg·ml^{-1} streptomycin
Neurobasal A medium	Life Technologies	Cell culture of myenteric ganglionic cells	10 % (v/v) foetal calve serum 10.000 units·ml^{-1} penicillin 10 mg·ml^{-1} streptomycin 0.5 mmol·l^{-1} glutamine
Advanced Dulbecco´s modified eagle medium/Ham´s F12 (DMEM/F12)	Life Technologies	Cell culture of intestinal muscle cells/ in vitro preincubation of intestinal muscle	4% (v/v) foetal calve serum 10.000 units·ml^{-1} penicillin 10 mg·ml^{-1} streptomycin
Collagenase type II	Biochrom, Berlin, Germany	Digestion of muscle layer and adherent tissue	stock solution 1 mg·ml^{-1}
Poly-L-lysin	Sigma Aldrich, Taufkirchen, Germany	Coating of coverslips and MEAs	5 µg·ml^{-1}
Laminin	Sigma Aldrich	Coating of MEAs	1 mg·ml^{-1}
Krebs-solution		Transport of the human mucosal biopsies	In mmol·l^{-1}: 116 NaCl; 1.3 $CaCl_2$; 3.6 KCl; 1.4 KH_2PO_4; 23 $NaHCO_3$; 1.2 $MgSO_4$. Set to a pH of 7.4 with NaOH/HCl.

Table 2.2: Solutions for the preparation

2.4.2 Preparation of myenteric ganglionic cells and intestinal muscle cells

The myenteric ganglia cells were isolated from five to nine days old rats as described by Schäfer et al. (Schäfer *et al.* 1999). The animals were killed by decapitation (approved by Regierungspräsidium Giessen, Giessen, Germany) and the abdominal cavity was opened with forceps and scissors following the linea alba. Starting from the anal ending, the whole intestine was removed using small scissors. The intestine was placed into Ca^{2+}- and Mg^{2+}-free Hank´s balanced salt (HBSS) solution. Under optical control with a binocular microscope (Olympus SZX9, Hamburg, Germany), the muscle layer was stripped off from the anal to the oral direction using two fine forceps. The muscle layer was then incubated in a vial containing 1 ml collagenase type II stock solution (1 mg·ml^{-1}; Biochrom, Berlin, Germany) and 1 ml HBSS without Ca^{2+} and Mg^{2+} (end concentration of collagenase: 0.5 mg·ml^{-1}) at 37 °C for 80 min. After the incubation period, the tissue was vortexed for 10 - 15 s in order to dissociate the pieces of intestinal muscle from the myenteric ganglia. The suspension was diluted 1:11 with HBSS and dispensed into 35 mm culture dishes. With the use of the binocular microscope, the net-like myenteric plexus pieces were collected with a micropipette and placed into warm (37 °C) Neurobasal medium. The remaining intestinal muscle cells were centrifuged and the HBSS was replaced with warm (37 °C) DMEM/F12 medium. Subsequently, the muscle cells were further dissociated with a syringe and two different needles (0.8 mm and 0.4 mm external diameter).

Depending on further use, 10 µl of the ganglionic cell suspension was seeded either on 10 mm coverslips coated with poly-L-lysin (5 µg·ml^{-1}) or microelectrode arrays coated with poly-L-lysin (5 µg·ml^{-1}) and laminin (1 mg·ml^{-1}). 20 µl of the muscle cell suspension was seeded on 10 mm coverslips coated with poly-L-lysin (5 µg·ml^{-1}). The ganglionic cells were cultured in Flexiperm® chambers (28 mm^2; Greiner Bio-One, Frickenhausen, Germany), whereas the muscle cells were cultured in 4-well-plates.

After 45 - 60 minutes, the cells had settled down, were covered with 290 µl Neurobasal medium (for the ganglionic cells) or 980 µl DMEM/F12 (for the muscle cells), and incubated at 37 °C in an atmosphere of 5 % (v/v) CO_2 in 95 % (v/v) air for at least 16 h.

2.4.3 Preparation of the intestine for isometric contraction measurements and Ussing chamber experiments

The animals were killed by a blow on the head followed by exsanguination (approved by Regierungspräsidium Giessen, Giessen, Germany). The abdominal cavity was opened following the linea alba, with relieving incisions along the costal arch. In order to bleed the animal, the heart was cut. Then the colon was cut through at the distal end with scissors. The rest of the colon was removed by a blunt preparation of the mesentery and transected caudally from the exit of the caecum. The colon was placed into ice-cold Parsons buffer gassed with 5 % (v/v) CO_2/95 % (v/v) O_2, which led to a relaxation of the intestinal muscle. Then the lumen was cleaned with Parsons buffer using a syringe. For some isometric contraction experiments other parts of the intestine were removed as follows: the duodenum was taken off directly behind the pylorus, the jejunal part originated from the approximate middle of the jejunum and the ileum was removed directly before the entrance to the caecum.

For some colonic preparations the intestinal muscle had to be stripped off. For this purpose, the colon was placed on a rod (diameter 5 mm). After a circular incision near the anal end with a blunt scalpel, the muscularis propria, together with the serosa, was stripped off in a proximal direction.

In order to remove other layers of the intestinal wall, the colon was opened longitudinally and spread on a glass plate moistened with Parsons buffer. Both endings of the tissue were fixed with glass slides and stretched in order to achieve a certain strain. Then the particular layers were removed:

Depending on the experiments, different preparations were performed (Figure 2.1).

For the isometric contraction measurements:

1) Full-thickness preparation: the whole intestinal wall was used.
2) Muscle-submucosa-lamina propria preparation: the epithelium was scraped off carefully with little pressure using the edge of a glass slide. Most of the lamina propria and the muscularis mucosae remained intact.
3) Muscle-submucosa preparation: the mucosa was removed. The tissue was incised with the sharp edge of a glass slide and then the mucosal layer was scraped off.
4) Muscle preparation: the whole intestinal muscle was stripped off and used for the isometric contraction measurements (see above).

For the Ussing chamber:

1) Full-thickness preparation
2) Mucosa-submucosa preparation: the intestinal muscle was stripped off as described above.
3) Mucosa preparation: after the intestinal muscle was stripped off, the mucosa was removed as described in the muscle-submucosa preparation, with the difference that more attention had to be paid to the integrity of the mucosal layer, since this layer was used in the experiment, whereas for the isometric contraction measurements the mucosal layer was discarded.

In order to confirm the success of the preparational method, the preparations were at least once stained with haematoxylin and eosin stain and microscopically examined.

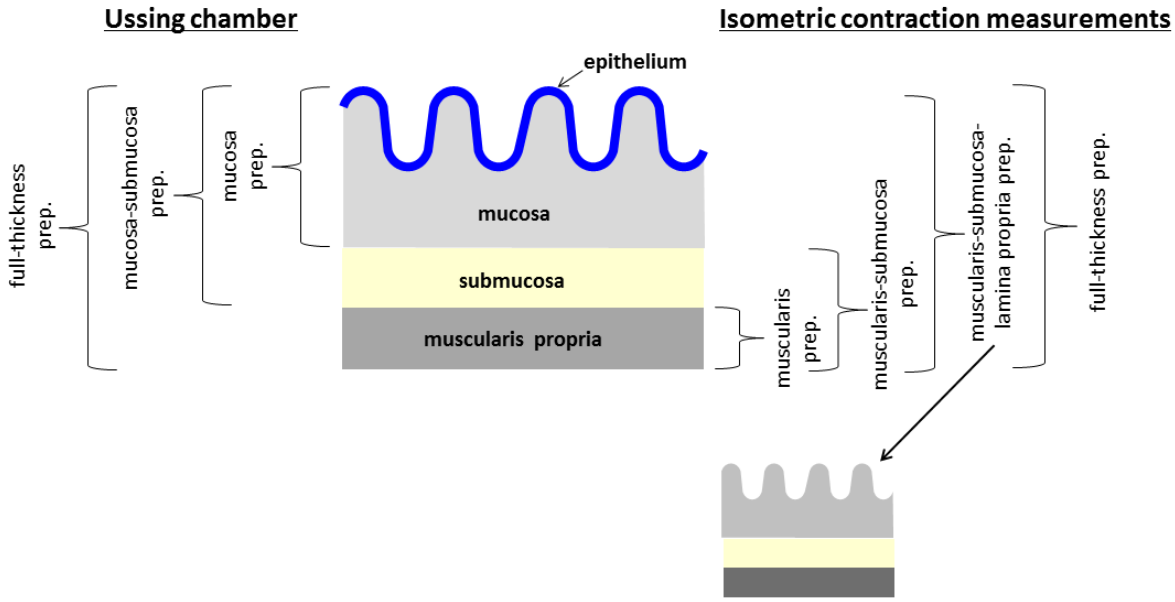

Figure 2.1: Illustration of the different layers of the colon and the usage for the specific preparations.

2.4.4 The human colonic mucosa biopsies

For the experiments with human mucosal biopsies two groups of patients were chosen: patients with ulcerative colitis and control patients without inflammatory disease. The ulcerative colitis group consisted of patients who underwent colonoscopy as a part of the clinical surveillance programme due to increased risk for development of colon cancer (Table 2.3). All patients except for two had no or few clinical symptoms and were considered to be in remission, whereas two patients showed activity according to the Mayo score (Lewis *et al.* 2008).

The control group consisted of patients who underwent colonoscopy for other reasons such as unspecific bleeding or altered bowel habits, but where the mucosa was macroscopically normal (Table 2.4). Thus, these control patients were 'disease controls', because they had intestinal symptoms but no inflammatory disease. The heterogeneity of the control group can be considered as a disadvantage; on the other hand it also reduces the risk of an error produced by a common disease denominator.

Ulcerative colitis patients		
Gender	**Age**	**Mayo score**
Female	22	0
Male	75	0
Male	33	1
Male	47	0
Male	40	0
Male	35	2
Female	35	0
Male	32	0
Male	30	0

Table 2.3: Ulcerative colitis patients

Control patients		
Gender	**Age**	**Reason for colonoscopy**
Female	33	Unspecific bleeding
Female	51	Constipation
Female	42	Unspecific bleeding
Female	69	Unspecific bleeding
Male	76	Loose stool containing mucus
Female	65	Unspecific bleeding

Table 2.4: Control patients

The evening before colonoscopy, the patients drank 4 l of an osmotic laxative (Laxabon®; BioPhausia, Stockholm, Sweden) in order to clean the intestine. Just prior to the colonoscopy, the patients were administered a premedication, consisting of 1 - 2 mg midazolam (Dormicum®; Roche, Basel, Switzerland) and 50 mg petidin (Petidin®; Meda, Solna, Sweden). During the whole procedure the heart rate and peripheral oxygenation was monitored with a pulse oxymeter. As part of the clinical diagnostics, up to 16 biopsies were taken from the caecum to the rectum according to the surveillance programme and histologically investigated by a pathologist. For the present study, seven biopsies were taken from the sigmoid colon and directly placed into oxygenated, ice-cold Krebs solution.

During the colonoscopy, the ulcerative colitis patient´s inflammatory state was evaluated by the gastroenterologist performing the procedure according to the Mayo score (Lewis *et al.* 2008). In the histological investigation, patients with a Mayo score of zero showed a normal or only slightly altered crypt architecture and a slight increase in infiltrating immune cells (eosinophils, neutrophils and plasma cells). The biopsies of patients with a Mayo-score of 1 - 2 had an acute inflammation with altered crypt architecture, infiltration of immune cells and cryptitis or crypt abscesses.

2.5 Microelectrode arrays (MEAs)

2.5.1 Solutions for MEA measurements

Solution	Source	Purpose	Concentration/supplements
Hank´s balanced salt solution (HBSS) with Ca^{2+}/Mg^{2+}	Life technologies, Darmstadt	MEA measurements	20 mmol·l^{-1} HEPES 10.000 units·ml^{-1} penicillin 10 mg·ml^{-1} streptomycin
Tergazyme solution	Sigma Aldrich, Taufkirchen, Germany	Enzymatic cleaning of the MEAs	10 mg·ml^{-1} in deionized water

Table 2.5: Solutions for MEA measurements

2.5.2 A short history of the microelectrode arrays (MEAs)

A microelectrode array (MEA) is a device that allows the measurement of action potentials in an extracellular manner from multiple cells at the same time. The first MEA was invented by Thomas in 1972 (Thomas *et al.* 1972) and was intended to overcome the limitations of single-cell techniques, such as patch-clamping or intracellular measurements with single electrodes (for review see Pine 2006). The chance to measure potentials from multiple sites and from a network of cells opened the possibility to examine spatial and temporal propagation of action potentials and the interaction between neurons.

In the early years, electrodes were fabricated of gold, sometimes platinized to reduce the impedance. Different insulation materials were used, such as photoresist, thermosetting polymers and silicon dioxide (Pine 2006). The MEAs were used for measuring cultured excitable cells, in the beginning chick myocytes and isolated snail ganglia, later dorsal root ganglia and neurons of the cervical ganglion (Pine 1980; Droge *et al.* 1986; Maroto *et al.* 2005).

In the eighties, further possibilities for application were explored, including other types of neurons, but also the measurement of slices, especially hippocampal slices and the retina (Jobling *et al.* 1981; Droge *et al.* 1986; Wheeler & Novak 1986). The MEAs enabled to measure the propagation of action potentials along a slice or – especially after light exposure – along the retina. The invention of FET transistor-coupled electrodes (Jobling *et al.* 1981) made it even possible to stimulate these slices or cultured cells electrically via one or more

electrodes. Long-term recordings performed with cultured cells as well as slices in organotypic culture for a period of several days (Welsh *et al.* 1995; Thiebaud *et al.* 1997) extended the knowledge about the plasticity of neural connections over time, with or without repeated stimulations. Chien and Pine (Chien & Pine 1991) combined the MEA-technique with voltage-sensitive dyes in order to measure not only action potentials but also to investigate subthreshold potentials.

Starting in the nineties, a lot of effort was done to control the growth of neurons on the chip and thus create artificial networks of neurons. Different kinds of coatings were applied and three-dimensional MEAs were built, with holes and tunnels for the axons and dendrites to grow into (Maher *et al.* 1999; Tooker *et al.* 2004; Marconi *et al.* 2012).

During the last decade, various types of MEAs were invented that allow using this technique for a lot of different applications. Among these, there are special thin MEAs that can be examined with high-power objectives, high-density MEAs with 265 electrodes for precise measurements of conduction velocity or synaptic delays, or perforated MEAs used for slices, that allow applying a negative pressure from below, and thus fixing the slice in the right position.

2.5.3 The principle of MEA measurements

Excitable cells are characterised by the ability of depolarisation induced by changes in membrane currents. The opening of ion channels, which is tantamount to the lowering of the membrane´s resistance, results in a change in membrane potential which can be measured by intracellular recordings. But the extracellular space has a resistance as well, and thus is conductive. Consequently, an action potential also leads to a change of voltage in the extracellular space. Although this change is very low compared to the intracellular voltage, it is still measureable and this can be performed with MEAs (Figure 2.2).

Well-established intracellular recording techniques, such as two-electrode voltage-clamp or – depending on the configuration - patch-clamping enable the investigation of this depolarisation in detail. However, there is a disadvantage of these techniques: since it is only possible to investigate one cell at a time, the neuronal interactions cannot be examined in a sufficient way. To some extend this can be compensated by the use of voltage-sensitive dyes. These dyes shift their spectral properties when being excited and thus indicate the depolarisation of a cell. It is possible to measure many cells at the same time, but

unfortunately these dyes have cytotoxic properties, so that the experimenter only gets a short peek in a range of seconds or minutes until the cell dies.

These handicaps can be overcome by microelectrode arrays. Because of the extracellular measurement with multiple electrodes, it is possible to receive information from many cells at the same time and – in contrast to voltage-sensitive dyes – over a long period of time. Measurements can be performed for minutes and hours and even for days if the cells are kept at constant pH and temperature conditions. Another advantage is the fact that the cells are cultured directly on the MEA: it is possible to measure the cells repetitively, which saves material and time.

Naturally, MEAs also have certain disadvantages. It is not possible to have a close view on the development of an action potential. The involvement of certain channels or sub-threshold potentials cannot be investigated. This purpose is served better with other electrophysiological techniques.

In intracellular measurements the amplitude of signals is usually in a mV-range. The signal detected with a MEA is 1000-times smaller (µV-range). The detection of this small signal requires a strong amplification and a minimal signal-to-noise ratio. The amplifier used in this study is the MEA1060 filter amplifier (Multichannel Systems, Reutlingen, Germany), which uses the SMD (Surface Mounted Devices) technology. It is very small and compact and does not only represent the interface with the MEA-probe, but also filters and amplifies the signal (Figure 2.3). The obtained data is transferred to the computer, digitized by MC Card (Multichannel Systems) and can be displayed and analysed by the software programme MC Rack (Multichannel Systems).

The MEA-amplifier has a broad bandwidth ranging from 0.1 Hz to 10 kHz. In order to enhance the signal-to-noise ratio, the recorded raw data can be filtered with MC Rack. In this study this was performed with a high-pass filter of 20 Hz. The gain of the amplifier is 1100 and is a fixed hardware property, meaning it cannot be changed by software controls.

The distance between the electrode and the cell is an important factor for the signal shape. The closer the cell is located to the electrode the stronger the signal. The maximal distance varies among the different cell types (Morin *et al.* 2005). Typically, the cell giving the signal is located in a radius of 30 µm around the electrode (User manual MEA, Multichannel Systems, Reutlingen, Germany).

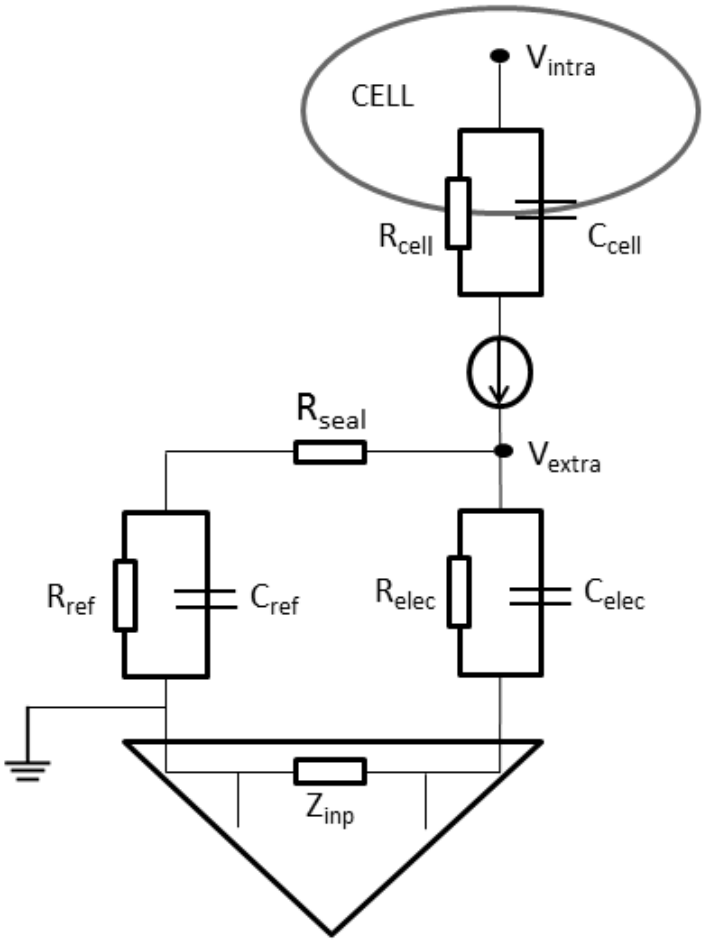

Figure 2.2: Simplified circuit diagram of a MEA-setup with an excitable cell
V_{intra}: intracellular potential; V_{extra}: extracellular potential; R_{seal}: sealing resistance; R_{elec} and C_{elec} resistance and capacitance of the recording electrode; R_{ref} and C_{ref} resistance and capacitance of the reference electrode Z_{input}: input impedance of the amplifier; R_{cell} and C_{cell} resistance and capacitance of the cell membrane.
Modified from Morin et al. 2005.

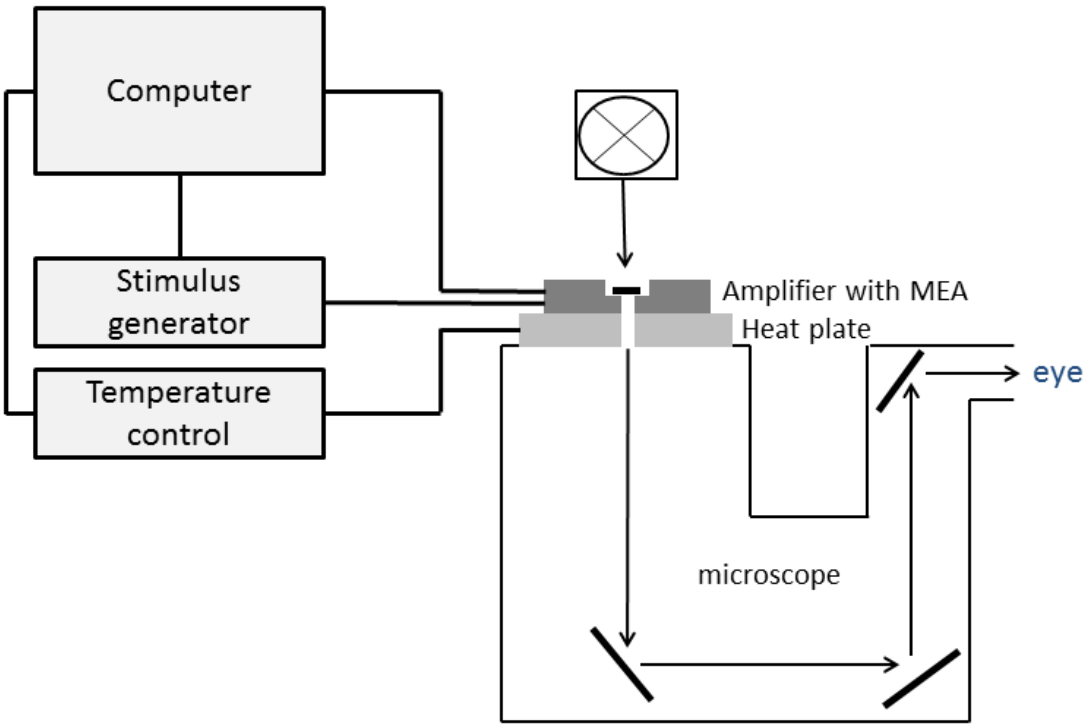

Figure 2.3: Illustration of a MEA-setup

2.5.4 The standard microelectrode array

The standard MEA used in this study is a glass chip with 60 electrodes (Multichannel Systems, Reutlingen, Germany; Figure 2.4). The electrodes are fabricated of titanium nitride (TiN), which is an extremely hard and stable material. It forms a microfold structure that increases the surface area and improves the signal-to-noise ratio. The electrodes have a flat and round shape and are embedded into the glass chip (Figure 2.5). The impedance ranges from 20 to 400 kΩ. The electrodes are connected to the contact pads via tracks, which are also fabricated of titanium nitride and are insulated with silicon nitride (Si_3N_4). These contact pads represent the connection between the MEA and the amplifier.

The electrodes have a diameter of 30 µm and are aligned in an 8 x 8 grid with an interelectrode distance of 200 µm. For grounding the bathing solution, the MEAs are equipped with an internal reference electrode.

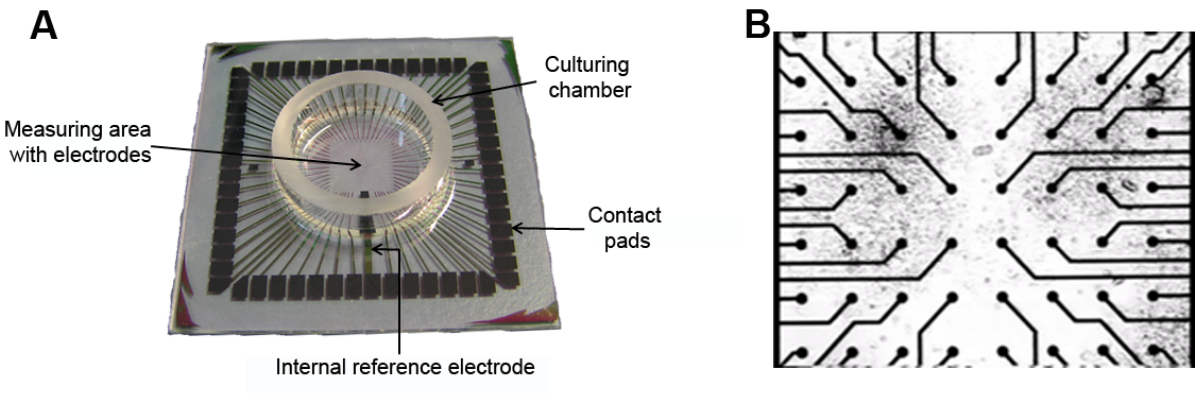

Figure 2.4 A: Image of a standard MEA-chip.
B: Microscopic picture of the measuring area of a MEA.
Shown are 48 of the 60 electrodes and myenteric ganglionic cells cultured on the MEA for 2 days.

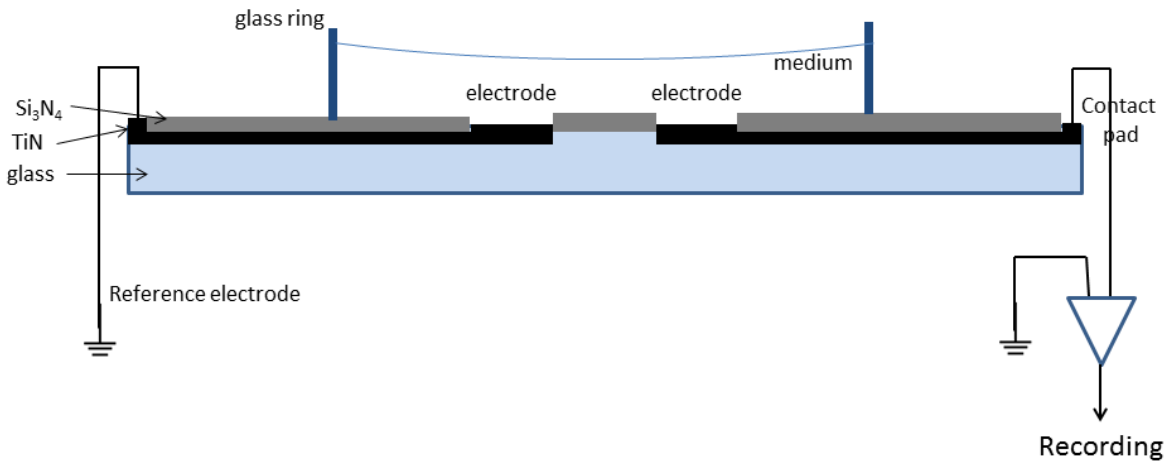

Figure 2.5: Schematic picture of a MEA-chip.
Exemplarily shown are one of the 60 recording electrodes (right side) and the internal reference electrode (left side).

2.5.5 The procedure of MEA measurements

Prior to the preparation, the MEAs were coated with 10 µl poly-L-lysin solution, which was left for evaporation. After this, 10 µl of laminin solution was pipetted onto the measuring area of the MEA and left there for 30 minutes, then it was removed (as described by Medert *et al.* 2013).

After the preparation, the cells were cultured for at least 12 hours. For measuring the MEAs, they were placed onto the microscopic stage and the amplifier plate was fixed on it. The reference electrode was chosen (usually number 15) and the setting information was downloaded to the amplifier using the software MEA Select (Multichannel Systems). After this, the programme MC Rack was opened and the traces of the electrodes were displayed. In case there was spontaneous activity in at least one electrode, the culture medium was replaced with the HBSS solution (see Table 2.5) using a pipette. This had to be done carefully to prevent a loosening of the cells. After waiting three to four minutes, the excitation level, which had been raised by the change of the medium, had returned to its former level and the recording was started. If the MEA showed no spontaneously active electrodes, it was placed back into the incubator for further culture and measured again the next day.

After starting the experiment, the baseline was measured for three to four minutes. Then the substance was carefully and softly administered using a pipette, without touching the MEA or the amplifier. Experiments with different forms of perfusion systems did not turn out to be successful because the increase in noise produced by the perfusion pump masked the small signals of the neurons.

In general, myenteric neurons seem to produce rather small amplitudes of action potentials compared to other neuronal cell types. The maximal signal size was around -40 µV, most signals only reached values of -15 to -20 µV. Thus it was essential to hold the noise level as low as possible (± 10 µV). After the administration of bradykinin, the response was measured for 12 minutes. The application of antagonists was carried out one minute before bradykinin was added.

After the experiments, the cells were washed with HBSS in order to remove the applied drugs. They were covered with Neurobasal medium and placed back into the incubator. After two to three hours, the cells had recovered and could be measured again. One MEA was used maximally three times per day.

For cleaning, the MEAs were incubated with the enzymatic solution Tergazyme (Table 2.5) overnight at room temperature.

2.5.6 Analysis of the MEA experiments

The obtained data was filtered and analysed with MC Rack. A high-pass filter of 20 Hz was applied in order to remove baseline fluctuations that might disturb the analysis. The spike rate was measured by counting those spikes passing a certain threshold. Due to differences among the MEAs, the threshold was set individually for each experiment. Depending if the electrode showed a negative or a positive spiking, the threshold was set 10 µV underneath or above the lowest/highest value of the noise. Although in an extracellular measurement of action potentials, the spike usually is negative, it is possible that the electrodes show positive spiking if the cell(s) giving the signal is (are) covering the recording electrode completely causing an 'pseudo-intracellular' measurement.

The baseline was measured just prior to the administration of the substance. The measurement of the response started 10 s after the administration, in order to exclude the detection of the artefact induced by the pipette.

The spike rate was measured in intervals with duration of 30 seconds in order to depict the course of the change in frequency induced by the substance. Only those electrodes were analysed that either were spontaneously active or started to show action potentials later on.

A few electrodes showed a much higher spiking rate than the others. These were defined as outliers and no longer considered for analysis, if the spike rates were higher than the 4-fold standard deviation of the other electrodes. Results were presented as means ± SEM of n active electrodes.

2.5.7 Waveform analysis

In order to distinguish signals from different neurons measured by the same electrode, a waveform analysis was performed using the spike sorting function of MCRack. One electrode is able to measure several cells in its surrounding area with each cell having another distance from the electrode. This difference in distance is reflected by different spike waveforms. With the waveform analysis up to three different units per electrode can be separated from each other and are considered as different neurons (Leibig *et al.* 2012). After administration of bradykinin, the percentage of responding neurons in relation to all active neurons was calculated. All neurons with an increase in frequency of action potentials higher than the absolute value of 0.3 Hz in response to bradykinin were defined as 'responding'.

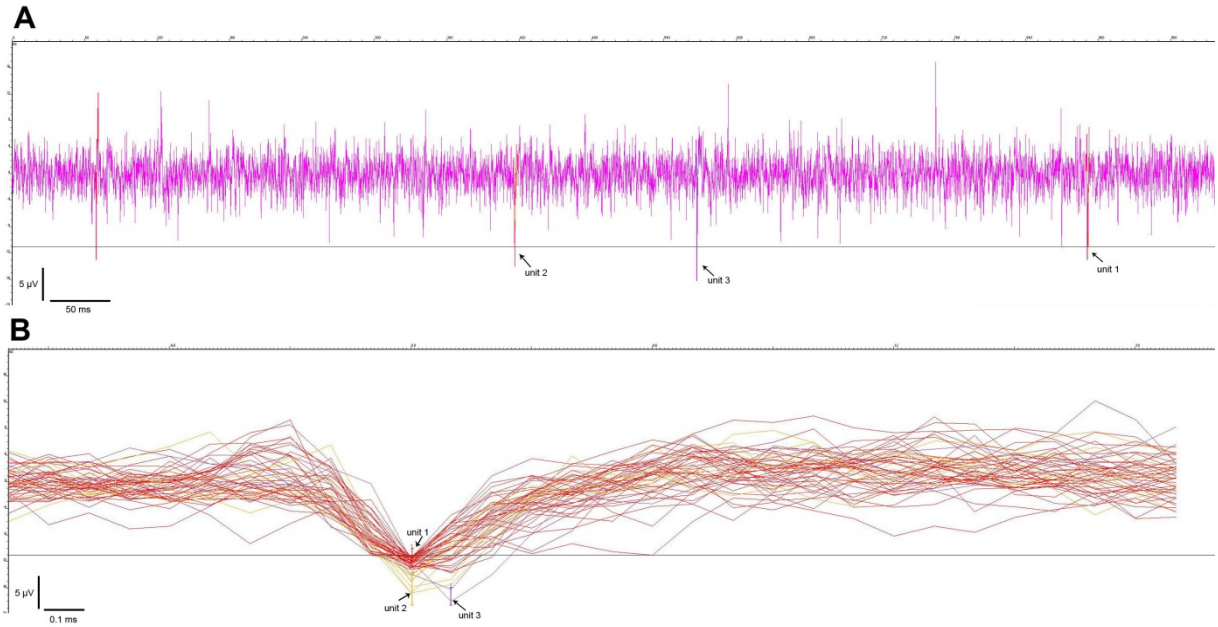

Figure 2.6: A: Representative tracing of firing activity of one MEA-electrode with different spike shapes being assigned to three different units (unit 1: red, unit 2: yellow, unit 3: purple).
B: Wave form analysis of the tracing seen in A.
Overlay of 50 spikes exceeding the threshold (-11 µV for this experiment). The vertical bars assign every spike to a certain unit depending on their amplitude and time line.

2.6 Immunofluorescence analysis

2.6.1 Solutions for immunocytochemistry (ICC) and immunohistochemistry (IHC)

Solution	Purpose	Concentration/supplements
Phosphate buffer (PB)	IHC; Rinsing of the tissue	80 Na_2HPO_4, 20 NaH_2PO_4 (in mmol·l^{-1}); pH 7.4 (adjusted with NaOH/HCl)
Phosphate buffered saline (PBS)	ICC; Rinsing of the cells	10 sodium phosphate buffer, 120 NaCl and 2.7 KCl (in mmol·l^{-1}); pH 7.4
PBS Triton-X (PBS-T)	ICC; Rinsing of the cells	0.05 % (v/v) Triton-X in PBS
Paraformaldehyde (PFA)	Fixation of cells and tissue	4% (w/v) PFA in PB Heated to 55°C during permanent stirring; after complete dissolving of the PFA, the solution was filtered and placed on ice
Blocking and antibody solution for ICC	Blocking of unspecific binding sites; dissolving of antibodies	10 % (v/v) donkey/goat serum dissolved in PBS-T
Blocking solution IHC	Blocking of unspecific binding sites	0.2 % (v/v) Triton-X, 1 % (w/v) bovine serum albumin (BSA), 0.5 % (w/v) milk powder, 1 % (v/v) donkey/goat serum dissolved in PB
Antibody solution IHC	Dissolving of antibodies	0.2 % (v/v) Triton-X, 1 % (w/v) BSA, 0.5 % (w/v) milk powder, 1 % donkey/goat serum, dissolved in PB
DAPI solution	Nuclear staining	300 nmol·l^{-1}; dissolved in PB.
Gelatin solution 1	Coating of the glass slides	5 g·l^{-1} aqua dest.; the solution was heated and mixed with 0.5 g·l^{-1} chromkaliumsulfate at 54°C, then filtered
Gelatin solution 2	Embedding of the tissue	18 g dissolved in 180 ml aqua dest.; the solution was heated to 37°C and filtered
Kresyl-violet	Inspection of the section plane (cryosections)	1 g·l^{-1} kresyl-violet acetate was dissolved in aqua dest. under stirring and warming; the solution was cooled down and 2.5 ml·l^{-1} glacial acetic acid was added; then filtered

Table 2.6: List of solutions used for immunofluorescence analysis

2.6.2 The principle of immunofluorescence analysis

The principle of the immunofluorescence analysis is based on the interaction of the epitopes of a certain antigen with the paratopes of specific antibodies. This interaction can be visualised with the aid of fluorescent markers, opening the possibility to investigate the presence and distribution of certain structures in tissue and cultured cells.

Most of the antibodies used are IgGs, either monoclonal or polyclonal. Polyclonal antibodies are obtained from immunised animals, meaning that they are produced by various different B-cells. Consequently, these antibodies bind to different epitopes of the same antigen, which results in a good sensitivity of these polyclonal antibodies. But at the same time, they sometimes produce unspecific background staining due to the lower specificity. In contrast, monoclonal antibodies are produced in vitro from a B-cell line, which has its origin in one specific B-cell. Thus the specificity of monoclonal antibodies is higher compared to polyclonal antibodies.

The antibodies consist of two antigen-binding regions, the F_{ab} (fragment antigen binding), and a crystallisable region, the F_c (Figure 2.7). The F_{ab} region binds specifically to a certain antigen, creating an antigen-antibody-complex, which is held together by multiple non-covalent bindings (Harlow and Lane 1988). The antigen-antibody complex is visualised by a secondary antibody carrying a fluorescent dye, called fluorochrome. It binds to the primary antibody and can be investigated using a fluorescent microscope (Coons 1958).

Due to the availability of different secondary antibodies, it is possible to detect more than one antigen. These double stainings give a clue about the localisation and morphological relation of different proteins. For these stainings, it is important to pay attention that the origin species of both primary antibodies differs, as well as the colour of the fluorochrome carried by the secondary antibodies. In this study double stainings were performed in order to investigate a possible co-localisation of the bradykinin receptors with neuronal markers.

2.6.3 Immunohistochemistry versus immunocytochemistry

Different protocols were used for the study of tissues by immunohistochemistry (IHC) or isolated cells by immunocytochemistry (ICC) (see 2.6.5). Firstly, the thickness of the tissue in the IHC compared to cells requires an extended fixation-period with PFA (12 hours vs. 15 minutes). Secondly, in the IHC the solutions need to have a higher penetrability than in the ICC. That is why the amount of Triton-X, a non-ionic surfactant, is higher in the IHC-solutions compared to that of the ICC. And thirdly, due to the various different cells types in most sections compared to one or two cell types in most cell cultures, the risk of unspecific background staining is much higher in the IHC. This is improved by the addition of BSA and milk powder, which coats all proteins in the sample and forces the antibody to compete for the specific antigen. In this study, both the IHC and the ICC were performed, the first with cryosections of the whole colon and the latter with cultured myenteric ganglionic cells and with dissociated intestinal muscle cells.

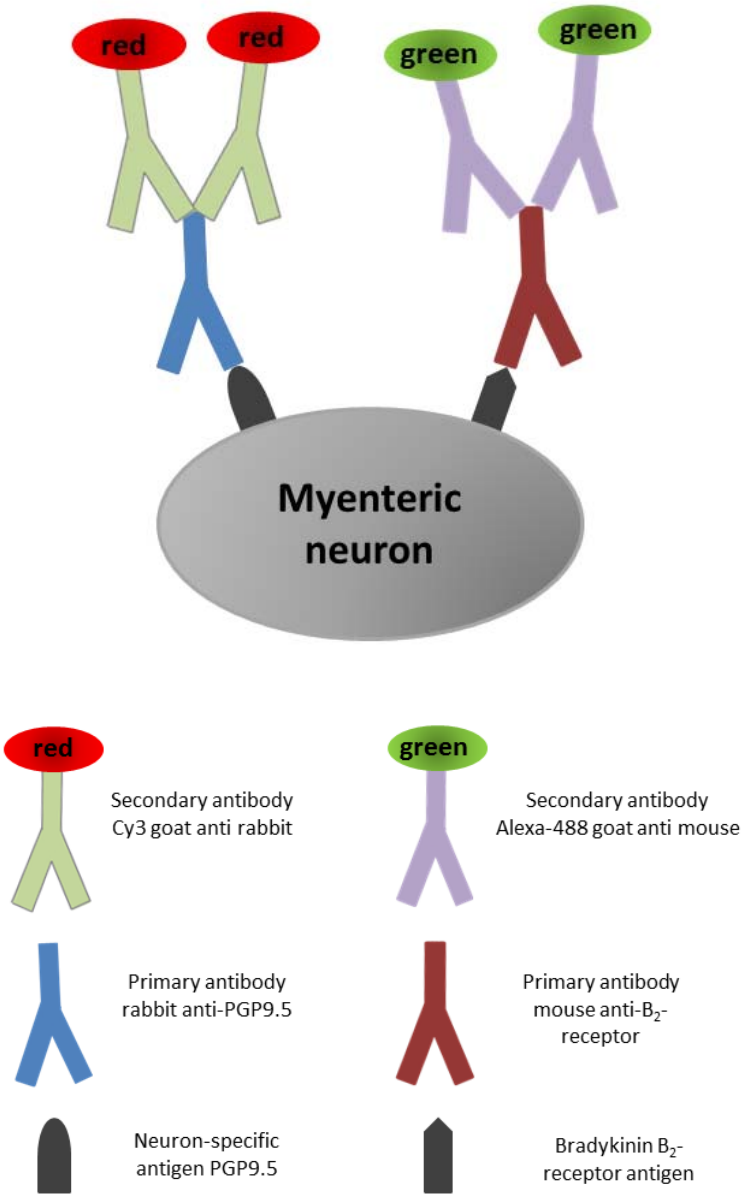

Figure 2.7: Principle of the double staining by indirect immunofluorescence using the example of the bradykinin B_2 receptor located on a myenteric neuron.
The primary antibodies bind with their F_{ab} region to the epitopes of the neuron-specific antigen PGP9.5 and the bradykinin B_2-receptor antigen, respectively. The secondary antibodies carrying a fluorochrom bind to the F_c region of the primary antibodies. The antigen-antibody-complex can be detected using a fluorescence microscope. If performing double stainings, it is important to ensure that the different primary antibodies do originate from different host species and that the secondary antibodies carry fluorochroms with different colours.

2.6.4 Used antibodies

2.6.4.1 Primary antibodies

Primary antibody	Target structure	Host species	Dilution	Manufacturer
Anti bradykinin B_1 receptor	Bradykinin B_1 receptor	Goat	1:50	Santa Cruz, Heidelberg, Germany
Anti bradykinin B_2 receptor	Bradykinin B_2 receptor	Mouse	1:200	Becton Dickinson, Heidelberg, Germany
Anti bradykinin B_2 receptor	Bradykinin B_2 receptor	Rabbit	1:20	Santa Cruz Heidelberg, Germany
Anti-PGP 9.5	Neurons	Rabbit	1:500	Millipore. Temecula, Canada
Anti-MAP2	Neurons	Mouse	1:250	Sigma-Aldrich, Taufkirchen, Germany
Anti-MAP2	Neurons	Rabbit	1:250	Sigma-Aldrich, Taufkirchen, Germany

Table 2.7: List of primary antibodies

2.6.4.2 Secondary antibodies

Primary antibody	Target structure	Colour	Dilution	Manufacturer
Alexa-488 donkey anti goat	Primary antibodies from the goat	Green	1:500	Invitrogen, Karlsruhe, Germany
Alexa-488 goat anti mouse	Primary antibodies from the mouse	Green	1:500	Invitrogen, Karlsruhe, Germany
Cy3 donkey anti rabbit	Primary antibodies from the rabbit	Red	1:800	Dianova, Hamburg, Germany
Cy3 goat anti mouse	Primary antibodies from the mouse	Red	1:800	Dianova, Hamburg, Germany

Table 2.8: List of secondary antibodies

2.6.5 The procedure of the immunohistochemistry (IHC) and immunocytochemistry (ICC)

2.6.5.1 Fixation with paraformaldehyde (PFA)

For the purpose of conservation, the tissue was fixed in 4 % (w/v) PFA. This solution leads to a cross-linkage of tissue proteins and thus preserves cellular structures.

IHC: the colon was prepared as described in 2.4.3, but without stripping off the muscle layer. Then the colon was cut into pieces with a size of about 1.5 x 3 cm and glued to an acrylic glass-holder with cyanoacrylate adhesive. It was taken care that the tissue fully covered the hole of the holder (Figure 2.8) (Schultheiss *et al.* 2002a). The holder with the tissue was kept in the PFA-solution for 12 hours at 4°C. After this incubation period, the tissue was rinsed with PB three times for five minutes.

ICC: after the preparation and culture period (2.4.2), the medium was removed with a pipette. The glass slips with the myenteric ganglionic cells were transferred to a 4-well-plate, whereas the glass slips with the muscle cells were left in their 4-well-plate. The cells were rinsed with PBS and then 500 µl of PFA was pipetted into each chamber. They were incubated on ice for 15 minutes. Then the PFA was removed and the cells were washed three times for five minutes with 500 µl PBS. In contrary to the IHC, the washing steps were not carried out on a shaker in order to prevent the cells from getting loose.

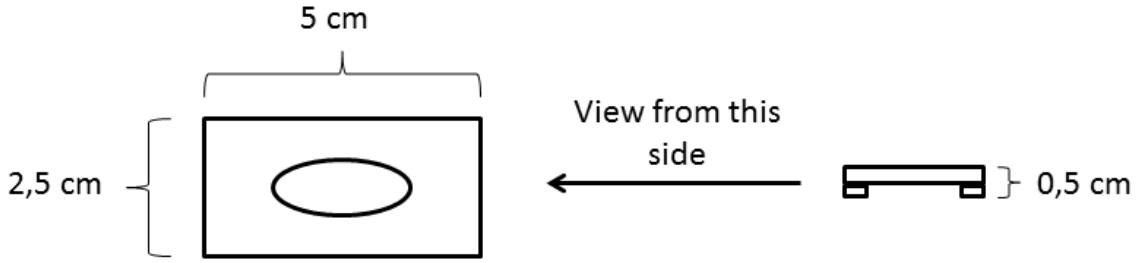

Figure 2.8: Illustration of the acrylic glass holder used for IHC.

2.6.5.2 Cryofixation (IHC)

The cryofixation was performed merely with the tissue for the IHC. After fixation with PFA and rinsing (2.6.5.1), the holder with the colon tissue was embedded in a glass dish containing liquid gelatine (2.6.1). It was taken care that the holder was fully covered with

gelatine, with a 0.5 cm gelatine layer underneath and above the tissue. After the solidification of the gelatine, the glass dish was placed on ice and the gelatine-tissue block was removed by cutting along the oval opening of the holder with a sharp scalpel. The removed tissue block was glued on a piece of cork with the embedding medium Tissue Tec® (Leica Instruments, Nussloch, Deutschland) and dunked for two minutes into isopentan, which has been cooled down with the aid of liquid nitrogen (temperature liquid nitrogen: -160 °C; temperature isopentan: ca. -80 °C). The tissue blocks were stored at -70 °C until further use.

2.6.5.3 Cryosections (IHC)

For the IHC, the tissue-gelatine-blocks were cryosectioned in a cryostat with a chamber-temperature of -18 °C (Leica CM 3050S; Leica Instruments, Nussloch, Deutschland). The frozen tissue-gelatine blocks were glued onto a movable holder with Tissue Tec® and cut into sections with a thickness of 4 µm. The sections were placed on the gelatine-coated glass slides. In order to confirm the section plane, the first sections were stained with a kresyl-violet solution for one minute and investigated under a microscope. If the sections plane turned out to be correct, more sections were produced and kept in the cooled chamber until further use.

2.6.5.4 Procedure of IHC

The cryosections were produced as described in 2.6.5.3. After this, the glass slides were transferred to a slide rack and placed into a plastic cuvette filled with 200 ml PB for rehydration. The cuvette was placed on a shaker for five minutes. This process was repeated with fresh PB two more times.

The next step was the blocking of unspecific binding sites, which was performed with the blocking solution as described in 2.6.1. The serum in the blocking solution contained antibodies binding to reactive sites and preventing the secondary antibody to bind unspecifically. The serum should come from the very species, from which the secondary antibody originated.

For the blocking step, the slides were placed upside down on an acrylic glass plate with two stripes of adhesive tapes serving as spacers. The short endings of the slides were placed on the tapes in order to get a capillary gap between the section and the plate. 200 µl of the

blocking solution was pipetted into this gap, and via capillary force the solution spread underneath the whole slide. The slides were then incubated at room temperature in a metal chamber laid out with moist paper tissue for 1 hour. After this, the slides were transferred to a fresh acrylic glass plate, and the primary antibody was pipetted underneath the slides with the same technique. The metal chamber was incubated at 4 °C for 12 hours. Then the slides were transferred to a slide rack and washed in PB as described in the rehydration step. The secondary antibody was applied in the same manner as the primary antibody, with the difference that this antibody had to be protected from light in order to prevent a fading of the fluorescent colour. All the following steps were performed in the dark as well. The incubation with the secondary antibody was carried out in a moist metal chamber for two hours at room temperature.

Then the slides were rinsed three times with PB again, and the nuclear staining with DAPI was performed, which is important for a better orientation in the tissue during the microscopic examination. DAPI intercalates mostly in adenosine- and thymine-rich regions of the DNA double helix and marks the nuclei of cells with a blue fluorescence if stimulated with ultraviolet light (Tanious *et al.* 1992). For this staining, the rack with the slides was transferred into a cuvette filled with DAPI and placed onto a shaker for five minutes. Then the slides were rinsed three times with PB again.

The last step was the covering of the slides. This was performed by placing one drop of Hydromount® (National diagnostics, Atlanta, Georgia, USA) on each section and covering it with a glass slip. The slip was fixed on the slide with a drop of clear nail polish and left for drying.

2.6.5.5 Procedure of ICC

After the fixation with PFA and the washing step described in 2.6.5.1, the unspecific binding sites were blocked. For this purpose, 500 µl of the blocking solution was pipetted into the wells and the plate was placed into a moist metal chamber for one hour. The administration of the antibodies and the washing steps were comparable to those of the IHC, with the difference that the solutions had a different composition (Table 2.6), and that all solutions were pipetted directly into the wells.

In the end, the coverslips were removed from the wells, placed upside down on a glass slide, which was equipped with a drop of Hydromount, and fixed with a small drop of clear nail polish.

2.6.5.6 Negative controls

In the IHC as well as in the ICC, negative controls were important to control the success of the immunofluorescent staining. For this purpose, for each slide a control slide was prepared, which was treated in exactly the same manner with the difference that the primary antibody was omitted. These negative controls should show no signal, when stimulated with the same wave length and exposure time, in order to confirm that the secondary antibody did not bind unspecifically. If there was a signal in the negative control, the IHC or ICC was discarded and repeated.

2.6.5.7 Microscoscopy

The analysis of the immunofluorescent staining was carried out with an Eclipse 80i microscope (Nikon, Düsselsdorf, Germany). The fluorochromes were stimulated with changeable light filters: the Cy3-fluorochromes were stimulated with a wave length of 510 - 530 nm and emitted light at a wave length of 630 - 660 nm. The Alexa-488-fluorochromes were stimulated with 450 - 490 nm and emitted at 510 - 530 nm. The nuclear staining DAPI was stimulated with 348 nm and emitted at 461 nm. The pictures were taken with a black and white camera (S/W camera Digital Slight DS 2 M BWc, Nikon). With the aid of the software programme NIS-elements 2.30 (Nikon), the pictures were displayed with different colours, depending on the emitted wave length. The Cy3-fluorochromes were shown in red, whereas the Alexa-488-fluorochromes were green and the DAPI-staining blue. Pictures were taken singularly at every wave length and then merged. This merging revealed the co-localisation of the signal with the nuclei, and – in the case of the double stainings – with other detected antigens. For the sake of comparability, the negative controls were always stimulated with the same exposure time as its corresponding positive slides.

For the purpose of illustration and documentation, the contrast and light intensity of the pictures were, when necessary, carefully processed with Adobe Photoshop. Signals that were to be compared were always processed in exactly the same manner.

Procedure	Reagents	Temperature	Duration
Fixation	PFA	Room temperature	12 hours (IHC)/ 15 min (ICC)
Cryofixation (only IHC)	Gelatine, tissue tec®, isopentan	Room temperature; liquid nitrogen: ca. -160 °C	Gelatine-embedding: ca. 1 hour isopentan: 2 min
Cryosections (only IHC)	Tissue Tec®, kresyl-violet	Cryostat: -70 °C	
Rehydration (only IHC)	PB	Room temperature	3 x 5 min
Blocking of unspecific binding sites	Blocking solution	Room temperature	1 hour
Incubation with primary antibody	Antibody solution + primary antibody	4 °C	12 hours
Rinsing	PB/PBS	Room temperature	3 x 5 min
Incubation with secondary antibody	Antibody solution + secondary antibody	Room temperature + light protection	2 hours
Rinsing	PB/PBS	Room temperature + light protection	3 x 5 min
Nuclear staining	DAPI-solution	Room temperature + light protection	5 min
Rinsing	PB/PBS	Room temperature + light protection	3 x 5 min
Embedding	1 drop hydromount per cryosection/ per glass slip	Room temperature + light protection	
Storage	Light protection	4 °C	

Table 2.9: Standard protocol for immunohistochemistry and immunocytochemistry

2.7 Ca^{2+}-imaging

2.7.1 Solutions for Ca^{2+}-imaging

Solution	Technique	Concentration
Standard Tyrode solution	Superfusion of the cells	In mmol·l^{-1}: 140 NaCl; 5.4 KCl; 10 HEPES; 1 $CaCl_2$; 1 $MgCl_2$; 12.2 glucose. Set to a pH of 7.4 with NaOH/HCl.
Ca^{2+}-free Tyrode solution	Superfusion of the cells	In mmol·l^{-1}: 140 NaCl; 5.4 KCl; 10 HEPES; 1 $MgCl_{2;}$ 12.2 glucose. Set to a pH of 7.4 with NaOH/HCl.

Table 2.10: Solutions for Ca^{2+}-Imaging

2.7.2 The principle of Ca^{2+}-imaging

Neuronal activity is accompanied by changes in the cytosolic Ca^{2+}-concentration. These changes can be detected with the Ca^{2+}-imaging technique, in which cells are loaded with specific fluorescent dyes (Figure 2.9). These dyes belong to two different groups: the wavelength stable dyes and the wavelength shifting dyes. When wavelength stable dyes bind to Ca^{2+}, they change the intensity of emission, but not the wavelength of excitation and emission. This differs from the wavelength shifting dyes. As the name implies, these dyes shift their wavelength, at which they are maximally excited, when binding to Ca^{2+} (maximum wavelength). The most common dye of this group is fura-2, which is also used in these experiments. Fura-2, which is bonded to Ca^{2+}, has its maximum wavelength at 340 nm, whereas the unbounded fura-2 has its maximum wavelength at 362 nm. The cells are excited at both wavelengths alternatively, and each emission is detected at 510 nm. It is important to mention that an excitation with a wavelength of exactly 362 nm is not effective, since this wavelength is too close to the isoemissive point of the spectral curve of fura-2 (Figure 2.10). Consequently, the excitation is performed at wavelengths of 340 nm and 380 nm. The quotient of the resulting emissions is calculated. These ratio measurements have certain advantages compared to measuring single emission wavelengths, such as independence from the absolute concentrations of the dye in the cell and factors like the size of the cell.

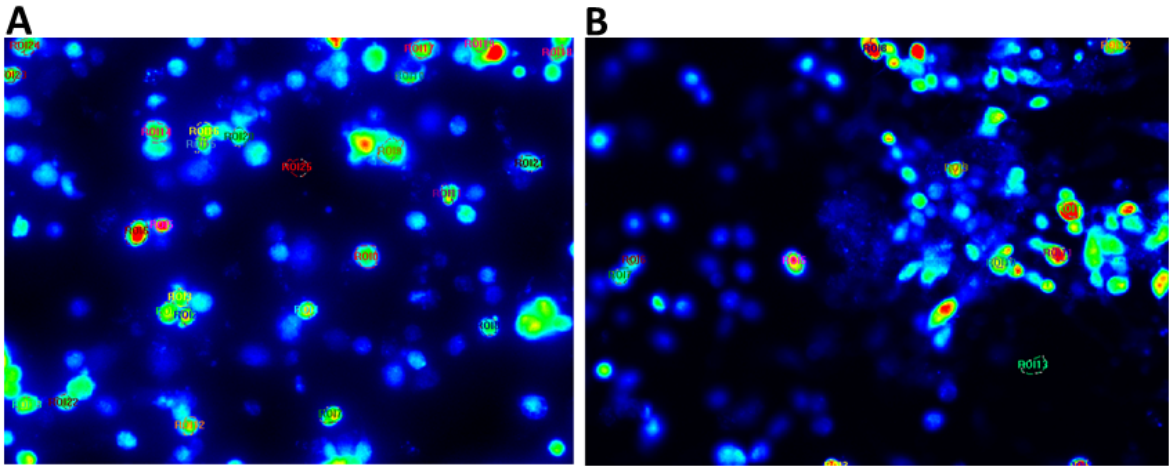

Figure 2.9: Picture of cells loaded with the fluorescent dye fura-2. Target cells are marked and defined as ´ROI´(region of interest).
A: dissociated intestinal muscle cells; B: myenteric ganglionic cells.

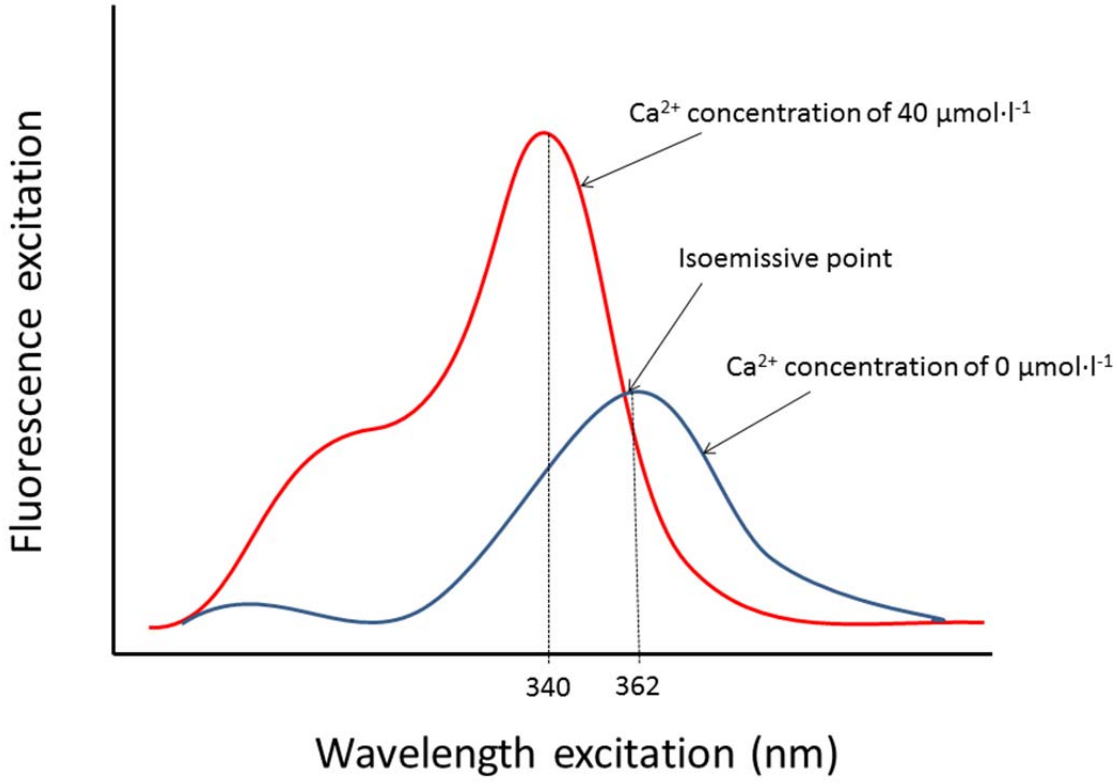

Figure 2.10: Excitation spectra of Fura-2 at different Ca^{2+}-concentrations
(Modified from Haughland, Handbook of Fluorescent Probes and Research Chemicals, 1996).

2.7.3 The fluorescent dye fura-2

Fura-2 is a Ca^{2+}-sensitive fluorescent dye, which has the structure of a Ca^{2+} chelator (Figure 2.11). Thus it has a high affinity for Ca^{2+} ions and binds them in chelate complexes. Figure 2.12 illustrates the dissociation curve of fura-2 with Ca^{2+} in dependency on the Ca^{2+} concentration. The dissociation constant (K_d), which represents the Ca^{2+}-concentration at which 50 % of the Ca^{2+} is bonded to fura-2, is at 224 nmol·l^{-1}. The smaller the K_d, the higher is the affinity for Ca^{2+}. The usual Ca^{2+} concentration in the cytosol is approximately 100 nmol·l^{-1}, consequently there is a sufficient leeway until fura-2 is saturated with Ca^{2+}.

Since fura-2 is negatively charged and unable to cross the cell membrane, an ester of this dye is used: fura-2 acetoxymethylester (fura-2 AM). Fura-2 AM is lipophilic and thus it can easily overcome the cell membrane. Once having entered, the cell´s unspecific esterases cleave the ester bonds and set free the uncharged form of fura-2, which is no longer able to penetrate the cell membrane (Tsien & Poenje 1986).

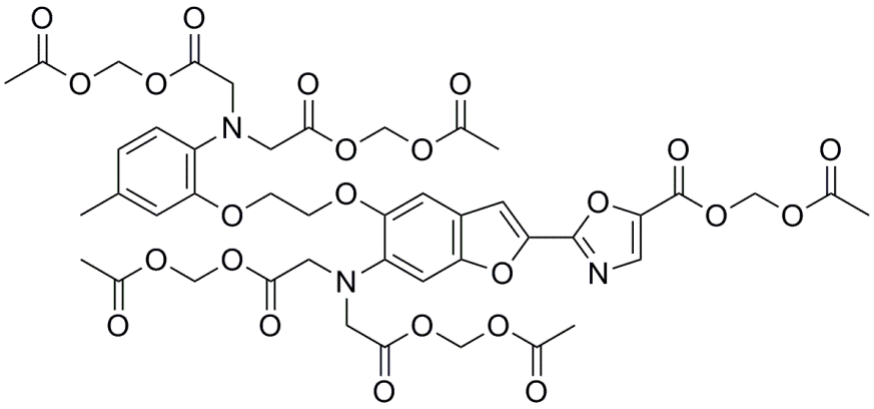

Figure 2.11: Structure of fura-2 AM

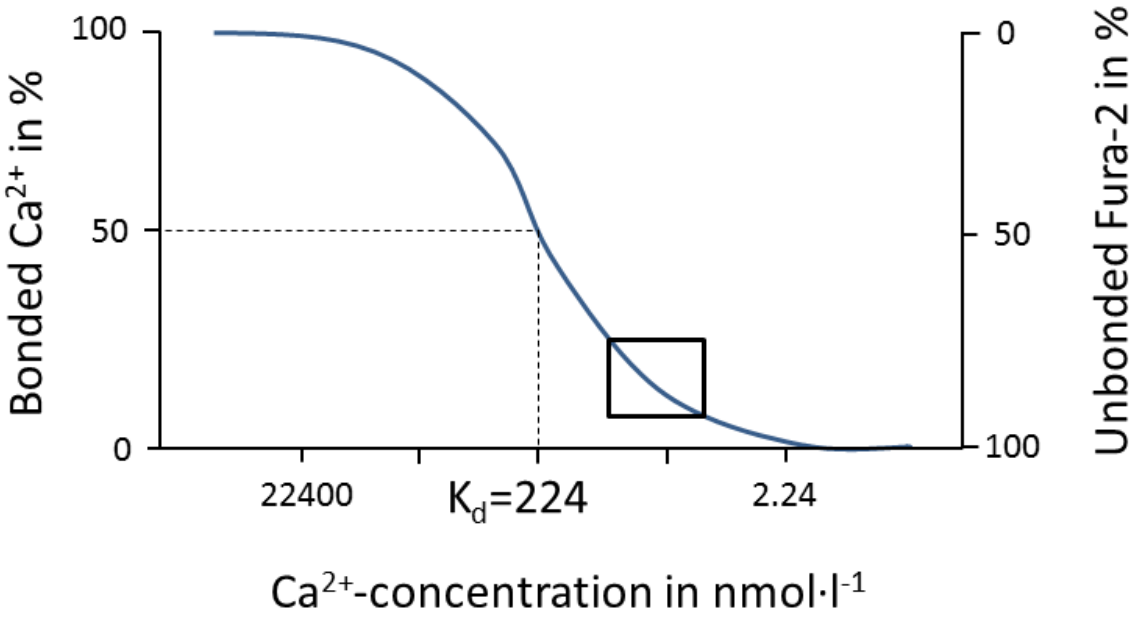

Figure 2.12: Dissociation curve of fura-2 with Ca^{2+} in dependency on the Ca^{2+}-concentration.
The square shows the range of the intracellular Ca^{2+}-concentration of cells under rest conditions. K_d= dissociation constant (modified from Haughland, Handbook of Fluorescent Probes and Research Chemicals, 1996).

2.7.4 The setup for the imaging-experiments

The fura-2 measurements were performed with an inverse light microscope (IX 50, Olympus), equipped with an epifluorescence setup (Figure 2.13). A xenon lamp produced light with alternating wavelengths of 340 and 380 nm, which was sent to the light conductor via a mirror. Another dichromatic mirror sent the light to the cover slip with the fura-2 loaded cells and excited the dye. The resulting emission had a wavelength of 510 nm and could pass the dichromatic mirror. A CCD-camera (charge coupled device, Till Photonics, Martinsried, Germany) recorded the emitted light and transferred it to a computer. The computer was equipped with the imaging software TILLvisION (Till Photonics) for displaying and analysing the obtained data. A movable mirror enabled to send the light either to the camera or to the eye.

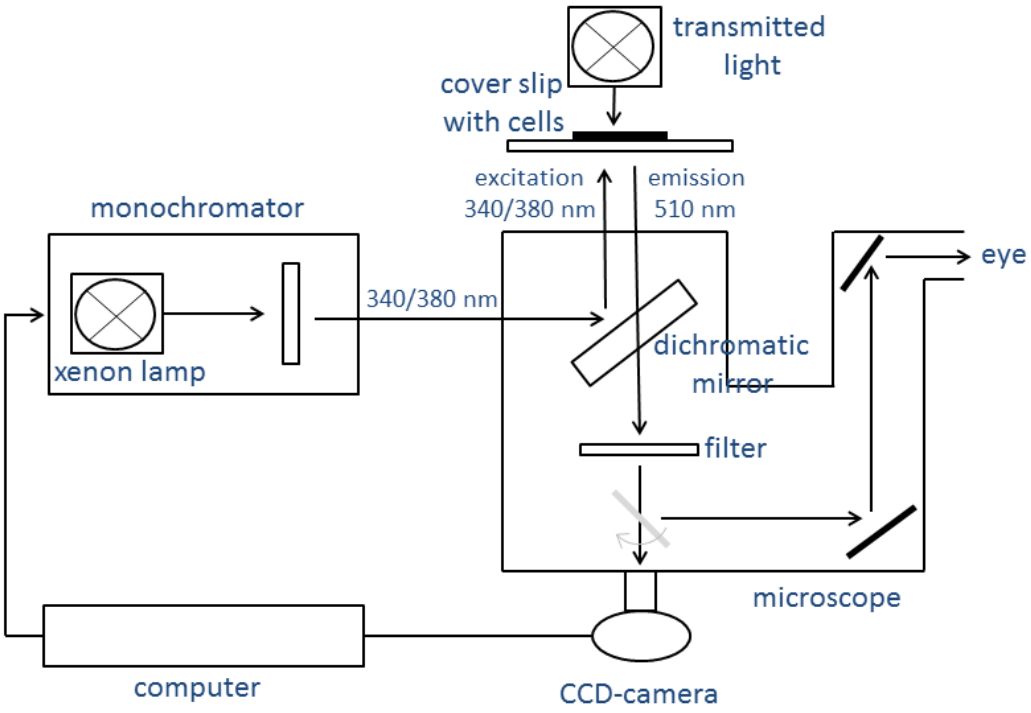

Figure 2.13: Illustration of the imaging set-up
(Picture modified by courtesy of M. Diener).

2.7.5 The experimental chamber and the perfusion system

The chamber consisted of a metal plate having a hole with a diameter of 1.1 cm. The cover slip was placed upon the hole and fixed with a teflon ring, which had a hole with the same diameter as the hole in the metal plate. The ring was screwed onto the metal plate in order to reach a tight seal between the teflon ring and the cover slip. The shape of the teflon ring formed a chamber with a volume of up to 1.5 ml. The whole device was placed onto the microscope stage and the perfusion system was installed.

The perfusion consisted of a system of pipes connected to a pump (type 11OSC.G18.CH5B; Ole Dich Instrumentmakers APS, Hvidovre Denmark). The perfusion speed was set at 250 $ml \cdot min^{-1}$.

2.7.6 Procedure and analysis of fura-2 measurements

The imaging experiments were performed with myenteric neurons as well as dissociated muscle cells obtained from the small intestine and the colon.

The cover slips were transferred to a 4-well-plate and covered with 500 µl standard Tyrode solution containing 6 µmol·l^{-1} fura-2 AM and 1.2 µg·ml^{-1} pluronic acid, which dispersed the fura-2 AM. The cover slips had to be protected from light, in order to prevent a bleaching of the dye. They were incubated at 37 °C for 60 minutes (muscle cells) and 75 minutes (neurons), respectively. Then the unbounded dye was washed away by changing the Tyrode buffer, the coverslips were transferred to the measuring chamber and placed onto the microscope stage. The perfusion system was installed. After the area of the glass slip to be measured was chosen using the light microscope, a picture was taken under UV-light and was displayed on the computer screen with false colours. Then the ROIs (regions of interest) were marked. In case of the myenteric neurons the cells were partly dissociated and partly still embedded in ganglia due to the preparational technique. In addition, there were a lot of glia cells in the cultures. The most successful measurements were made with clusters of cells, but it had to be taken care that the cells were not too piled. In order to avoid the marking of glia cells, the ROIs were chosen under light microscopic control.

At the beginning of the experiment, the cells were covered with Tyrode solution and a baseline was measured. In the experiments using bradykinin and its receptor agonists, the substance was carefully administered with a pipette. Then the change in the fura-2 ratio was detected for either 20 minutes (neurons) or for 8 minutes (muscle cells). This difference is due to the response pattern of both cell types. The antagonists were diluted in standard Tyrode solution and superfused for five minutes via the perfusion system. The Ca^{2+}-free, as well as the Mn^{2+}-containing Tyrode solution was applied in the same way. After this, bradykinin was administered as described above. After each experiment, a viability control was performed with either KCl (for the neurons) or carbachol (for the muscle cells). KCl depolarises the cell, which leads to an increase of cytosolic Ca^{2+} level, and carbachol binds to the G_q-protein coupled muscarinic receptors and thus increases the Ca^{2+}-concentration.

During the experiments with the intestinal muscle cells, the spontaneous, but also the stimulated contractions and movements of the cells disturbed the measurements. Consequently, these experiments were performed in the presence of 5 µmol·l^{-1} nifedipine, which inhibits the contraction of the muscle cells by blocking the dihydropyridine-sensitive L-type calcium channels (Ragy & Elbassuoni 2012).

A reaction to a substance had to fulfil two requirements in order to be considered as a response of the cell: the amplitude of the ratio increase after administration had to exceed

1) the absolute value of 0.05 and 2) the 4-fold of the standard deviation calculated from the baseline.

Due to nifedipine, the muscle cells did often not respond to carbachol in a sufficient way, so in these experiments the requirement for inclusion to the analysis was a response either to bradykinin or to carbachol. Some cells responded to bradykinin with a biphasic reaction, with the first negative peak being very small. Consequently, the requirement for the negative peak to be considered as a cell reaction, was to exceed the 2-fold of the standard deviation, instead of the 4-fold as used for the positive peak.

Using the imaging software TILLvisION, the protocol for the measurement was defined and the acquired data was displayed and analysed. Every 5 seconds the dye was excited with a pair of light pulses (340 and 380 nm). The exposure time was 20 ms for each pulse. The emitted signals were detected and the ratio was calculated by the software. It was displayed as a curve, which rose in response to an increase of cytosolic Ca^{2+} level and fell in response to a decrease of cytosolic Ca^{2+} level. The obtained data was analysed with spread sheet software (Microsoft Excel).

2.7.7 Manganese quenching

2.7.7.1 The theory of manganese quenching

A possibility to directly investigate the Ca^{2+} influx from the extracellular space is the manganese quenching technique (Hallam *et al.* 1988). As Mn^{2+} is accepted as substrate by many Ca^{2+} transporting enzymes, it enters the cell via the same pathways as native Ca^{2+} (e.g. via store operated or voltage-dependent Ca^{2+} channels). Once inside the cytosol, it irreversibly binds to fluorescent markers, in this case fura-2, and quenches its fluorescent activity. Therefore, the fura-2 fluorescence decreases in dependence on time. If then a substance is added, which induces a Ca^{2+} entry above the basal Ca^{2+} influx, the decline in the fura-2 fluorescence accelerates, since more Mn^{2+} enters the cell and quenches fura-2. This change in the slope of the fluorescence can be measured and quantified. In order to avoid interferences of the Mn^{2+} quench with changes in the cytosolic Ca^{2+} concentration (which themself affects the fura-2 fluorescence), these measurements are performed at a single

wave length of 360 nm i.e. the isoemissive wave length, at which the fura-2 fluorescence is independent from the cytosolic Ca^{2+} level.

2.7.7.2 The procedure of manganese quenching experiments

The glass slides were prepared as described in 2.7.6. After measuring the baseline, a Tyrode solution containing Mn^{2+} ($5 \cdot 10^{-4}$ mol·l^{-1}) was perfused into the chamber. After five minutes, bradykinin or bovine serum albumin (BSA, used as carrier for bradykinin), was added using a pipette and the change in the fura-2 fluorescence was measured for 20 minutes.

Those neurons exhibiting a visible change in the slope of the fura-2 fluorescence were considered as responding. The Δ slope was calculated by comparing the slope prior to the administration to the slope after the administration of the substance.

2.8 Polymerase-chain-reaction (PCR)

2.8.1 Solutions and kits

Solution/kit	Components	Purpose	Manufacturer
NucleoSpin RNA XS		RNA extraction from myenteric ganglionic cells	Macherey Nagel (Düren, Germany)
NucleoSpin RNA L		RNA extraction from intestinal muscle cells	Macherey Nagel (Düren, Germany)
Reverse transcription kit 'Masterscript'	dNTP mix (10 mmol·l^{-1}), random hexamers, RT-PCR buffer, Masterscript RT enzyme, Primer RNase inhibitor	Reverse transcription for standard PCR	5 prime (Hamburg, Germany)
RT-kit 'M-MLV Reverse Transcriptase'	5x First Strand Buffer, M-MLV reverse transcriptase, DTT (0.1 mol·l^{-1})	Reverse transcription for real time PCR	Life technologies (Darmstadt, Germany)
dNTP mix		Reverse transcription for real time PCR	Sigma Aldrich (Taufkirchen, Germany)
Random hexamers		Reverse transcription for real time PCR	Applied Biosystems (Foster City, CA, USA)
DEPC-water	0.1 % (v/v) diethylpyrocarbonat (DEPC) in aqua dest., autoclaved	Reverse transcription for real time PCR	Sigma Aldrich (Taufkirchen, Germany)
MasterTaq kit	Taq DNA polymerase, 10x Taq buffer	Standard PCR	5 prime (Hamburg, Germany)
RNase-free water		Reverse transcription for standard PCR; Standard PCR	Sigma Aldrich (Taufkirchen, Germany)
TAE-buffer		Gel electrophoresis	MP Biomedicals, (Santa Ana, CA, USA)

Loading buffer	Gel electrophoresis	Peqlab (Erlangen, Germany)
TaqMan® Gene Expression Master Mix	Real time PCR	Applied Biosystems (Foster City, CA, USA)

Table 2.11: Solutions and kits used in the PCR

2.8.2 The principle of the PCR

The PCR is a widely used technique that enables to quantify a specific sequence of nucleic acids. Preconditioned that the exact DNA sequence of a certain gene is known, the PCR is able to amplify this sequence, and thus prove the existence or non-existence of the gene. The reverse transcription PCR (RT-PCR) uses the same principle, with the difference that it amplifies messenger RNA (mRNA), which has been converted to the so called complementary DNA (cDNA) in advance. It proves not only the existence, but also the expression of a gene. A further development of the RT-PCR is the quantitative real time RT-PCR, also called real time PCR or qPCR, which allows evaluating the strength of expression.

The PCR has three stages (Figure 2.14): 1) denaturation, 2) annealing, 3) elongation. In the first step, the denaturation, the DNA is cleaved into single strands by heating it to 92 – 98 °C. Then the temperature is decreased to the primer-specific annealing temperature in order to bind the primers to the specific sequence of DNA. In the third step the temperature is increased to 72 °C, and the DNA polymerase starts to bind nucleotides to the single strands, producing two newly-formed double-strands. This cycle is repeated 30 - 35 times until a sufficient amount of the target DNA is produced.

Primers are short DNA strands that serve as a starting point for the DNA polymerase. They are complementary to those sequences on the DNA, which flank the target gene and thus are essential for the specific amplification of a gene.

The DNA polymerase is isolated from the germ Thermophilus aquaticus and is able to withstand high temperatures. This makes this enzyme very valuable for the PCR reaction, because the enzyme survives the denaturation step.

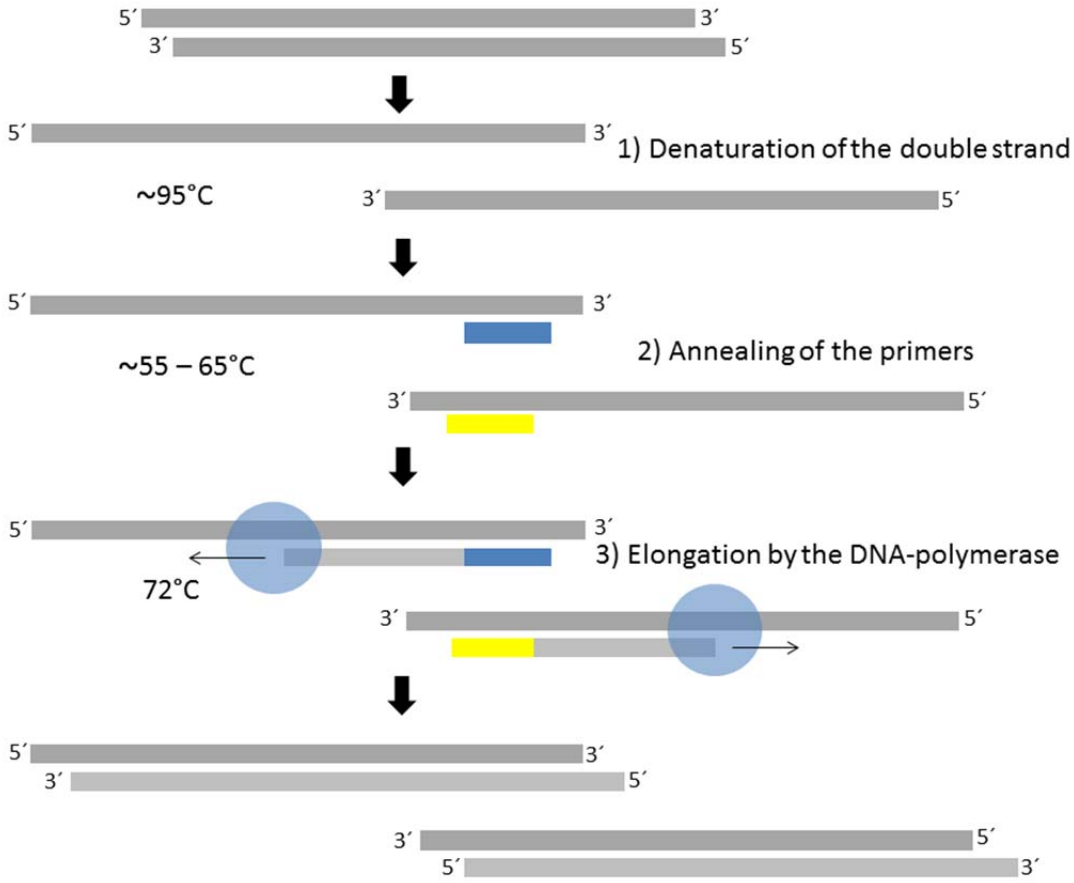

Figure 2.14: A simplified scheme of one PCR cycle

2.8.3 The reverse transcription PCR (RT-PCR)

The RT-PCR consists of two steps: the reverse transcription and the actual PCR. The reverse transcription transforms mRNA to double-stranded complementary DNA (cDNA), and the PCR amplifies this cDNA. Two different protocols of reverse transcription were used: one for the conventional PCR (2.8.3.2) and another for the qPCR (2.8.3.3).

2.8.3.1 RNA extraction

Firstly, the mRNA had to be obtained from the sample. This was performed using a RNA extraction kit. Depending on the cell types, two different kits were applied (Table 2.11). The amount of neurons was very small, so the mRNA had to be extracted with a special kit for cultured cells according to the user manual (NucleoSpin RNA XS, Macherey Nagel, Düren, Germany). The intestinal muscle was difficult to lyse with conventional RNA extraction, so a special protocol in combination with a RNA extraction kit was applied according to the protocol of the supplier (Support protocol for difficult-to-lyse tissue using NucleoSpin RNA II, Macherey Nagel). The amount of obtained RNA was determined using a spectrometer (Eppendorf BioPhotometer plus; Hamburg, Germany) and the RNA was stored at -20 °C until further use.

2.8.3.2 Reverse transcription (RT) for the standard PCR

In the reverse transcription, the obtained RNA was transformed to the double-stranded complementary DNA. This was done by the RNA-dependent DNA-polymerase. In this study the reverse transcription was performed with the RT-kit ‘Masterscript’ (Table 2.11). The incubations were carried out in a thermocycler (Mastercycler gradient; Eppendorf, Hamburg, Germany).

As a first step, the template RNA was incubated for 5 minutes at 65 °C with deoxyribonucleotides (dNTP) and random hexamer primers (mastermix 1, Table 2.12). The random hexamer primers are sequences of six nucleotides, which bind randomly to the RNA and give a starting point for the transcription. In a next step, the RNA-primer mix was mixed with a RT-PCR buffer, the Masterscript RT enzyme and a primer RNase inhibitor (mastermix 2, Table 2.13) and incubated for 60 minutes at 42 °C. As a control, one sample was prepared with water instead of RNA. One further sample was run without addition of the enzyme

reverse transcriptase (RT^- control). This control sample did not show a band in the subsequent PCR amplification and electrophoresis, confirming that no DNA contaminations had occurred.

As a last step the samples were diluted 1:10 with RNase-free water and stored at -80 °C.

Mastermix 1 (standard PCR)	Volume (per sample)	Incubation
RNAse-free water	1 µl	
dNTP mix (10 mmol·l^{-1})	2 µl	5 minutes
Random hexamers	1 µl	65°C
Template RNA	6 µl	

Table 2.12: Composition of mastermix 1 (standard PCR) for the cDNA-synthesis

Mastermix 2 (standard PCR)	Volume (per sample)	Incubation
RNAse-free water	3.5 µl	
RT-PCR buffer	4 µl	60 minutes
(25 mmol·l^{-1} Mg^{2+})		42°C
Masterscript RT enzyme	2 µl	
Primer RNase inhibitor	0.5 µl	

Table 2.13: Composition of mastermix 2 (standard PCR) for the cDNA-synthesis

2.8.3.3 Reverse transcription for the real time qPCR

The reverse transcription for the qPCR was performed with the RT-kit 'M-MLV Reverse Transcriptase' (Table 2.11). One sample was prepared with water instead of template RNA and served as control.

Mastermix 1 (real time)	Volume (per sample)	Incubation
DEPC water	1 µl	
dNTP mix (10 mmol·l^{-1})	1 µl	10 minutes
Random hexamers	1 µl	65 °C
Template RNA	8 µl	

Table 2.14: Composition of mastermix 1 (real time) for the cDNA-synthesis

Mastermix 2 (real time)	Volume (per sample)	Incubation
DEPC water	2 µl	1. 60 minutes
5x First Strand Buffer	4 µl	37 °C
(15 mmol·l^{-1} Mg^{2+})		2. 5 minutes
M-MLV reverse transcriptase	1 µl	90 °C
DTT (0.1 mol·l^{-1})	2 µl	

Table 2.15: Composition of mastermix 2 (real time) for the cDNA-synthesis

2.8.4 The standard PCR

The purpose of this PCR was to investigate the expression of the bradykinin B_1 and B_2 receptor in the intestinal muscle. The cDNA was obtained as described in 2.8.3.1. The PCR was performed in the thermocycler, which was used for the reverse transcription as well (2.8.3.2).

The PCR-mastermix MasterTaq (Table 2.11) consisted of the following components:

	PCR-Mastermix	
Taq DNA polymerase		1.25 U
10x Taq Buffer:	KCl	50 mmol·l^{-1}
	Tris-HCl	30 mmol·l^{-1}
	Mg^{2+}	1.5 mmol·l^{-1}
	Igepal®-CA360	0.1 % (v/v)
	dNTP	200 µmol·l^{-1} of each dNTP

Table 2.16: Composition of the mastermix used in the PCR reaction

For the PCR-reaction the following components were used per sample:

	B_1 receptor
cDNA	1 µl
Primer B_1-receptor (sense)	1 µl
Primer B_1-receptor (antisense)	1 µl
PCR-Mastermix (Table 2.16)	10 µl
RNase-free water	12 µl

Table 2.17: Composition of the PCR reaction for the B_1 receptor
One sample was prepared with water instead of template RNA and served as a control.

	B_2 receptor
cDNA	1 µl
Primer B_2-receptor (sense)	1 µl
Primer B_2-receptor (antisense)	1 µl
PCR-Mastermix (Table 2.16)	10 µl
RNase-free water	12 µl

Table 2.18: Composition of the PCR reaction for the B_2 receptor
One sample was prepared with water instead of template RNA and served as a control.

The amplification was performed using the following programme:

1.cycle			2. - 40. cycle			Final incubation	
denaturation	94 °C	10 min					
denaturation	94 °C	1 min	denaturation	94 °C	1 min		
annealing	60 °C	1 min	annealing	60 °C	1 min		
elongation	72 °C	2 min	elongation	72 °C	2 min		
Final incubation						72 °C	60 min

Table 2.19: Incubation programme for the standard PCR

2.8.4.1 Primers for the standard PCR

All primers were purchased from MWG-Biotech AG (Ebersberg, Germany) and are listed in the following table:

Target	Sequence	bp	Source
B_1 receptor	$^{5'}$-GTGGTCAGCGGGGTCATCAAGG-$^{3'}$ (sense)	22	http://www.ncbi.nlm.nih.gov/nuccore/U66107
	$^{5'}$-GGAAAGCGAAGAAGTGGTAAGG-$^{3'}$ (antisense)	22	
B_2 receptor	$^{5'}$-GCCTTCCGGATGGTTTCA-$^{3'}$ (sense)	18	http://www.ncbi.nlm.nih.gov/nuccore/M59967
	$^{5'}$-TGGTGTTGGAGGTTGTTTGATA-$^{3'}$ (antisense)	22	

Table 2.20: Primers for the standard PCR

2.8.4.2 Gel electrophoresis

The purpose of the gel electrophoresis is the separation of the amplified DNA. For preparing the gel, 3 g agarose was mixed with 100 ml TAE-buffer and heated to 100 °C. Then it was left to cool down, until it reached a temperature of 60 – 70 °C. 5 µl of the staining substance Roti®-safe was added. The gel was filled into the electrophoresis chamber and left there for solidification. Then the samples were mixed with a loading buffer and pipetted onto the gel. The applied voltage was 50 V and the duration 2 hours.

The DNA-bands were visualised with fluorescent light with a stimulation wavelength of 312 nm in a transilluminator (Peqlab). The documentation was performed with the software programme BioCapt 11.03 (Vilber Lourmat, Eberhardszell, Germany).

2.8.5 The quantitative real time PCR (qPCR)

The qPCR is a method, which simultaneously amplifies and detects DNA sequences. In the conventional PCR the product of the amplification is usually visualised by gel electrophoresis. However, it is difficult and inaccurate to use the intensity of the stained bands as a measure for the amount of mRNA in the sample. This limitation is overcome by the qPCR, which takes advantage of the kinetics of the amplification (Figure 2.15). Initially, the amount of amplified DNA doubles after each cycle of the PCR reaction; it rises exponentially. Later the curve goes into a linear phase because of the decline of dNTPs and primers, but also because of the accumulation of pyrophosphate. In the end, the curve reaches a plateau phase, in which only small amounts of DNA are produced. In the qPCR the amount of produced DNA is visualised by the fluorescence resonance energy transfer (FRET): two special chromophores can be excited with light of a specific wavelength. Thereupon, both chromophores emitt light of another specific wavelength. In the FRET, the emitted light of the first chromophore has the same wavelength as the light needed to excite the second. This leads to an energy transfer among both chromophores if they are localised close to each other. As a result, merely light with the wavelength of the second chromophore is emitted. In qPCR special hybridising probes which are equipped with these chromophores start with the energy transfer when integrated into the newly formed DNA. Thus, it is possible to gain information about the amount of produced DNA by measuring both emission wavelength and setting them in relation to each other. Usually this is done by a relative quantification using the reaction kinetics described above.

For this quantification, the cycle number is determined, at which the fluorescent signal for the first time is stronger than the background staining. This cycle number is called C_T-value. Variations induced during RNA extraction or by different amounts of the templates are normalised by comparing the C_T-value to the C_T-value obtained from the simultaneous amplification of a reference gene (in this study: ß-actin). The resulting value is called ΔC_T-value. Finally this value is compared to the so called calibrator, which is in this study the template of those neurons, which have not been cultured at all (reference sample). This value ($\Delta\Delta C_T$) was designated as numeric value 1 in order to calculate the relative quantity (RQ) of cDNA of the other samples, representing x-fold differences compared to the control sample.

ΔC_T (target gene) = C_T (target gene) – C_T (reference gene)

$\Delta\Delta C_T = \Delta C_T$ (target gene) - ΔC_T (target gene in the reference sample)

Relative quantity (RQ) = $2^{-\Delta\Delta C_T}$

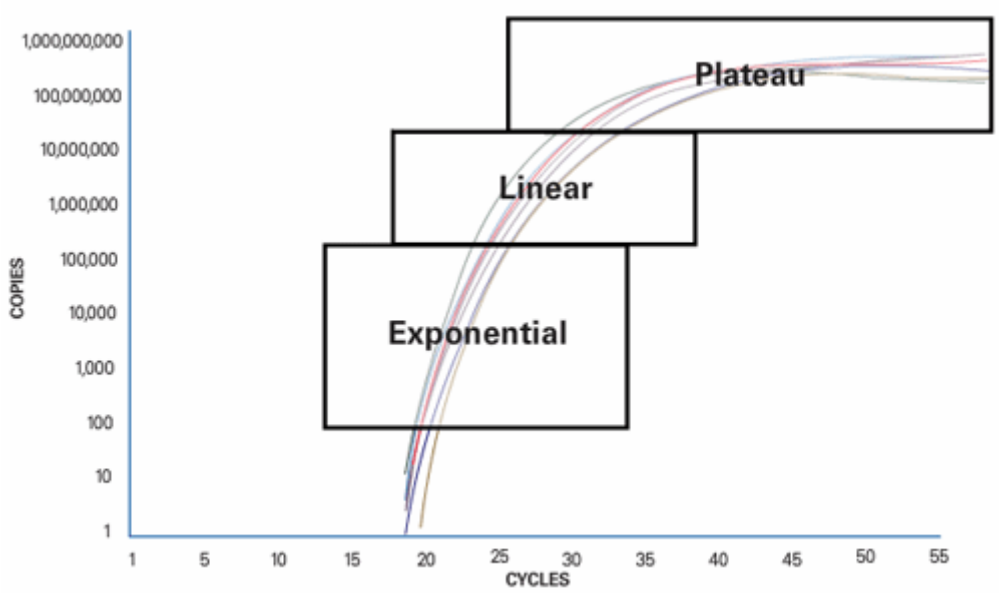

Figure 2.15: Amplification curve of a PCR
From: Applied Biosystems 'Real Time PCR vs. Traditional PCR vs. Digital PCR'.

2.8.5.1 Procedure of the real time PCR

The real time PCR was performed in a StepOnePlus™ Real-Time PCR System (Applied Biosystems, Foster City, CA, USA). The PCR-Mix was pipetted into the reaction plate (MicroAmp® Fast 96-Well Reaction Plate; Applied Biosystems) placed on a plate holder (MicroAMP TM 96-Well Support Base; Applied Biosystems). Then the cDNA was added (Table 2.21, one sample was prepared with water instead of cDNA and served as a control). The plate was covered with an optical adhesive cover (Applied Biosystems) and placed into the real time cycler. The programme used for the amplification is described in Table 2.22. The relative quantity was calculated according to the formulas described in 2.8.5.

PCR-Mix	cDNA
5 µl TaqMan® Gene Expression Mastermix 0.5 µl Primer	+ 4.5 µl

Table 2.21: PCR-Mix used in the real time PCR

1.cycle			2.-44. cycle		
Activation of the polymerase	50 °C	2 min			
Denaturation	95 °C	15 s	Denaturation	95 °C	15 s
Annealing + elongation	60 °C	30 s	Annealing + elongation	60 °C	30 s

Table 2.22: Programme for the real time PCR

2.8.5.2 Primers

The primers used were TaqMan® Gene Expression Assays (Applied Biosystems, Foster City, CA, USA) and are listed in the following table:

assay ID	gene (rattus norvegicus)
Rat ACTB Endogenous Control (VIC/MGB Probe, Primer Limited)	β- Actin
Rn02064589_s1	B_1 receptor

Table 2.23: Primers used in the real time PCR

2.9 The Ussing chamber

2.9.1 Solutions

Solution	Purpose	Composition
Parsons buffer solution	Standard Ussing chamber	In mmol·l^{-1}: 107 NaCl; 4.5 KCl; 25 $NaHCO_3$; 1.8 Na_2HPO_4; 0.2 NaH_2PO_4; 1.25 $CaCl_2$; 1 $MgSO_4$; 12.2 glucose. Set to a pH of 7.4 with NaOH/HCl.
Krebs solution	Square wave current Ussing chamber	In mmol·l^{-1}: 116 NaCl; 1.3 $CaCl_2$; 3.6 KCl; 1.4 KH_2PO_4; 23 $NaHCO_3$; 1.2 $MgSO_4$. Set to a pH of 7.4 with NaOH/HCl.

Table 2.24: Solutions for the Ussing chamber experiments

2.9.2 Structure of the Ussing chamber

The Ussing chamber technique was invented in the fifties by the Danish physiologist Hans H. Ussing (Ussing & Zerahn 1951) and enables to measure electrogenic transport across the epithelium of different organs. The Ussing chamber used nowadays differs slightly from the model built by Ussing and Zehran and is also referred to as the modified Ussing chamber. In this thesis work two different Ussing chamber setups were used: the experiments with the rat tissue were performed in a standard Ussing chamber, whereas the human mucosal biopsies were investigated in an Ussing chamber using the square wave current pulse analysis. The latter experiments were performed under the kind supervision of Henrik Sjövall and Jenny Gustafsson at the Department of Medical Biochemistry and Cell Biology at the University of Gothenburg, Sweden.

The standard Ussing chamber was built from acrylic glass and could be disassembled into two halves (Figure 2.16). Screws made of acrylic glass held both halves together. In order to have a water-proof seal, a thin silicon film was applied at the contact surface. The tissue with a size of 1 cm^2 was fixed with the aid of fine metal pins between both halves of the chamber and thus separated the two compartments. The volume of the compartments was 3.5 ml. The upper side of the chamber was equipped with openings for changing buffer solution or applying substances. During the whole experiments, the buffer solution was gassed with 5 %

(v/v) CO_2/95 % (v/v) O_2 and kept at a temperature of 37 °C. Under these conditions the tissue preserved its epithelial functions up to 6 hours (Diener *et al.* 1989).

The electrodes for measuring the potential difference (PD electrodes) and those for injecting the short-circuit current (I_{sc} electrodes) were both connected via agar bridges to the bathing solution.

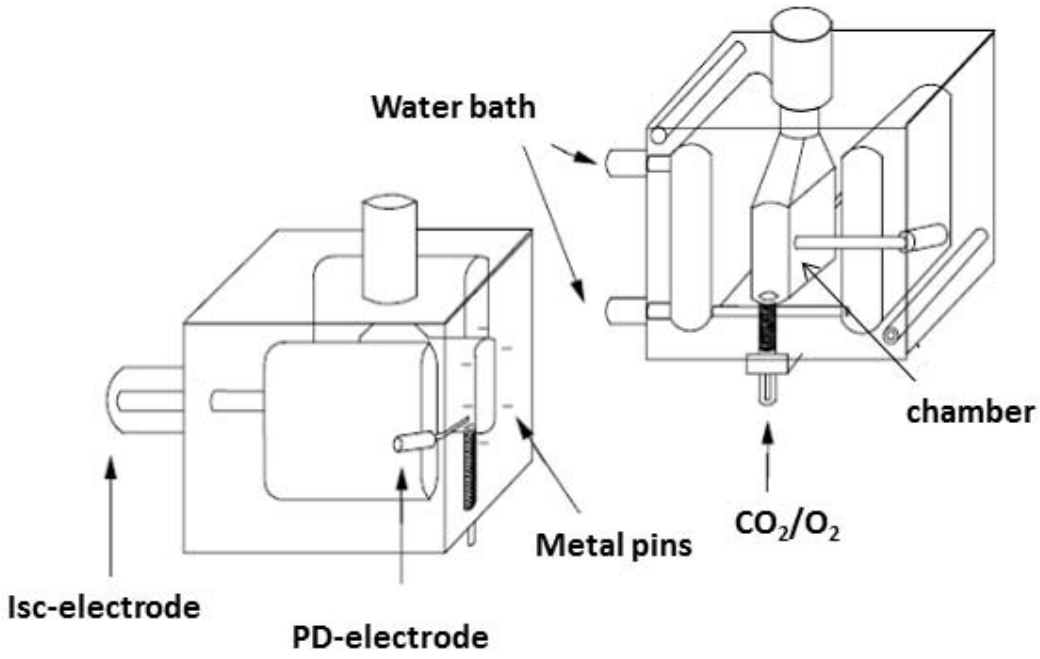

Figure 2.16: Schematic picture of a standard Ussing chamber.
Modified picture by courtesy of M. Diener.

The setup for performing the Ussing pulse analysis slightly differed from the standard Ussing chamber setup. This Ussing chamber (Warner instruments, Hamden, USA) was also built of acrylic glass and could be disassembled, but it was held together with a metal ring. The tissue was mounted on a circular thin plastic disc that completely covered the small hole in the middle of the disc. Another disc of the same type was placed upon the tissue, so that the tissue was held between both discs. The area of the tissue being exposed via the holes was 0.03 cm^2. The discs were placed on one chamber half and fixed with metal pins. Then the chamber was reassembled and placed into a chamber rack. Each compartment of the chamber was filled with 2 ml Krebs solution. On the mucosal side, the Krebs solution contained additionally 5.7 $mmol \cdot l^{-1}$ Na-pyruvate, 5.13 $mmol \cdot l^{-1}$ Na-L-glutamate and 10

mmol·l^{-1} D-mannitol. On the serosal side, the D-mannitol was replaced by 10 mmol·l^{-1} D-glucose. The potential difference was measured with a pair of Ag/AgCl electrodes (Radiometer, Denmark), which were connected to the bathing solution via agar bridges (0.9 % (w/v) NaCl/4 % (w/v) agar; Marine Bioproducts, Canada). The I_{sc} electrodes were placed directly into the bathing solution.

2.9.3 The principle of the Ussing chamber

2.9.3.1 The epithelium as an electrical circuit

The epithelial tissue can be seen as an electrical circuit as shown in Figure 2.17. The epithelium is comparable to a capacitor (C_e), because it consists of a thin insulation layer with conducting material on both sides and thus is able to store energy in an electrical field. When the tissue is clamped to a potential difference of zero, the short-circuit current (I_{sc}) flows through the subepithelial resistance (R_s) and the epithelial resistance (R_e), which are arranged in series and form together the tissue resistance (R_t).

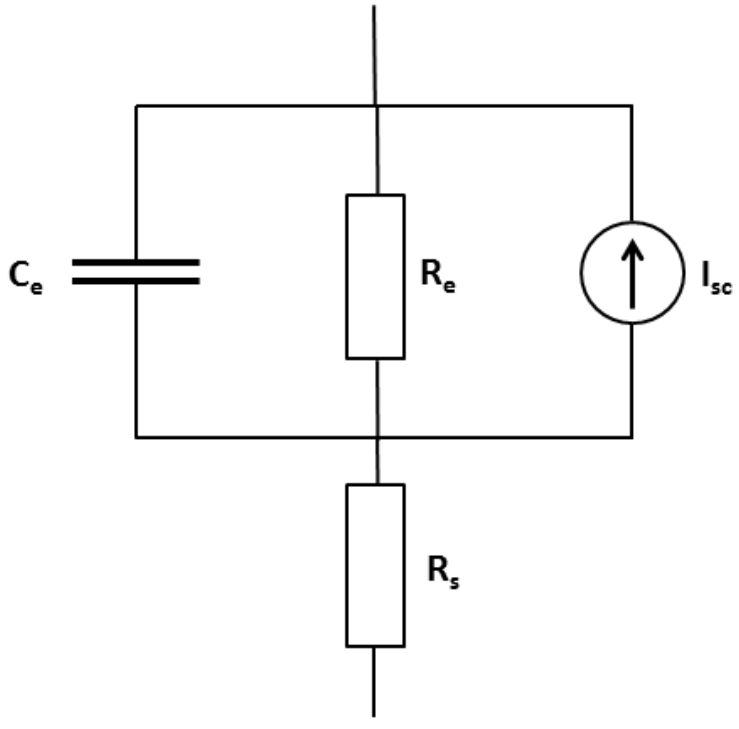

Figure 2.17: Electrical circuit representing the tissue.
Consisting of a parallel resistor (R_e), capacitor (C_e) and current generator (I_{sc}) and a serial subepithelial resistance (R_s).

2.9.3.2 The standard Ussing chamber

The tissue fixed in the Ussing chamber had a mucosal and a serosal side, separated in the chamber. Ion transport across the epithelium created a potential difference, which was clamped to zero by injection of exactly the amount of current that cancelled the potential difference (voltage-clamp mode). This current is called short-circuit current (I_{sc}) and gives information about the electrogenic transport across the epithelium. It is constantly applied and adjusted every 6 seconds. An increase in I_{sc} is created by an active transport along the epithelium, which either can be a net cation transport from the mucosal to the serosal side or a net anion transport from the serosal to the mucosal side. In this study the I_{sc} is given as $\mu Eq \cdot h^{-1} \cdot cm^2$ ($1\ \mu Eq \cdot h^{-1} \cdot cm^{-2} = 26.9\ \mu A \cdot cm^{-2}$), meaning the charge movement per time and free tissue surface.

In addition the tissue resistance (R_t) and conductivity was detected by injecting an additional current pulse with an amplitude of ± 50 µA (above and below the level of the I_{sc}) and a duration of 200 ms once every minute. From the resulting voltage response, the R_t could be calculated using Ohm´s law:

$$R_t = U/I.$$

The tissue conductivity (G_t) was the reciprocal value of the resistance:

$$G_t = I/U.$$

The I_{sc} and the additional current pulse were injected via the I_{sc} electrodes (Ag/AgCl-electrodes), whereas the potential difference was measured by the potential electrodes (Figure 2.16). These were placed as close as possible (1 mm) to the tissue in order to avoid a loss of potential difference due to the resistance of the bathing solution.

2.9.3.3 The Ussing pulse measurements

The standard Ussing chamber is an established method for investigating epithelial properties. However, it has some drawbacks and that is why alternative Ussing measurements were introduced. One of these is the Ussing pulse measurement. The

standard Ussing technique was often criticised for considering the resistance of the subepithelial tissue equal to the resistance of the bathing solution. This idea evolved from the first Ussing experiments performed on the frog skin, which is a very tight tissue. However, other tissues have another structure and so the subepithelial resistance has to be taken into account in order to prevent a systemic error in the calculation of the I_{sc} (Hemlin *et al.* 1988).

Because of these considerations, the Ussing pulse measurement was established. This technique is based on the theory that a square wave current, which acts on a resistance-capacitor element, shows a delayed voltage increase, with a time course dependent on the relation between the resistor (R_e) and the capacitor (C_e) (Figure 2.18). When the current step ends, the C_e is discharged again with the same time course. The initial rapid increase in voltage shown in the first phase of Figure 2.18 is due to the charging of the subepithelial resistance, whereas the second mono-exponential phase of the curve is produced by the epithelial resistance. By plotting the voltage logarithmically against time, we receive a linear function, which can be extrapolated back to the time point, when the current pulse terminated (t=0).

$$V(t) = V_t \cdot e^{-t/(R \cdot C)}$$

$$V(0) = V_0 \cdot e^{-0/(R \cdot C)} \rightarrow V(0) = V_0 \cdot 1 \rightarrow V_0$$

From this value the R_e can be calculated using Ohm´s law:

$$V(0) = I \cdot R_e \rightarrow R_e = V(0)/I$$

The resulting R_e only reflects the epithelial resistance without the subepithelial resistance.

Another important advantage of the Ussing pulse technique is that it gives information about the capacitance of the tissue that can be calculated from the time constant of the discharge of the C_e.

$$V(t) = V_0 \cdot e^{-t}/(R \cdot C) \rightarrow C = (t_2 - t_1)/(R \cdot \ln(V_1/V_2))$$

V_1 and V_2 are the voltages at two selected time points t_1 and t_2 of the mono-exponential phase of the curve.

The capacitance that is proportional to the membrane area can therefore serve as a marker for the epithelial size, thickness and constitution and is often used to investigate exocytosis (Bertrand *et al.* 1998; Bertrand *et al.* 1999). In this study, a change in capacitance was used to monitor mucin exocytosis. Of course, it has to be noted that this increase in capacitance could also be due to the release of other substances. However, Gustafsson et al. (Gustafsson *et al.* 2012) demonstrated recently that the C_e response to carbachol was absent in the colon of mice deficient in the intestinal mucin muc2. Thus, the carbachol induced change in C_e depends on mucus production and mucus release.

The short-circuit current I_{sc} is also calculated according to Ohm´s law

$$I_{sc} = PD / R_e$$

The values for the I_{sc} are higher in this setup compared to the I_{sc} measured with the standard Ussing chamber, which can be explained by the more correct compensation of Re.

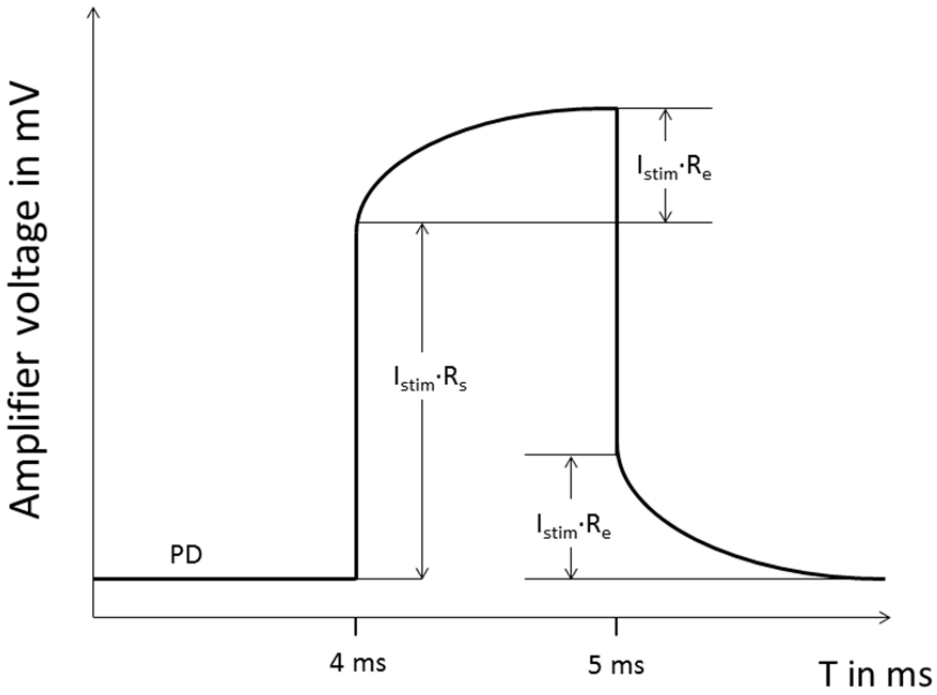

Figure 2.18: The voltage measured by the amplifier after injection of a square wave current pulse.
Modified from: http://goto.glocalnet.net/medimet/The%20Ussing%20Pulse%20Measurement%20Method.PDF

2.9.4 The procedure of the Ussing measurements

2.9.4.1 Procedure of the standard Ussing measurements

The tissue was prepared as described in 2.4.3 and mounted onto the metal pins (2.9.2) using two forceps. The two halves were clamped together and each filled with 3.5 ml Parsons buffer solution (Table 2.24). Before starting the voltage-clamp mode (2.9.3), the tissue was measured in the open-circuit mode for a few minutes. In this mode a direct measurement of the potential difference was performed, without injecting current. Due to a spontaneous secretion of Cl^- and HCO_3^- (Strabel & Diener 1995), the mucosal side usually became negative compared to the serosal side. The next step was the 60 min equilibration phase, which was performed in the voltage-clamp mode. Then the substances were applied with a pipette according to the protocol. Automatic voltage-clamp equipment (Aachen Microclamp; Ing. Büro für Mess- und Datentechnik, Dipl. Ing. K. Mußler, Aachen, Germany) constantly measured the short-circuit current, the conductivity and the potential difference and automatically subtracted the potential difference of the electrodes and the resistance of the bathing solution. At the end of each experiment, the values and graphs were printed. For further processing, the data was transferred to a spread-sheet programme (Lotus 123). The baseline was defined as the average of the values obtained three minutes before the administration of the respective substance. The highest value after the administration was defined as the peak and the difference between baseline and peak was called ΔI_{sc}.

2.9.4.2 Procedure of the Ussing pulse experiments

Before starting the experiment, the chambers were assembled and filled with Krebs solution. The potential difference of the electrodes and the bathing solution was measured and in case of chambers with a PD > 1 mV, the agar bridges were changed.

In order to mount the mucosal biopsies obtained as described in 2.2, the chambers were disassembled and the tissue was carefully placed onto the plastic disc, covering the hole completely. The disc was fixed on the metal pins and the other disc was placed upon it. Then the chambers were reassembled and placed into the rack. The chamber-halves were filled with 2 ml Krebs solution each. On the mucosal side the Krebs solution contained additionally 5.7 $mmol \cdot l^{-1}$ Na-pyruvate, 5.13 $mmol \cdot l^{-1}$ Na-L-glutamate and 10 $mmol \cdot l^{-1}$ D-mannitol. The

agar bridges were installed and the tissue was left to equilibrate for 30 min. During this period, only the PD was measured. After this, the current-electrodes were placed into the bathing solution and the stimulation was started. Baseline values were measured for 30 min, followed by addition of substances using a pipette. The responses were measured for 30 min, and after each experiment, the tissue was placed into 4 % (w/v) paraformaldehyde solution for further histological examination.

Data was analysed with spread-sheet software (Microsoft Excel) and the following properties were measured and calculated:

Property of the tissue	**Calculation**
Potential difference PD (mV)	Measured PD – PD(electrodes + bathing solution)
Specific Resistance R_e ($\Omega \cdot cm^2$)	Measured resistance · surface area
Capacitance C_e ($\mu F \cdot cm^{-2}$)	Measured capacitance/surface area
Short circuit current I_{sc} ($\mu A \cdot cm^{-2}$)	Measured current/surface area

Table 2.25: Measured properties and calculations for the Ussing pulse experiments

2.10 Isometric contraction measurements

2.10.1 Solutions

Solution	Composition
Parsons buffer solution	In mmol·l^{-1}: 107 NaCl; 4.5 KCl; 25 $NaHCO_3$; 1.8 Na_2HPO_4; 0.2 NaH_2PO_4; 1.25 $CaCl_2$; 1 $MgSO_4$; 12.2 glucose. Set to a pH of 7.4 with NaOH/HCl
Advanced Dulbecco´s modified eagle medium/Ham´s F12 (DMEM/F12)	4 % (v/v) fetale calve serum 10.000 units·ml^{-1} penicillin 10 mg·ml^{-1} streptomycin

Table 2.26: Solutions for isometric contraction measurements

2.10.2 The principle of the isometric contraction measurements

The isometric contraction measurements were performed in an organ bath that enables to maintain the integrity of isolated organs for several hours. An isometric contraction is a static contraction, without any change of the muscle length. The force, with which the muscle pulls at the force transducer, is measured. Thus the contraction or relaxation of a muscle can be detected. In this study, the effect of bradykinin and bradykinin receptor agonists on the contractility of different parts of the intestine and on different layers of the colon was investigated.

2.10.3 The structure of the organ bath

The organ bath (yielded by courtesy of Sanofi Aventis, Frankfurt, Germany) consisted of a chamber filled with 10 ml Parsons buffer, which was surrounded by a water bath that was heated to 37 °C (Figure 2.19). Through an opening on the ground of the chamber the buffer solution was gassed with 5 % (v/v) CO_2/95 % (v/v) O_2. The lower part of the intestine was fixed with a thread to the ground of the chamber, whereas the upper part was knotted to the force transducer. A contraction or relaxation was detected by the force transducer and the strain was transformed to voltage, amplified in the amplifier and displayed and analysed with the computer.

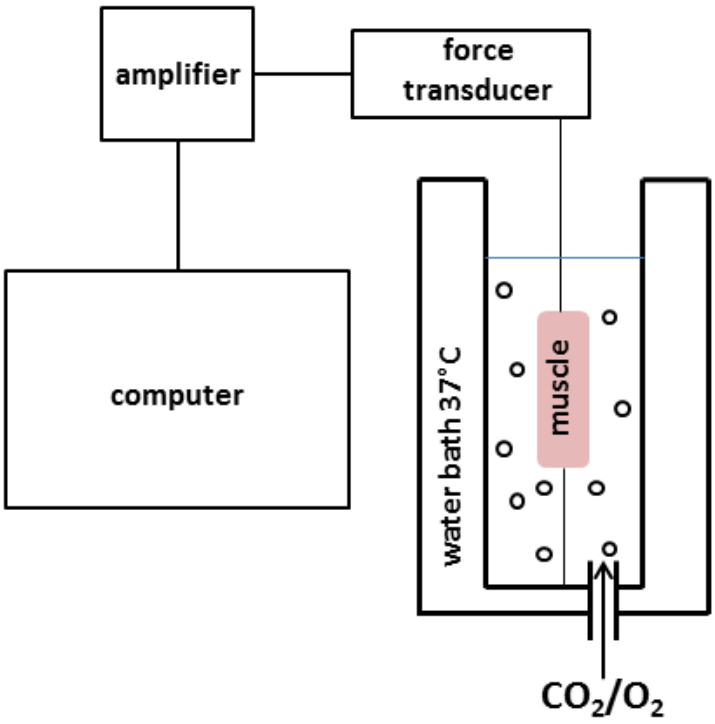

Figure 2.19: Schematic picture of the organ bath

2.10.4 The procedure of the organ bath

After the tissue was prepared as described in 2.4.3, a 2 cm long piece was pulled on a plastic rod with a diameter of 3 mm. Threads were knotted to both ends and the tissue was placed into the chamber, filled with warm and gassed Parsons buffer solution. The lower part was fixed by wrapping a loop of the thread around the hook on the ground of the chamber. The upper part was fixed in the same manner to the force inducer. The pretension was set at 1.5 g. Due to the thinness of the tissue, the layer-experiments were performed with a pretension of only 1 g. The pretension was adapted by lifting or lowering the force transducer electrically.

After an equilibration phase of 10 minutes, the pretension was lowered to the actual tension under which the measurement should be performed, which was 1 g and 0.5 g for the layer-experiments, respectively. The baseline was detected for five more minutes and then the substance was added with a pipette. It was important not to touch the thread with the pipette. After the addition of the substance the resulting contraction or relaxation was measured for ten minutes. As viability control, carbachol ($5 \cdot 10^{-5}$ mol·l^{-1}) was administered after each experiment.

In one set of experiments the tissue was incubated for 5 hours in order to upregulate the B_1 receptor. This was carried out in 5 % (v/v) CO_2/95 % (v/v) O_2-gassed DMEM/F12 (Table 2.2). The medium was changed every 45 – 60 minutes.

Further analysis was performed with spread-sheet software (Microsoft Excel). The baseline was defined as the average force measured one minute prior to the administration of the substance, whereas the response was the maximum or minimum reached within five minutes after administration. Only those experiments with a positive response to the viability control were included into the analysis.

2.11 Statistics

The results are presented as mean values ± standard error of the mean (SEM) or as original curves. In case the results are shown as columns, the height of the columns displays the mean value and the error indicators stand for the SEM.

The n-count represents the measured neurons or muscle cells in the Ca^{2+} imaging experiments, the analysed electrodes in the microelectrode array measurements, the intestinal pieces in the isometric contraction measurements and the number of preparations in the real time PCR and RT-PCR. In the Ussing chamber experiments (standard as well as square wave analysis) n stands for the number of the tissues measured. Independently from the n-count, each experiment was repeated with tissue from at least three animals.

A probability value of $p < 0.05$ was considered as a significant difference. In order to compare two groups, either the Student´s t-test or the Mann-Whitney-U-test was applied; the decision which one to choose was made with the help of an F-test. If more than two groups were to be compared, a one-way ANOVA with a subsequent analysis of linear contrasts with the Tukey´s test was applied. The Chi-squared test was used for calculating whether there was a significant difference in the number of responding cells between different groups. The calculations were performed with WinSTAT (R. Fitch Software, Bad Krozingen, Germany).

3 Results

3.1 Evaluation of the method of microelectrode arrays (MEA)

1.1.1 Adaptation of culturing conditions for rat myenteric ganglia

The preparation of rat myenteric ganglia (2.4.2) was based on the method described by Schäfer et al. (Schäfer *et al.* 1997). A few minor modifications were established, as the electrical activity of the neurons seemed to be increased by these procedures. Especially the digestion step was changed: it turned out that the neurons exhibited more frequently spontaneous activity, when they were incubated in collagenase only one time for 80 minutes. Repeated digestion obviously changed their electrical properties, although their morphology examined with a light microscope was unaltered. Figure 3.1 shows an example of an immunocytochemical staining of the neurons and glia cells grown on a microelectrode array. As described by Murakami et al. (Murakami *et al.* 2009), the culture consisted of roughly two-third glial cells and one-third neurons. During culture, the number of glia cells in relation to the neurons increased, since the glia cells were - in contrast to the neurons - able to undergo mitosis.

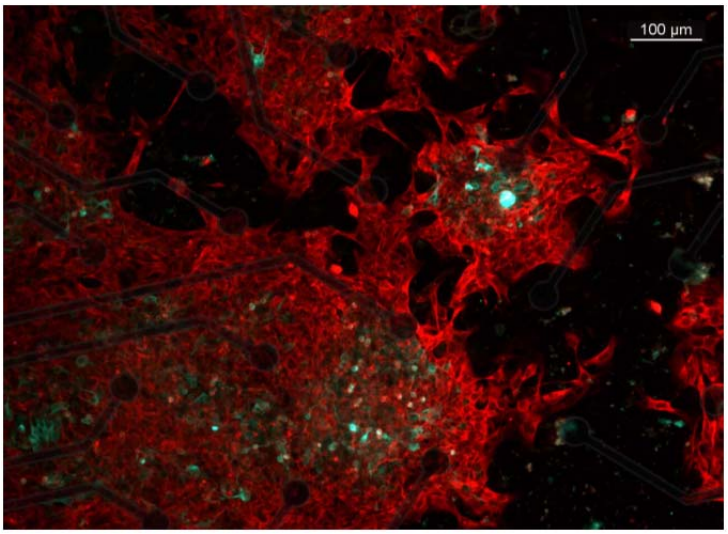

Figure 3.1: Immunocytochemical staining of rat myenteric ganglionic cells cultured on a microelectrode array for 2 days.
Neurons were marked with an antibody against MAP2 (green) and glial cells with an antibody against S-100 (red). A cell nucleus staining was performed with DAPI (blue). For better orientation, the immunocytochemical photo was merged with a light microscopic photograph of the same microelectrode array depicting the positions of the electrodes relatively to the cells.

3.1.1 Determination of the threshold for the detection of action potentials measured with microelectrode arrays

In order to allow a clear differentiation between noise and action potentials, basic measurements of the spontaneous activity of myenteric neurons were performed. After the administration of tetrodotoxin (10^{-6} mol·l^{-1}), a blocker of voltage-dependent Na^+-channels, which suppresses the propagation of action potentials in nerve cells (Catterall 1980), no spontaneous spike activity could be detected. This proved that the spikes measured with the microelectrode arrays were in fact action potentials (Figure 3.2). These measurements also enabled to find a rule for the threshold determination used for the spike detection. As described in 2.5.5, the frequency was calculated by counting the spikes passing a certain threshold, which can be set individually for each microelectrode array. The experiments with tetrodotoxin showed that a threshold of 10 µV underneath or above the lowest/highest value of the noise of the respective microelectrode array (dependent if the electrode showed negative or positive spikes) made it very unlikely to detect noise instead of spikes.

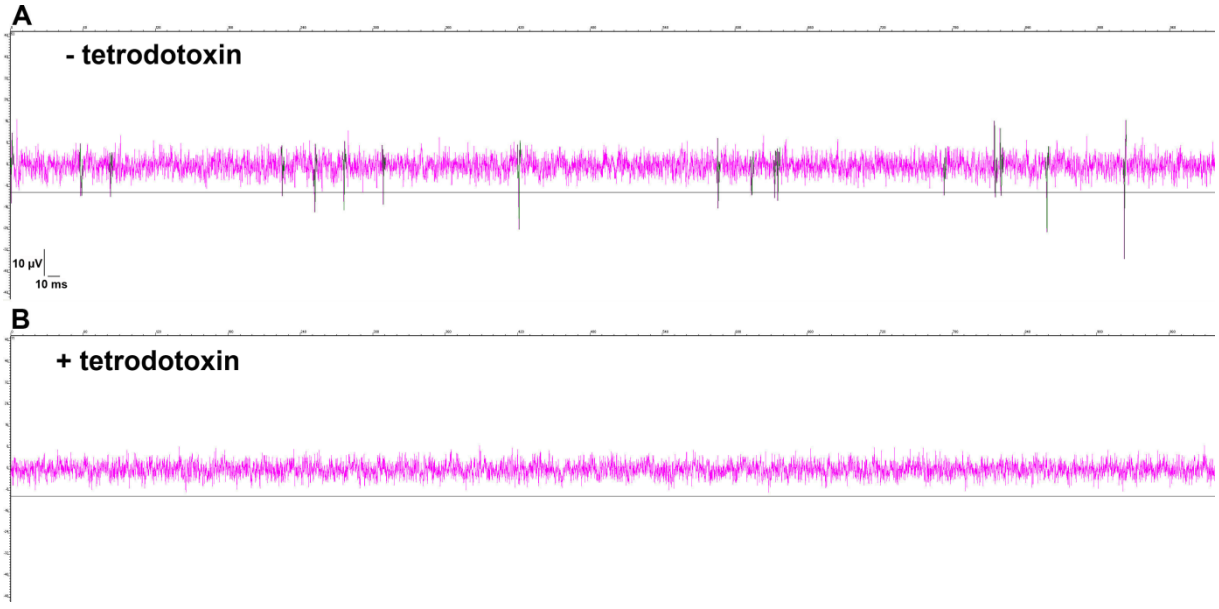

Figure 3.2: Original tracing of a microelectrode array measurement of rat myenteric neurons in the absence (A) or the presence (B) of the neurotoxin tetrodotoxin (10^{-6} mol·l^{-1}).
Action potentials exceeding the threshold (horizontal black line) were detected by the analysis software and are marked in green. In the presence of tetrodotoxin, no spike exceeded the threshold. Typical experiment from n = 20.

3.1.2 The influence of glia cells on the electrical activity of myenteric neurons

During the first measurements of spontaneous activity, it was noticeable that most myenteric neurons showed an activity between day 1 and day 3 after preparation. Only very few microelectrode arrays carried neurons that exhibited electrical activity later than day 3, measured either as spontaneous spike activity or after depolarisation by increasing the extracellular K^+ concentration to 30 $mmol \cdot l^{-1}$ with KCl. Many other studies using microelectrode arrays were performed with neurons from the central nervous system, which show a quite different activity pattern. Gross & Schwalm (Gross & Schwalm 1994) described that spinal cord neurons from foetal mice started to show spontaneous activity after 1 - 2 weeks and stayed active up to 10 months. Potter & DeMarse (Potter & DeMarse 2001) maintained active embryonic dissociated cortical neurons from the rat for more than 9 months. However, judged from a morphological point of view, the myenteric ganglia cultured on the microelectrode arrays in the present study looked viable: the glial cells and neurons started to grow radially in all directions and the neurites built connective fibres between the ganglia. Beginning at day 4, the cells built aggregates, as described by Jessen et al. for enteric neurons in culture (Jessen *et al.* 1983) (Figure 3.3). So the viability of the cells during cell culture is unlikely to play a role in the early cessation of electrical activity.

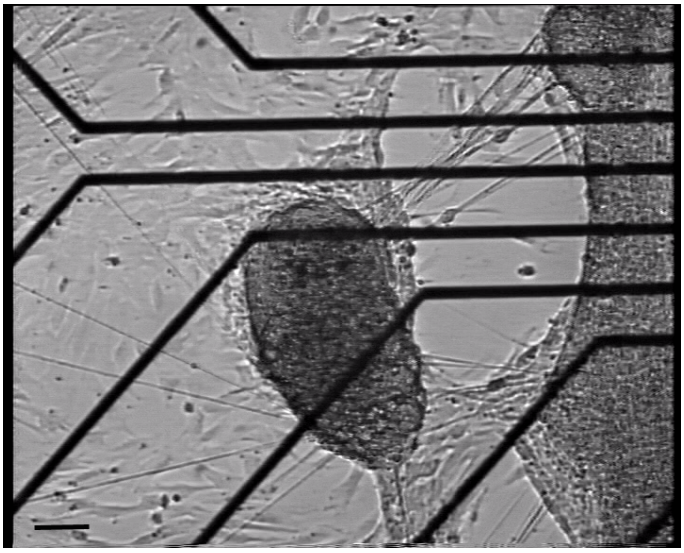

Figure 3.3: Light microscopic picture of myenteric ganglionic cells grown on a microelectrode array for six days.
The black lines are the tracks leading to the electrodes. The picture shows how the ganglionic cells start to build aggregates and interconnecting fibres after a prolonged period of culturing. Horizontal scale bar: 50 µm.

The hypothesis evolved that the glial cells, by growing and proliferating during the culture period, may build an insulation layer, which might prevent the electrodes from detecting the action potentials generated by the neurons. In order to prove this theory, measurements of spontaneous activity of myenteric neurons grown on microelectrode arrays in the presence and absence of cytosine ß-D-arabinofuranoside (10^{-5} mol·l^{-1}), a mitosis inhibitor suppressing the glial growth (Negishi *et al.* 2003; Murakami *et al.* 2007), were performed.

The light microscopic examination proved the success of the mitosis inhibition; the glial growth was suppressed and the remaining glia underwent their natural cell death without having been able to perform mitosis (Figure 3.4). However, Figure 3.5 shows that the mean frequency of action potentials did not differ between those microelectrode arrays cultured with cytosine ß-D-arabinofuranoside and those without. Furthermore, the ß-D-arabinofuranoside-treated cells did not exhibit a longer duration of spontaneous activity compared to the control neurons (data not shown). These results imply that overgrowth by the glia cells is not the reason for the cessation of spontaneous activity in myenteric neurons after day 3.

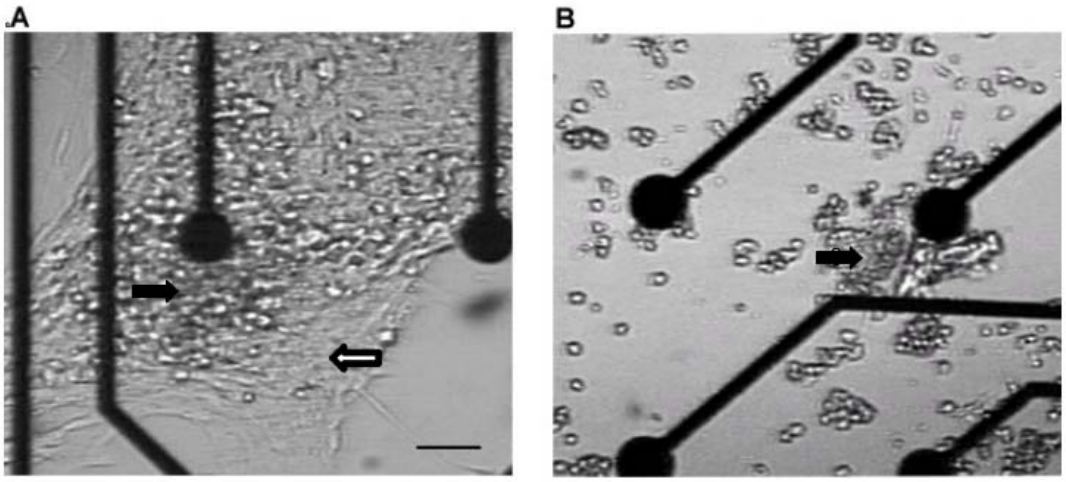

Figure 3.4: Light microscopic picture of myenteric ganglionic cells after three days of cultivation on a microelectrodes array with (B) and without (A) cytosine ß-D-arabinofuranoside (10^{-5} mol·l^{-1}).
The black lines with the round heads are the tracks and electrodes of the microelectrode arrays. Filled arrows: neurons; open arrows: glia cells. Horizontal scale bar: 50 µm. The pictures illustrate the successful suppression of the glial growth. Exemplary pictures from three independent experiments. Horizontal scale bar: 30 µm.

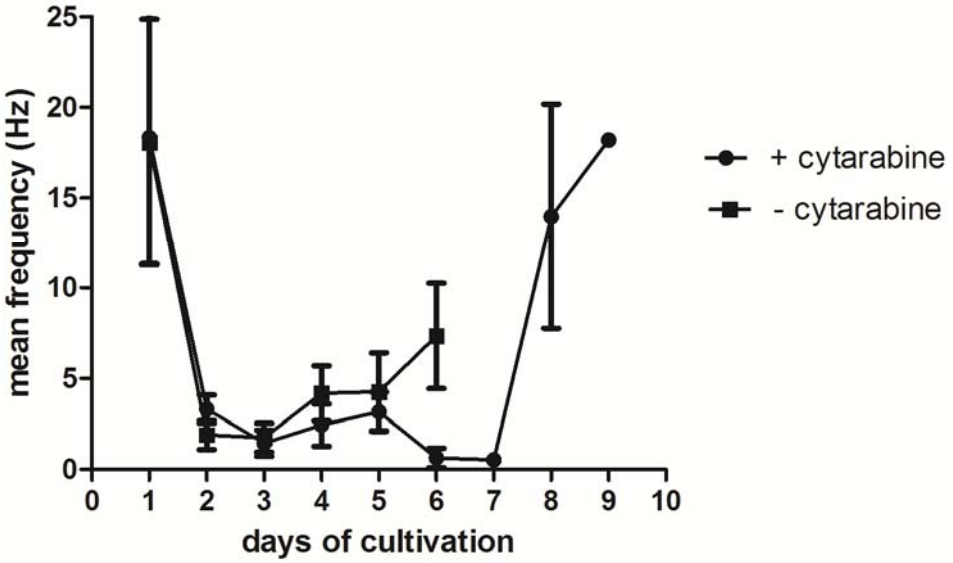

Figure 3.5: The effect of the mitosis inhibitor cytosine ß-D-arabinofuranoside (10^{-5} mol·l^{-1}) on the spontaneous activity of myenteric neurons measured with microelectrode arrays.
Shown is the mean frequency in Hz of the spontaneous action potentials in dependence on the duration of cultivation in days. The dots show those microelectrode arrays cultured in the presence of cytosine ß-D-arabinofuranoside, whereas the squares show those microelectrode arrays cultured without cytosine ß-D-arabinofuranoside. The value for day 9 in the cytosine ß-D-arabinofuranoside group is obtained from only one electrode; consequently there is no error indicator for this value. The other values are means ± SEM; n = 3 – 17.

3.2 The effect of bradykinin on myenteric neurons

3.2.1 The effect of bradykinin on the frequency of action potentials

As a preliminary microelectrode array experiment, four different concentrations of bradykinin ($2 \cdot 10^{-10}$ mol·l^{-1} – $2 \cdot 10^{-7}$ mol·l^{-1}; n = 9 – 18) were tested. Bradykinin induced an increase in action potential frequency at all four concentrations (data not shown). These responses were, however, small at the two lowest concentrations. Therefore, an intermediate concentration of $2 \cdot 10^{-8}$ mol·l^{-1} was selected for the further experiments.

The time course of the change in action potential frequency evoked by bradykinin ($2 \cdot 10^{-8}$ mol·l^{-1}) followed a typical biphasic pattern. After an initial increase ('1st peak') occurring within 30 – 90 s after administration of bradykinin, a second increase could be detected ('2nd peak'), which occurred within 120 – 720 s after administration (Figure 3.6A). The electrical activity decreased between both peaks without reaching the former baseline. As a control experiment, buffer containing only bovine serum albumin (BSA), which was used as carrier for bradykinin to prevent adsorption at the wall of the storage tubes, was applied. Administration of this BSA-containing buffer (Figure 3.6B) only evoked an initial increase in action potential frequency, which suggests that in part the stimulation of mechanosensitive neurons may contribute to the first peak of the bradykinin response, but did not evoke a long-lasting stimulation of the excitability of the myenteric neurons. The averaged baseline activity of the neurons was 0.12 ± 0.06 Hz. The bradykinin-induced first increase reached an average frequency of 1.09 ± 0.50 Hz followed by the second increase of 1.38 ± 0.36 (n = 34; Figure 3.7), which was reached 2 to 12 min after administration of the kinin.

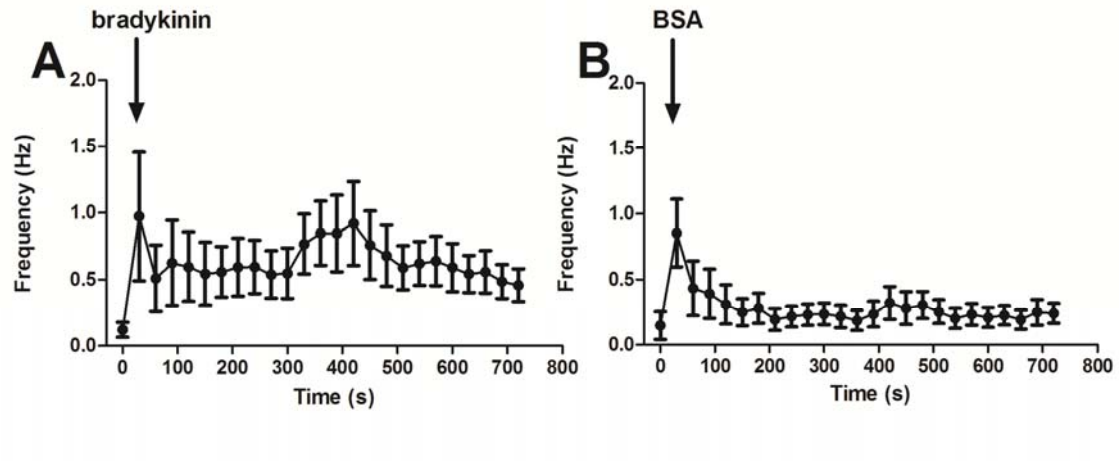

Figure 3.6: The effect of bradykinin ($2 \cdot 10^{-8}$ mol·l^{-1}; A) or of its carrier BSA (0.1 % (w/v); B) on the electrical activity of myenteric neurons cultured on microelectrode arrays.
A: After measuring the baseline, bradykinin (left arrow) was administered at t = 30 s to the buffer solution and the frequency of action potentials was measured for 720 s in intervals of 30 s. The graph shows mean (symbols) ± SEM (bars) of 34 electrodes.
B: shows the control experiment in which BSA (right arrow) was administered instead of bradykinin (n = 22).

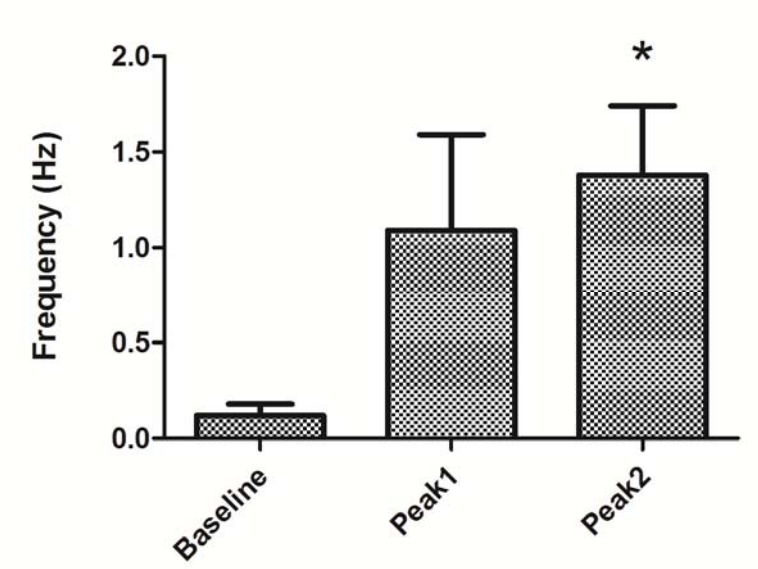

Figure 3.7: The effect of bradykinin ($2 \cdot 10^{-8}$ mol·l^{-1}) on the electrical activity of myenteric neurons cultured on microelectrode arrays.
Shown is the frequency of action potentials in Hz for the baseline, the 1st peak (measured within 30 – 90 s after administration of bradykinin) and the 2nd peak (reached within 120 – 720 s after administration). The columns represent the mean values and the bars show the SEM. n = 34; * P < 0.05 versus baseline.

In an additional series of experiments, a waveform-analysis (see 2.5.7) was performed in order to distinguish the response of individual neurons to bradykinin in microelectrode array measurements. This analysis revealed that two out of 16 analysed neurons responded with only the first peak, two (out of 16) with only the second peak and three (out of 16) exhibited both peaks. Overall, seven (out of 16) neurons responded to bradykinin (Figure 3.8).

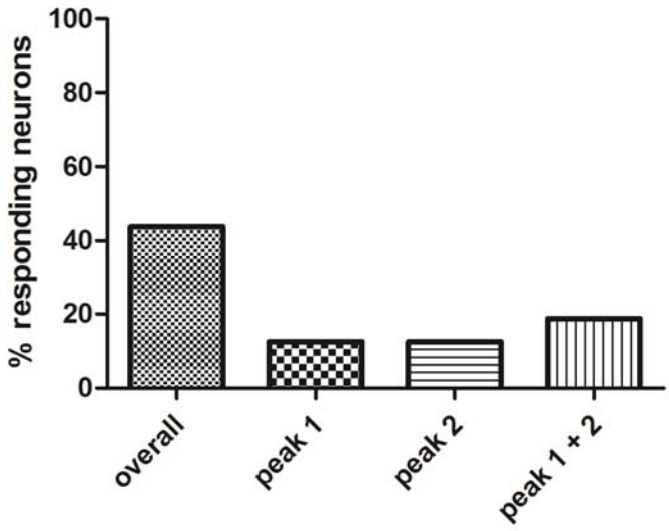

Figure 3.8: Waveform-analysis of the bradykinin-induced change in electrical activity of myenteric neurons measured with microelectrode arrays.
As described in 2.5.7, the spike shape and amplitude was analysed and assigned to different units representing single neurons. Data is presented as percentage of neurons responding to bradykinin ($2 \cdot 10^{-8}$ mol·l^{-1}) compared to the number of spontaneously active neurons. The first column shows the overall response and the second and third column represent the percentage of neurons responding with solely a 1st (30 - 90 s after administration) and 2nd (later than 120 s after administration) peak, respectively. The fourth column shows the percentage of neurons responding biphasically. For statistics, see 3.2.1; n = 7.

3.2.2 The changes in cytosolic Ca^{2+}-concentration induced by bradykinin

There are different signal transduction pathways known for bradykinin, most of them leading to an increase of the cytosolic Ca^{2+} concentration, either by an influx from the extracellular space or by a release from intracellular stores (see 1.2.2). Especially the depolarisation of a cell, in this case induced by bradykinin-evoked action potentials, can cause the opening of voltage-dependent Ca^{2+} channels resulting in an influx of Ca^{2+} into the cytosol (Lacinova 2005).

In order to find out whether the induction of action potentials by bradykinin observed in the microelectrode array experiments is paralleled by changes in the cytosolic Ca^{2+} concentration, myenteric ganglia were loaded with the Ca^{2+}-sensitive dye fura-2. From 20 neurons, which responded to a K^+ depolarization used as viability control, in eight neurons an increase of the cytosolic Ca^{2+} concentration was evoked by bradykinin ($2 \cdot 10^{-8}$ mol·l^{-1}). The bradykinin response consisted – similar as it was observed in the microelectrode array measurements - of two phases; an initial, transient increase (‘1st peak‘) was followed by a secondary rise (‘2nd peak‘) of the fura-2 ratio signal (Figure 3.9). However, this pattern was not observed in all neurons responding to bradykinin; four out of eight neurons showed a biphasic response (as shown in Figure 3.9), whereas one out of eight responding cells only exhibited the first transient peak and three out of eight only exhibited the late response (Figure 3.10B). The rise in the fura-2 ratio during the first peak amounted to an average of 0.19 ± 0.06, whereas the second peak reached an average of 0.14 ± 0.03 (n = 20) (Figure 3.10A).

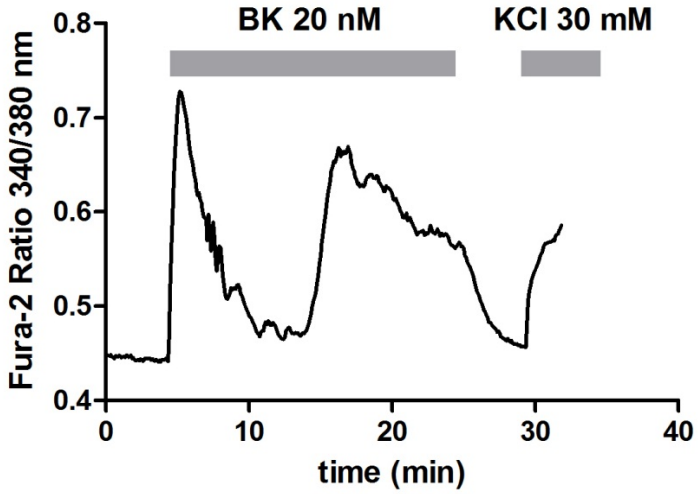

Figure 3.9: The effect of bradykinin (BK; $2 \cdot 10^{-8}$ mol·l^{-1}, left grey bar) on the cytosolic Ca^{2+} concentration of myenteric neurons.
Representative tracing from n = 20. KCl ($3 \cdot 10^{-2}$ mol·l^{-1}, right grey bar) served as viability control. For statistics, see 3.2.2.

3.2.3 The bradykinin receptors involved

Bradykinin binds to two receptors: the constitutively expressed B_2 receptor, which can be found in several tissues throughout the body, and the B_1 receptor, which can be induced in vivo by e.g. tissue damage or inflammation. In order to investigate the involvement of these two receptor types, changes in cytosolic Ca^{2+} concentration in response to a B_1 receptor agonist (des-arg^9-bradykinin) and a B_2 receptor agonist (hyp^3-bradykinin) were measured (for review of the drugs see Leeb-Lundberg 2005).

The effect of bradykinin on the cytosolic Ca^{2+} concentration was mimicked by these selective B_1 and B_2 receptor agonists (Figure 3.10). Both the B_1 agonist des-arg^9-bradykinin (10^{-7} mol·l $^{-1}$) as well as bradykinin B_2 agonist hyp^3-bradykinin (10^{-7} mol·l^{-1}) evoked a change of the fura-2 signal in myenteric neurons. Out of 24 neurons responding to the viability control (see Methods for description of the threshold for acceptance of a response), six neurons responded to des-arg^9-bradykinin. One of these six neurons showed merely a 1st peak; two of six cells responded only with a late (2nd) peak. In three of six neurons des-arg^9-bradykinin induced a biphasic change in the fura-2 signal. Hyp^3-bradykinin induced a change in the fura-2 ratio in 13 of 19 cells responding to the viability control. Two of 13 cells showed only a 1st peak; four of 13 cells only a late (2nd) peak, and seven of 13 neurons responded in a biphasic manner. The change in the fura-2 ratio induced by des-arg^9-bradykinin reached an average 1st peak of 0.11 ± 0.02 and an average 2nd peak of 0.14 ± 0.04 (n = 24; Figure 3.10A). When hyp^3-bradykinin was administered, the neurons responded with an average change in the fura-2 signal amounting to 0.31 ± 0.11 for the 1st peak and 0.21 ± 0.04 for the 2nd peak (n = 19; Figure 3.10A).

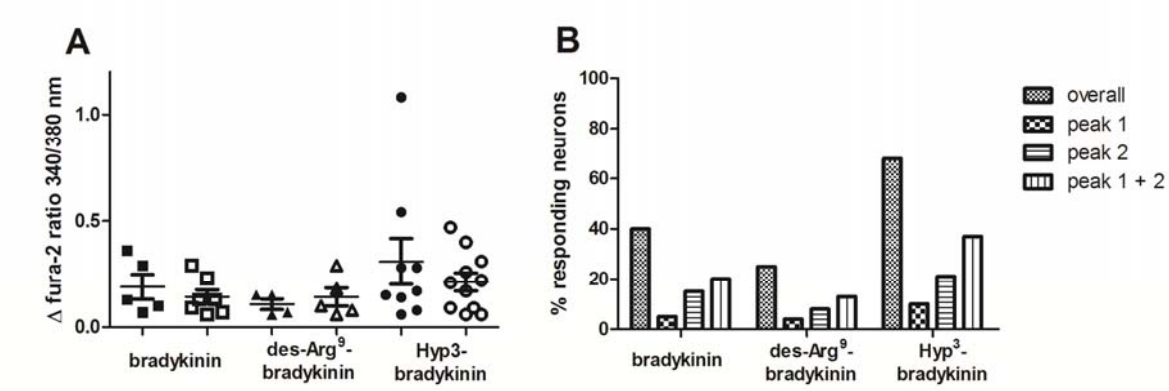

Figure 3.10: The effect of bradykinin ($2 \cdot 10^{-8}$ mol·l^{-1}), the B_1 agonist des-arg^9-bradykinin (10^{-7} mol·l^{-1}) and the B_2 agonist hyp^3-bradykinin (10^{-7} mol·l^{-1}) on the cytosolic Ca^{2+}-concentration in myenteric neurons.

A: The increase of the fura-2 ratio above the former baseline (Δ fura-2 ratio) induced by the respective test substance, presented as single data points for the 1st peak (reached within 10 minutes after administration; filled signs) and the 2nd peak (reached later than 10 minutes after administration; open signs). Large horizontal bars: means; small horizontal bars: SEM; n = 19 - 24.

B: Percentage of viable neurons showing a change in the cytosolic Ca^{2+}-concentration in response to the test substance, subdivided into groups of neurons showing merely an early 1st peak, merely a late (2nd) peak, and those having both peaks, respectively. The columns entitled 'overall' represent the percentage of neurons showing any kind of response (peak 1, peak 2 or both peaks). n = 19 - 24. For statistics see 3.2.3.

These results were confirmed by microelectrode measurements evaluating the effect of bradykinin ($2 \cdot 10^{-8}$ mol·l^{-1}) in the presence of the B_1 receptor blocker des(Arg^{10},Leu^9)-kallidin (10^{-6} mol·l^{-1}) and the B_2 receptor blocker HOE 140 (10^{-6} mol·l^{-1}) (for review of the drugs, see Leeb-Lundberg 2005). In order to suppress the release of neurotransmitters so that each response of a neuron must represent a direct stimulation of the respective neuron (and not a stimulation of neighbouring cells innervating this neuron), these measurements were carried out in a buffer solution devoid of divalent cations. Bradykinin induced a triphasic change in excitability, with a 1st phase showing an increase of frequency, a 2nd inhibitory phase consisting of a fall underneath the former baseline, and a 3rd phase exhibiting a rise in frequency of action potentials (Figure 3.11).

In the presence of both blockers, the 1st and the 2nd phase induced by bradykinin were reduced, but without reaching a level of statistical significance (Table 3.1). However, these findings taken together with the results from the imaging-experiments showing that the agonists of both receptors mimic the effect of bradykinin, strongly suggest that both the B_1 and the B_2 receptors are involved in this effect in cultured myenteric neurons.

Additionally, the blocker experiments demonstrate that the 1st phase, being analogous to the 1st peak in the Ca^{2+} containing buffer solution, is at least partially mediated by bradykinin itself, since it is reduced in the presence of the blocker(s). However, mechanosensitive neurons seem to be involved in the evolvement of the 1st peak as well, since MEA-measurements in the presence of Gd^{3+} (10^{-4} mol·l^{-1}) a blocker of mechanogated ion channels, which mediate the response to mechanical stimulation in mechanosensitive neurons (Hamill & McBride 1996), reduced the first peak induced by bradykinin by half (data not shown).

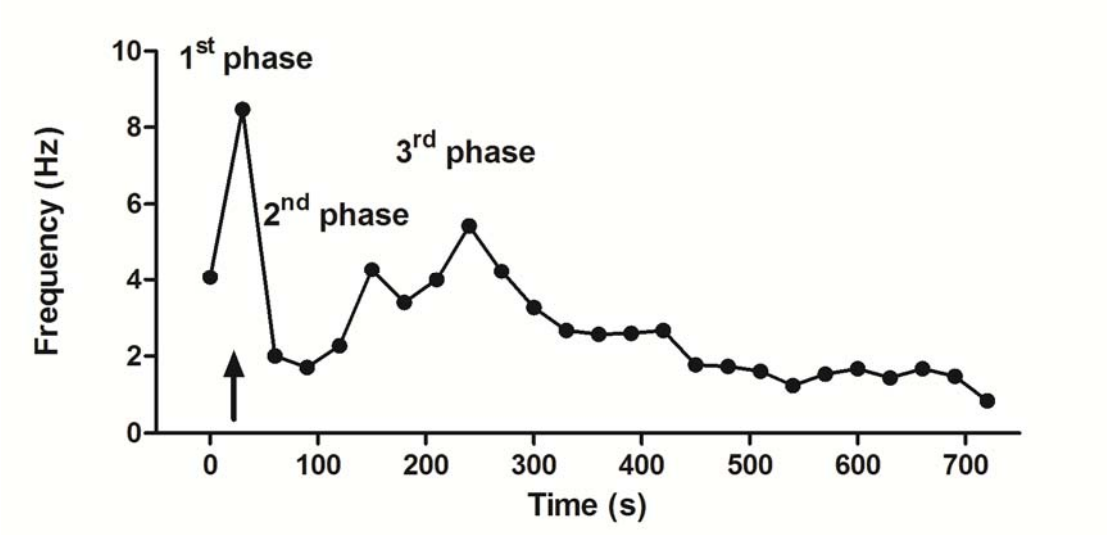

Figure 3.11: The effect of bradykinin ($2 \cdot 10^{-8}$ mol·l^{-1}) on the frequency of action potentials in myenteric neurons measured with microelectrode arrays in the absence of Ca^{2+}.
Shown is a typical tracing from n = 45. The frequency was measured for 720 s in intervals of 30 s and is shown as dots. The first dot represents the baseline prior to the administration of bradykinin (arrow). In the absence of Ca^{2+} in the buffer solution, bradykinin induced a triphasic change of frequency, with a 1st, a 2nd and a 3rd phase.

	Frequency of action potentials (Hz)		
	1st phase	**2nd phase**	**3rd phase**
Bradykinin alone	3.11 ± 0.70	0.94 ± 0.21	2.42 ± 0.57
Bradykinin + B_1/B_2 blocker	1.28 ± 0.26	0.73 ± 0.20	1.47 ± 0.36

Table 3.1: The effect of bradykinin alone and in the combined presence of the B_1 receptor antagonist des(Arg^{10},Leu^{9})-kallidin(10^{-6} mol·l^{-1}) and the B_2 receptor antagonist HOE 140 (10^{-6} mol·l^{-1}) on the electrical activity of myenteric neurons measured with microelectrode arrays in the absence of Ca^{2+}.
The bradykinin response exhibits three phases: The 1st phase occurs within 30 – 90 s after administration of bradykinin, the 2nd phase within 120 – 180 s and the 3rd phase later than 180 s after administration. Values are means ± SEM of the frequency of action potentials in Hz; n = 18 – 26.

In order to confirm the expression of both bradykinin receptor types on myenteric neurons on a morphological level, neuronal cells were labelled with antibodies against the neuronal markers MAP2 and PGP 9.5, respectively, and then double-stained with antibodies against the B_2 or the B_1 receptor. Figure 3.12A demonstrates a localisation of the B_2 receptor on glia as well as neurons, with a more intensive staining on neurons. This finding is consistent with previous observations at rat myenteric ganglia published by Murakami et al. (Murakami *et al.* 2007).

The inducible B_1 receptor is generally considered not to be expressed under basal conditions, but is upregulated e.g. under inflammatory conditions (Calixto *et al.* 2004). In accordance with this general model, no signal for the B_1 receptor was found in freshly dissociated rat myenteric ganglia (‘0 days‘; Figure 3.12B). However, already after one day in vitro incubation under cell culture conditions, a clear immunocytochemical signal for this receptor could be detected (Figure 3.12B), suggesting an upregulation of the B_1 receptor during cell culture.

This upregulation of the B_1 receptor was confirmed by real time PCR (Figure 3.13). The results show that the expression of B_1 receptor mRNA after three, six and ten hours of incubation increases relatively to the expression directly after preparation (‘0 hours‘).

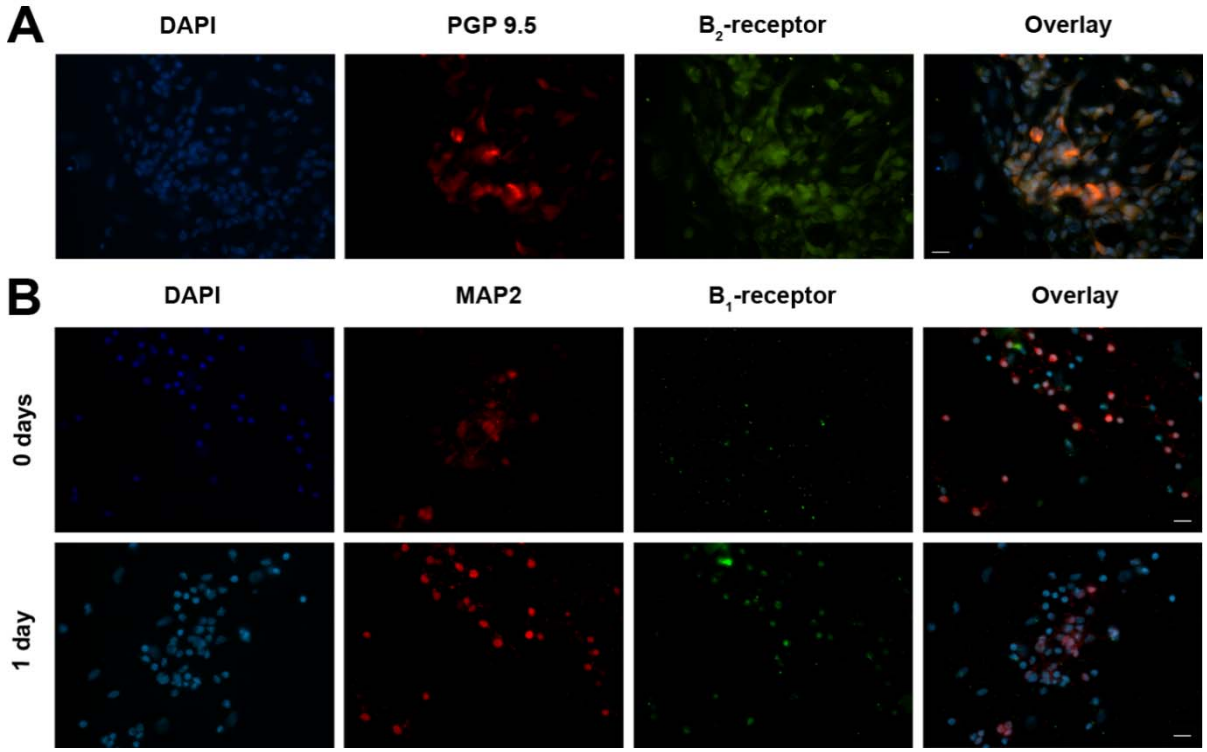

Figure 3.12: Immunocytochemical staining of myenteric ganglionic cells for bradykinin receptors.
A: Double staining with the nuclear marker DAPI (blue), the neuronal marker PGP 9.5 (red) and the B_2 receptor (green). The right picture is an overlay of all three markers. The pictures reveal that the B_2 receptor is located on the neurons as well as on the glia cells, with a slightly stronger signal on the neurons. Typical results from three independent experiments. Horizontal scale bar: 100 µm.
B: Double staining with the neuronal marker anti-MAP2 (red) and the B_1 receptor (green). In the first row, cells are fixed and stained directly after preparation (‘0 days‘) and show no signal for the B_1 receptor, whereas after one day of cultivation (second row, ‘1 day‘) a signal can be detected. This illustrates the upregulation of the B_1 receptor. Furthermore the second rows shows that the B_1 receptor is - similar as the B_2 receptor - located on both neurons and glia cells. Typical results from three independent experiments. Horizontal scale bars: 100 µm.

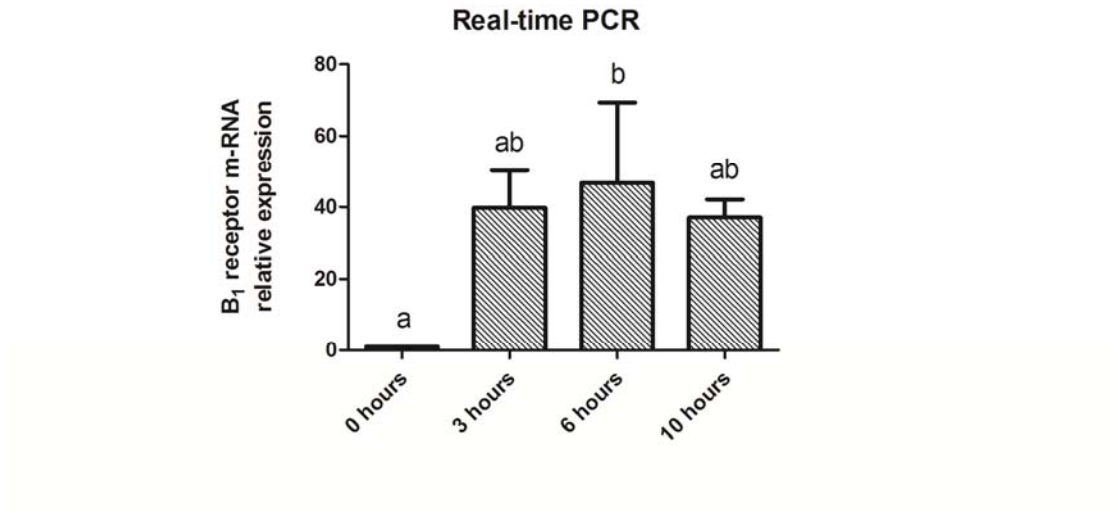

Figure 3.13: Relative expression of B_1 receptor mRNA in myenteric ganglia cells after different time spans of cell culture.
Values are mean (bars) + SEM (lines); n = 3 for all time points except the 10 h time period, in which one value with a very high mRNA expression was qualified as statistical outlier and was therefore excluded. Statistically homogenous groups are marked with the same letter (a, b). $P < 0.05$ (one-way analysis of variances followed by linear contrast analysis via Tukey test).

3.2.4 The involvement of prostaglandins in the mediation of the bradykinin-induced effect on myenteric neurons

The increase in the cytosolic Ca^{2+} concentration induced by bradykinin at enteric neurons has been reported to be – at least partially – mediated by prostaglandins in different parts of the enteric nervous system such as rat myenteric (Gelperin *et al.* 1994; Murakami *et al.* 2007) or guinea pig submucosal neurons (Hu *et al.* 2004b). In order to find out, whether this is also the case for the increase in frequency of action potentials induced by bradykinin, the effect of bradykinin on myenteric neurons grown on microelectrode arrays was tested in the absence and presence of piroxicam, a cyclooxygenase inhibitor (Carty *et al.* 1980).
Piroxicam (10^{-5} mol·l^{-1}) apparently reduced both bradykinin-induced peaks in action potential frequency (Figure 3.14). This effect did, however, not reach statistical significance due to the high variability. Nevertheless, in light of the data published in the literature (see above), it seems likely that prostaglandins play, at least partially, a role in the mediation of bradykinin-induced change of electrical activity in rat myenteric neurons also under the experimental conditions I used.

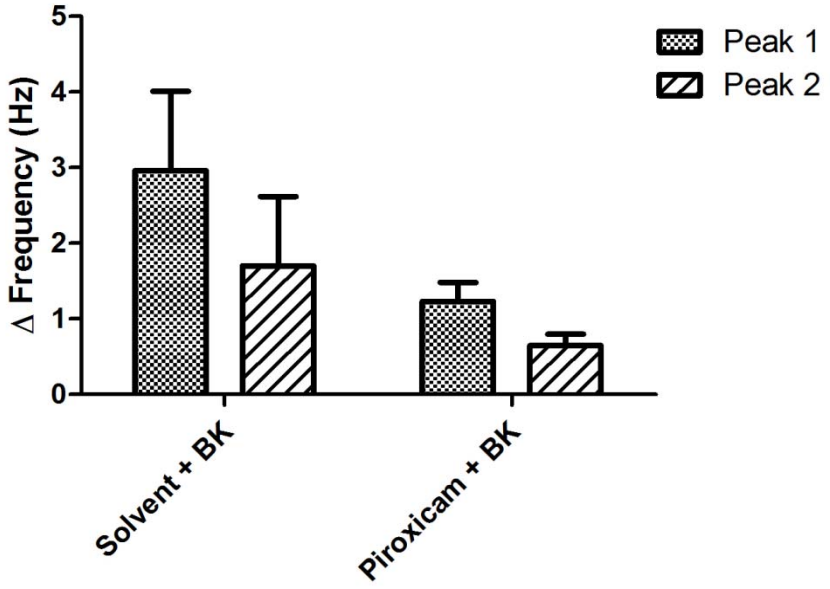

Figure 3.14: Effect of bradykinin (BK; $2 \cdot 10^{-8}$ mol·l^{-1}) in the presence (right two bars) of piroxicam (10^{-5} mol·l^{-1}) and in the presence of solely the solvent of piroxicam (ethanol; 0.01 % (v/v); left two bars).
Shown is the increase in action potential frequency above the former baseline (Δ frequency) induced by bradykinin 30 – 90 s (peak 1) or later than 120 s (peak 2) after administration of the kinin. Values are means (bars) + SEM (lines); n = 19 - 24.

Several studies showed that bradykinin induces a release of prostaglandins by glia cells (Ishimoto *et al.* 1996; Hsieh *et al.* 2007), which ascribes to these cells an important part in the mediation of the bradykinin-induced effect on neurons. To investigate how glia cells modify the electrical activity of myenteric neurons, microelectrode array measurements were performed with cells being cultured with the mitosis-inhibitor cytosine ß-D-arabinofuranoside.

As described above, already after one day in culture, the ganglionic cells incubated with cytosine ß-D-arabinofuranoside (10^{-5} mol·l^{-1}) showed a strong decrease in the amount of glia cells. After three days of culturing, only sporadic glia cells could be detected (Figure 3.4B), whereas under control conditions glia cells spread and covered large parts of the area (Figure 3.4A).

After the administration of bradykinin, the change in electrical activity was measured. As shown in

Figure 3.15, the suppression of glial growth with cytosine ß-D-arabinofuranoside did not diminish the stimulation of action potentials by bradykinin. Quite to the contrary, the first peak was even increased significantly in the cytosine ß-D-arabinofuranoside-treated ganglionic cells. This might be due to the abolition of the insulating effect on the electrical connection between the neurons and the electrodes caused by the glia. Therefore, glia cells seem not to play a major part in the modification of the bradykinin-induced change in electrical activity measured with microelectrode arrays.

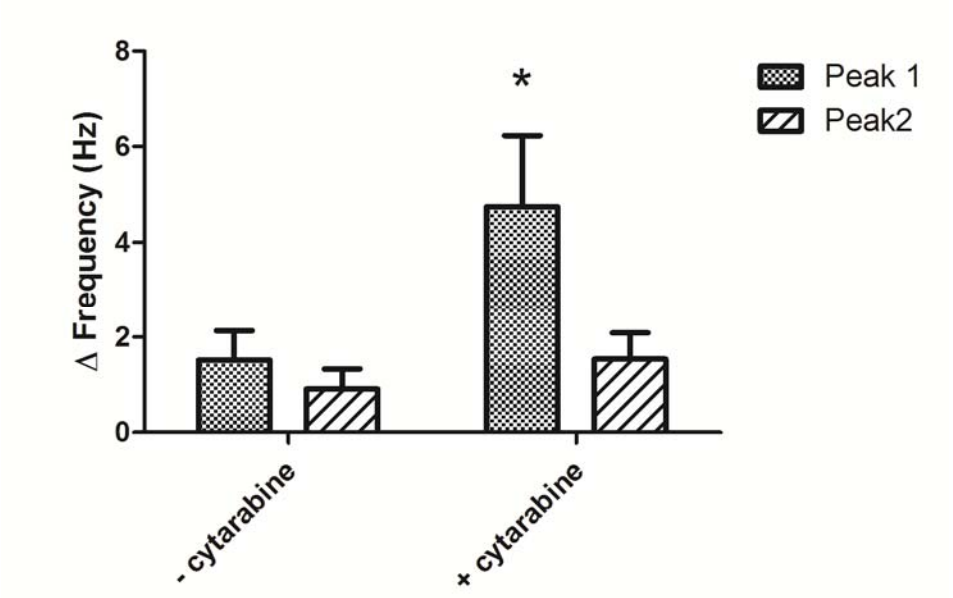

Figure 3.15: The effect of bradykinin ($2 \cdot 10^{-8}$ mol·l^{-1}) on the electrical activity of myenteric neurons cultured in the presence (right columns) and absence (left columns) cytosine ß-D-arabinofuranoside (10^{-5} mol·l^{-1}).

Given is the increase in action potential frequency above the former baseline (Δ frequency) induced by bradykinin 30 – 90 s (peak 1) or later than 120 s (peak 2) after administration of the kinin. Values are means (bars) + SEM (lines); n = 20 - 21. * $P < 0.05$ versus corresponding peak in the group cultured without cytosine ß-D-arabinofuranoside.

3.2.5 The signal transduction of the bradykinin receptors

Bradykinin receptors are G_q-protein coupled receptors which upon stimulation induce a change in the cytosolic Ca^{2+} concentration via the IP_3 pathway in most tissues (Prado *et al.* 2002; Leeb-Lundberg 2005). In order to test whether this holds also true for rat myenteric neurons, the effect of bradykinin ($2 \cdot 10^{-8}$ mol·l^{-1}) on the excitability of myenteric neurons grown on microelectrode arrays was measured in the presence and absence of YM-254890 (10^{-7} mol·l^{-1}), which is a potent inhibitor of G_q-proteins (Takasaki *et al.* 2004). As shown in Figure 3.16, YM-254890 reduced the bradykinin-induced 2nd peak significantly. It is unclear, why the 1st peak was not reduced, but since in the following experiments the 1st peak was inhibited by blockers of the G_q-protein related signal cascade, it is likely that the mechanical stimulation during the administration plays a role in the accruement of this 1st peak.

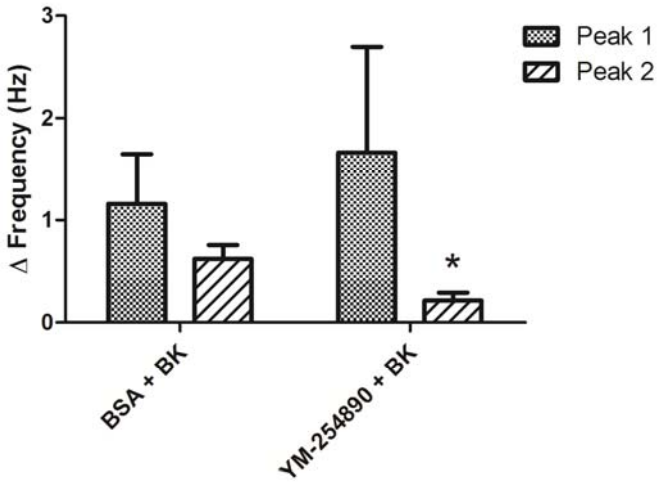

Figure 3.16: The effect of bradykinin ($2 \cdot 10^{-8}$ mol·l^{-1}) on the electrical activity of myenteric neurons in the presence of YM-254890 (10^{-7} mol·l^{-1}; right two bars) or in the presence of buffer containing bovine serum albumin (BSA; 0.1 % (w/v); left two bars), which was used as carrier for of YM-254890 to prevent adsorption of this peptide to the wall of the storage vessels.
Given is the increase in action potential frequency measured with microelectrode arrays above the former baseline (Δ frequency) induced by bradykinin 30 – 90 s (peak 1) or later than 120 s (peak 2) after administration of the kinin. Values are means (bars) + SEM (lines); n = 20-21. * $P < 0.05$ versus corresponding peak in the BSA group.

G_q protein-coupled receptors often induce a change in the cytosolic Ca^{2+} concentration via the IP_3 pathway. In order to find out if this is also the case for bradykinin stimulating myenteric neurons, we examined the effect of bradykinin on the cytosolic Ca^{2+} concentration in the presence and absence of 2-APB, a drug known to inhibit IP_3-receptors (Maruyama *et al.* 1997). However, 2-APB (10^{-4} mol·l^{-1}) had no effect on the bradykinin-evoked changes in the cytosolic Ca^{2+} concentration (Figure 3.17A). Neither the early rise (1st peak) nor the late rise (2nd peak) of the fura-2 ratio signal induced by the kinin ($2\cdot10^{-8}$ mol·l^{-1}) was altered in the presence of this drug indicating that a release of stored Ca^{2+} from cellular organelles via IP_3 receptors does not mediate this response.

In contrast, the effect of bradykinin was dependent on an influx of Ca^{2+} from the extracellular space. When the myenteric ganglia were superfused with a Ca^{2+}-free buffer solution, the effect of bradykinin ($2\cdot10^{-8}$ mol·l^{-1}) was almost abolished (Figure 3.17B). Out of 34 tested neurons, which showed a reaction in the viability control, only four neurons responded to bradykinin in the absence of Ca^{2+} (in the presence of Ca^{2+}, 17 out of 24 viable neurons showed a response). The amplitude of the fura-2 signal induced by bradykinin in this remaining group (i.e. the four neurons still responding to bradykinin under nominal Ca^{2+}-free conditions) was nearly unchanged. This inhibition in the majority of cells strongly suggests that the influx of Ca^{2+} from the extracellular space plays a prominent role in the majority of myenteric neurons for the bradykinin-induced change in cytosolic Ca^{2+} concentration.

In neurons the predominant pathway for influx of extracellular Ca^{2+} is provided by voltage-dependent Ca^{2+} channels, which are activated during depolarisation (Lacinova 2005). These channels are blocked by different divalent cations such as Ni^{2+} (Zamponi *et al.* 1996). In order to investigate the contribution of voltage-dependent Ca^{2+} channels in the bradykinin-evoked increase in the cytosolic Ca^{2+} concentration, the effect of bradykinin ($2\cdot10^{-8}$ mol·l^{-1}) was tested in the presence and absence of Ni^{2+} ($5\cdot10^{-3}$ mol·l^{-1}). In the presence of Ni^{2+}, the number of neurons responding to bradykinin with a rise in their cytosolic Ca^{2+} concentration was reduced from 37 % (19 out of 51 viable cells) under control conditions to 20 % (9 out of 45 viable cells) in the presence of this inhibitor (Figure 3.17C). This inhibition, however, did not reach statistical significance.

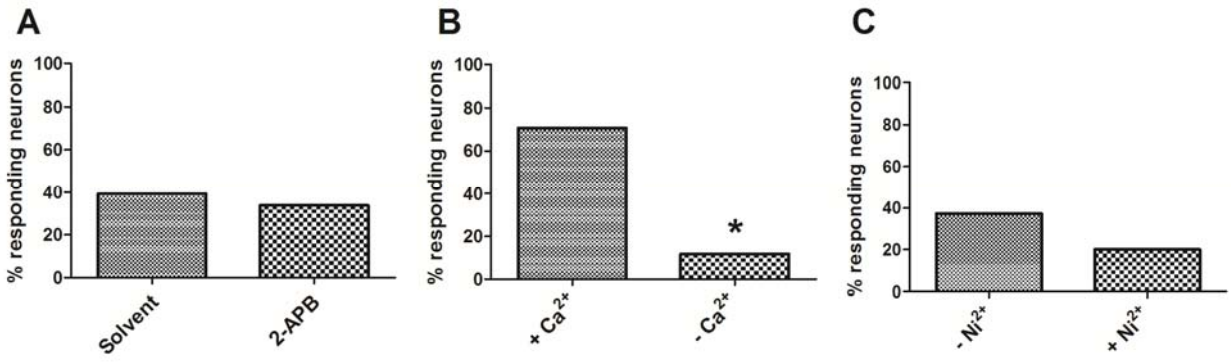

Figure 3.17: The effect of bradykinin ($2 \cdot 10^{-8}$ mol·l^{-1}) on the cytosolic Ca^{2+}-concentration of myenteric neurons measured under different conditions.
Shown is the percentage of neurons responding to bradykinin with a change in cytosolic Ca^{2+} concentration in relation to the number of viable neurons.
A: Effect of bradykinin in the presence and absence of the IP_3 receptor blocker 2-APB (10^{-4} mol·l^{-1}) and the solvent 2-ABP (DMSO), respectively; n = 74 - 80.
B: Effect of bradykinin in the presence and absence of Ca^{2+} in the buffer solution; n = 24 – 34. For statistics see text. * $P < 0.05$ versus the group measured in the presence of Ca^{2+}.
C: Effect of bradykinin in the presence and absence of the Ca^{2+} channel blocker Ni^{2+} ($5 \cdot 10^{-3}$ mol·l^{-1}); n = 45 – 51. For statistics see text.

In order to confirm the origin of the Ca^{2+} as well as shedding light on the mechanisms underlying the biphasic response induced by bradykinin, experiments with manganese quenching (see 2.7.7) were performed. In general, the neurons showed a moderate decrease of the isoemissive fura-2 signal after administration of Mn^{2+}, indicating that they have a rather low open probability of Ca^{2+} channels in the plasma membrane. After administration of bradykinin, in 15.5 % (16 out of 103 measured cells) the fall in the fura-2 signal was accelerated. This response lasted between 1 and 19 seconds (in average 7 seconds). One out of 103 cells showed a biphasic response. All other responses occurred lather than 10 minutes after administration of bradykinin and can therefore be referred to as '2nd peak'. In the presence of the carrier for bradykinin, bovine serum albumin (BSA; 0.1 % (v/v)), only 3 out of 94 neurons (3.2 %) responded with a fall in the slope of the fura-2 fluorescence. The Δ slope of the response did not differ between bradykinin and BSA (data not shown).

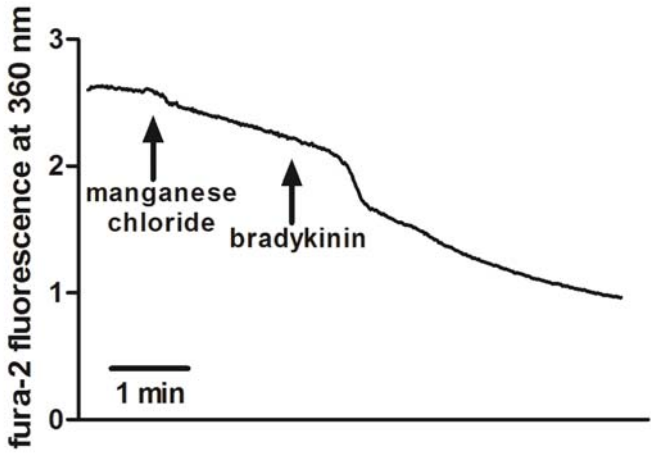

Figure 3.18: Typical tracing of the effect of bradykinin ($2 \cdot 10^{-7}$ mol·l^{-1}) on the fura-2 signal in a manganese quenching experiment.
The left arrow shows the application of manganese chloride ($5 \cdot 10^{-4}$ mol·l^{-1}), which leads to a decrease in the fura-2 signal. The right arrow marks the administration of bradykinin ($2 \cdot 10^{-8}$ mol·l^{-1}). Typical experiment from n = 103; for statistics see text.

3.3 The neuronal regulation in the bradykinin-induced increase in short-circuit current in the rat distal colon

It has been shown in different studies that bradykinin induces a chloride secretion in the rat, rabbit and human colon and in guinea pig ileum (Cuthbert & Margolius 1982; Musch *et al.* 1983; Diener *et al.* 1988; Baird *et al.* 2008). In several studies an involvement of enteric neurons was described, as the kinin-induced secretion was partially inhibited by the neurotoxin tetrodotoxin (Diener *et al.* 1988; Green *et al.* 2003; Baird *et al.* 2008). However, these studies were performed either at mucosa-submucosa- or mucosa-preparations focusing on the role of secretomotor neurons within the submucosal plexus. Since the myenteric plexus might influence epithelial secretory and absorptive processes as well, e.g. via interconnections to the submucosal plexus (Auerbach 1864), but also due to direct projections of myenteric neurons to the mucosa (Cajal 1911; Müller 1920), we aimed to find out whether the myenteric plexus is involved in the chloride secretion induced by bradykinin. For this purpose, Ussing chamber experiments were performed using different preparations, in which individual layers of the colonic wall had been dissected. As a readout for chloride secretion, short-circuit current (I_{sc}) was measured, which increases during induction of electrogenic anion secretion (or electrogenic cation absorption) across the epithelium.

The concentration-dependent change in short-circuit current in response to bradykinin, the B_2 receptor agonist hyp^3-bradykinin, and the B_1 receptor agonist des-arg^9-bradykinin was measured in different preparations containing different parts of the enteric nervous system: the full-thickness preparation (containing the myenteric, the submucosal and the mucosal plexus), the mucosa-submucosa preparation (the muscle layer with the myenteric plexus was removed), and the mucosa preparation (the muscle layer with the myenteric plexus and the submucosa with the submucosal plexus were removed). For illustration of the preparation see 2.4.3. Between each administration of the kinin, the buffer solution was changed three times in order to prevent desensitisation against bradykinin (Diener *et al.* 1988).

The results are shown in Figure 3.19. Bradykinin (10^{-9} – 10^{-7} mol·l^{-1} at the serosal side) and hyp^3-bradykinin (10^{-9} – 10^{-7} mol·l^{-1} at the serosal side) induced a concentration-dependent increase in I_{sc} in all three preparations (Figure 3.19A+B). However, for both peptides this

increase in I_{sc} was strongly reduced in the full-thickness preparations. Des-arg^9-bradykinin (10^{-9} – 10^{-7} mol·l^{-1} at the serosal side) had only minimal effects on the I_{sc} in both full-thickness and mucosa-submucosa preparations (Figure 3.19C) suggesting that bradykinin B_1 receptors do not play a role in the regulation of transepithelial chloride secretion.

In order to find out whether the impaired effect of bradykinin on the I_{sc} in full-thickness preparations is due to a stimulation of inhibitory neurons in the myenteric plexus by bradykinin, measurements in the presence of the neurotoxin tetrodotoxin (10^{-6} mol·l^{-1} at the serosal side) were performed. In the full-thickness preparation neither bradykinin, nor hyp^3-bradykinin nor des-arg^9-bradykinin had an effect on the I_{sc}, when tetrodotoxin was present (Figure 3.20A). However, in the mucosa-submucosa preparation hyp^3-bradykinin induced an increase in I_{sc} (Figure 3.20B).

This shows that the reduced response in full-thickness preparations is not due to an activation of inhibitory neurons by bradykinin. It is most likely that the intestinal muscle forms a diffusion barrier, which hinders the bradykinin to reach the epithelium.

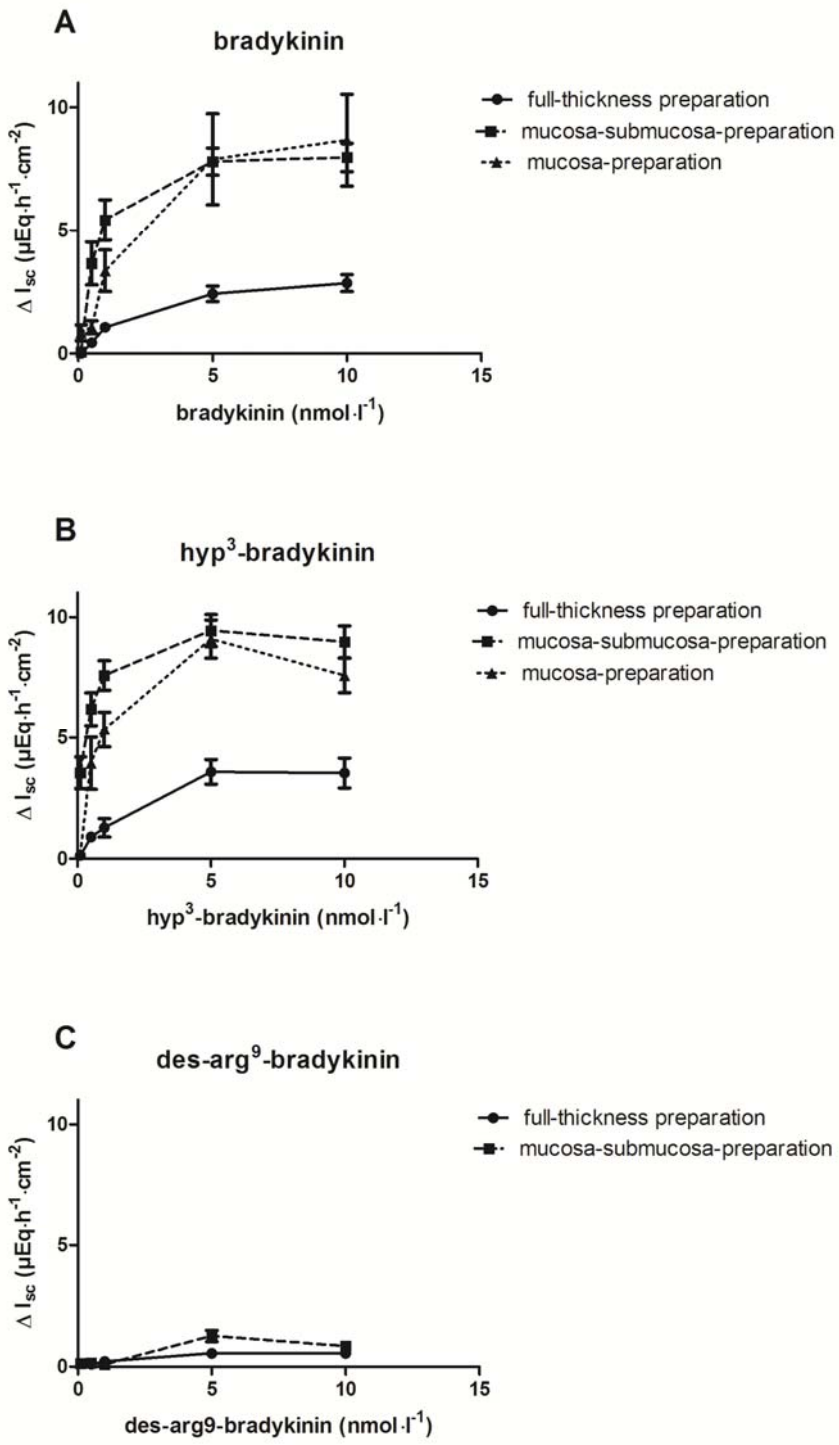

Figure 3.19: Concentration-response curves (10^{-9} – 10^{-7} mol·l^{-1} at the serosal side) for bradykinin (A), the B_2 agonist hyp^3-bradykinin (B), and the B_1 agonist des-arg^9-bradykinin (C) in Ussing chamber experiments.

Shown is the increase in short-circuit current (Δ I_{sc}) above the former baseline measured just before the administration of the respective test substance. The solid line shows experiments with full-thickness preparation, the dashed line represents mucosa-submucosa preparations, and the dotted line stands for the experiments with mucosa preparations. Shown are means (symbols) ± SEM (bars); n = 7 - 9.

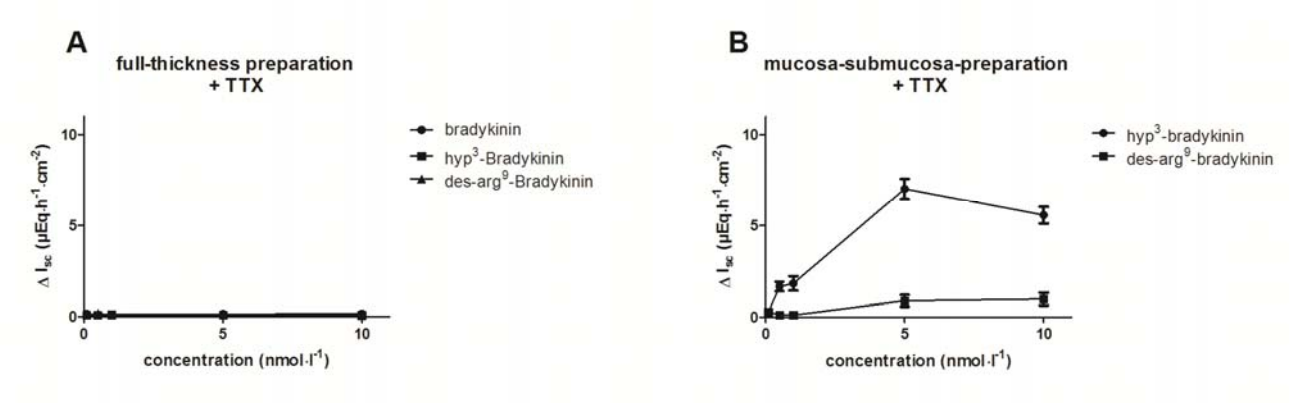

Figure 3.20: Concentration-response curves (10^{-9} – 10^{-7} mol·l^{-1} at the serosal side) for bradykinin, hyp^3-bradykinin and des-arg^9-bradykinin in Ussing chamber experiments in the presence of tetrodotoxin (10^{-6} mol·l^{-1} at the serosal side).

The change in short-circuit current (Δ I_{sc}) above the former baseline detected right before the respective administration of the test substance measured in full-thickness preparations (A) and mucosa-submucosa preparations (B). Shown are means (symbols) ± SEM (bars); n = 7 - 8.

3.4 The differences in bradykinin-induced chloride and mucus secretion between control and ulcerative colitis patients

Bradykinin has been described to be centrally involved in different models of experimental colitis in mice and rats (Stadnicki *et al.* 1998b; Kamat *et al.* 2002; Hara *et al.* 2007; Hara *et al.* 2008), as well as in inflammatory bowel diseases (IBD) in humans (Stadnicki *et al.* 2003b; Devani *et al.* 2005; Stadnicki *et al.* 2005). However, these studies with human samples concentrate on the expression of enzymes and receptors of the bradykinin system on a morphological or molecular biological level. Functional studies of the involvement of bradykinin with human biopsies have not been performed so far.

Thus, we performed a study, in which we compared the effect of bradykinin on the ion and mucus secretion in control tissue with samples from patients suffering from inflammatory bowel diseases (see 2.4.4) using Ussing pulse measurements. These experiments were performed at the Department of Medical Biochemistry and Cell Biology at the University of Gothenburg (Sweden) under the kind supervision of Henrik Sjövall and Jenny Gustafsson. Since this study was limited in time, the results must be regarded as preliminary.

In Ussing pulse experiments (2.9.3.3) not only changes in short-circuit current (ΔI_{sc}) representing changes in electrogenic ion transport, but also changes in epithelial capacitance (ΔC_e) are measured. The latter parameter enables to conclude on the mucus-secretion by the goblet cells via exocytosis (Gustafsson *et al.* 2012).

Figure 3.21A shows the change in I_{sc} induced by kinins in tissue from patients with ulcerative colitis and tissue from patients, who were not suffering from inflammatory bowel disease, but underwent colonoscopy for other reasons (‘control patients‘). The left two columns show that bradykinin ($2 \cdot 10^{-8}$ mol·l^{-1} at the serosal side) induced an increase in I_{sc}. However, there was no significant difference between control and ulcerative colitis patients. The right two columns show that the B_2 agonist hyp^3-bradykinin (10^{-7} mol·l^{-1} at the serosal side) induced a change in I_{sc} as well; but this agonist induced a much stronger increase in I_{sc} than native bradykinin (bradykinin: 0.54 ± 0.33 µEq·h^{-1}·cm^{-2}, n = 8; hyp^3-bradykinin: 2.20 ± 0.52 µEq·h^{-1}·cm^{-2}, n = 7). This higher sensitivity to the B_2 receptor agonist was lost in tissues from ulcerative colitis, as hyp^3-bradykinin (10^{-7} mol·l^{-1} at the serosal side) induced there only an increase in I_{sc} of 0.45 ± 0.64 µEq·h^{-1}·cm^{-2} (n = 9).

A similar effect can be observed for the mucus secretion (Figure 3.21B). Bradykinin ($2 \cdot 10^{-8}$ mol·l^{-1} at the serosal side) induced a weak mucus secretion in both control and ulcerative colitis patients (left two columns). However, the mucus secretion induced by hyp^3-bradykinin (10^{-7} mol·l^{-1} at the serosal side; right two columns) in control patients was much stronger compared to native bradykinin (bradykinin: 0.84 ± 0.54 µF·cm^{-2}, n = 8; hyp^3-bradykinin 2.27 ± 1.0 µF·cm^{-2}, n = 7), but was abolished in ulcerative colitis patients. The B_1 agonist des-arg^9-bradykinin (10^{-7} mol·l^{-1}) had neither an effect on ion secretion nor on mucus release (data not shown), indicating a B_2 receptor-mediated response. These results suggest a functional deficiency in kinin-regulated mucus secretion in inflammatory bowel disease.

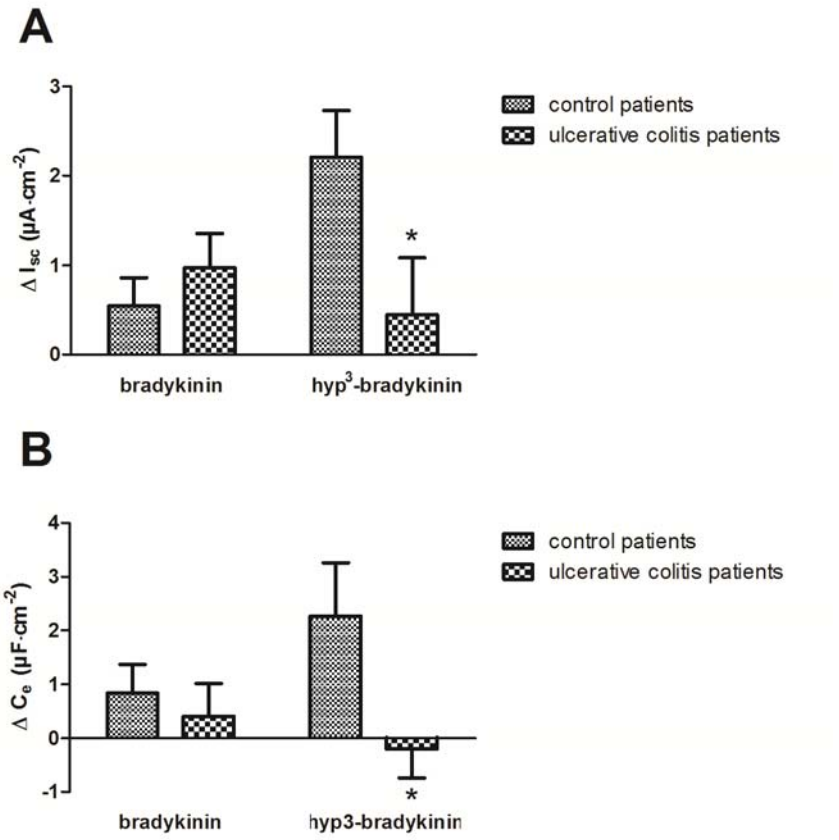

Figure 3.21: The effect of bradykinin ($2 \cdot 10^{-8}$ mol·l^{-1} at the serosal side; left columns) and the B_2 agonist hyp^3-bradykinin (10^{-7} mol·l^{-1} at the serosal side; right columns) on the short-circuit current (I_{sc}) and the epithelial capacitance (C_e) of control and ulcerative colitis patients.
A: Effect of both agonists on short-circuit current as difference to the former baseline (ΔI_{sc}).
B: Increase of the capacitance above the former baseline (ΔC_e).
Values are means (columns) ± SEM (bars); n = 7 - 9. * $P < 0.05$ versus the effect of hyp^3-bradykinin in the group of control patients.

In a next step the involvement of enteric neurons in bradykinin-induced mucus secretion was investigated. Although the biopsies used for these experiments were mucosal biopsies and thus theoretically devoid of the myenteric and submucosal plexus, we were interested if there was still a neuronal regulation, e.g. via neurons of the mucosal plexus, which – in addition to submucosal neurons – control epithelial ion transport (Andres *et al.* 1985).

Figure 3.22A shows the effect of bradykinin ($2 \cdot 10^{-8}$ mol·l^{-1} at the serosal side) on the change in I_{sc} in the presence and absence of tetrodotoxin (10^{-6} mol·l^{-1} at the serosal side), comparing the samples from the control with those from the ulcerative colitis patients. For both groups the effect of bradykinin was reduced when measured in the presence of tetrodotoxin, although merely in the group of control patients this reduction reached a level of statistical significance. Figure 3.22B illustrates a similar reduction of bradykinin-induced mucus secretion in the presence of tetrodotoxin. This effect could only be observed in control patients; the inhibition of bradykinin-induced mucus secretion by tetrodotoxin in the ulcerative colitis group was marginal. These results indicate an involvement of neurons in the effect of bradykinin on the human mucosal biopsies.

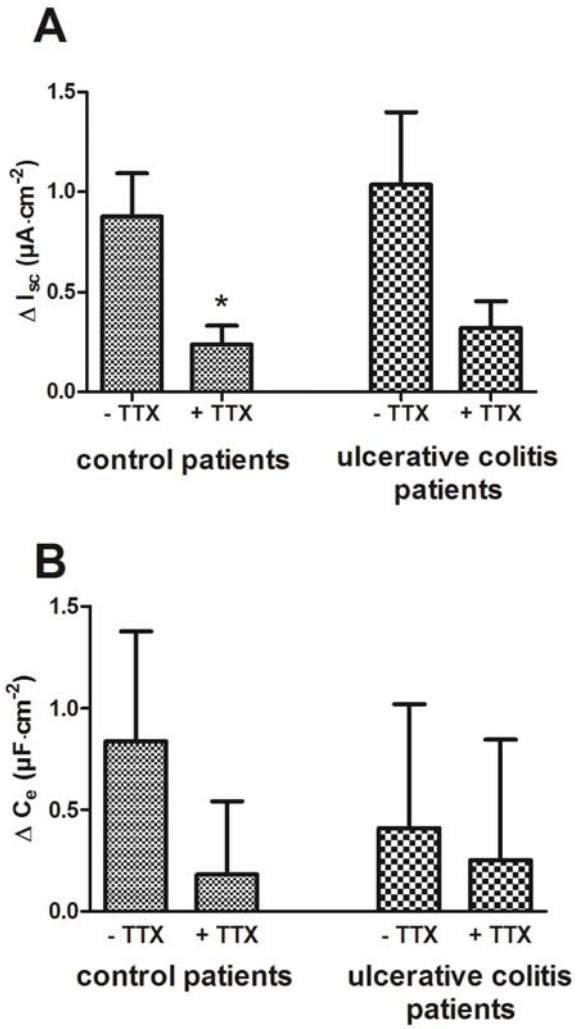

Figure 3.22: The effect of bradykinin ($2 \cdot 10^{-8}$ mol·l^{-1} at the serosal side) on the short-circuit current (I_{sc}) and the capacitance (C_e) of control (left columns) and ulcerative colitis patients (right columns) in the presence and absence of tetrodotoxin (10^{-6} mol·l^{-1} at the serosal side).
A: The increase of the short-circuit current above the former baseline (ΔI_{sc}).
B: The increase of the capacitance above the former baseline (ΔC_e).
Values are means (columns) ± SEM (bars); n = 5 – 9.

3.5 The effect of bradykinin on the contractility of the rat intestinal muscle

3.5.1 The segment-dependent effect of bradykinin on the contractility of the rat intestine

It has been shown that the rat duodenum responds to bradykinin in a biphasic manner, i.e. a relaxation followed by a contraction (Altinkurt & Ozturk 1990; Feres *et al.* 1992; Ozturk *et al.* 1993; Wassdal *et al.* 1999a; Wassdal *et al.* 1999b). However, there is only marginal knowledge about the changes in motility induced by bradykinin in other segments of the rat intestine (Elliott *et al.* 1960).

Thus changes in isometric force induced by bradykinin were investigated at the different segments (duodenum, jejunum, ileum and colon) of rat intestine. In concentration response experiments performed with full-thickness preparations of different segments of the gut, bradykinin turned out to be most effective at a concentration of 10^{-7} mol·l^{-1} (data not shown). Therefore, this concentration was chosen for the following experiments.

As reported in the literature (see above), in my study full-thickness preparations of the duodenum responded to bradykinin (10^{-7} mol·l^{-1}) with a pronounced relaxation followed by a secondary contraction (Figure 3.23, Table 3.2). In average, muscle tone fell by -0.47 ± 0.04 g below the former baseline and increased then transiently by 0.31 ± 0.04 g (n = 7). The jejunum showed a weaker relaxation and a stronger contraction compared to the duodenum. In contrast, in the ileum the initial relaxation was very small and was followed by a quite strong contractile response, which amounted to 1.04 ± 0.32 g (n = 6). In the colon, the change in contractility evoked by the kinin was similar as in the duodenum; a pronounced relaxation was followed by a weak contraction (Figure 3.23, Table 3.2).

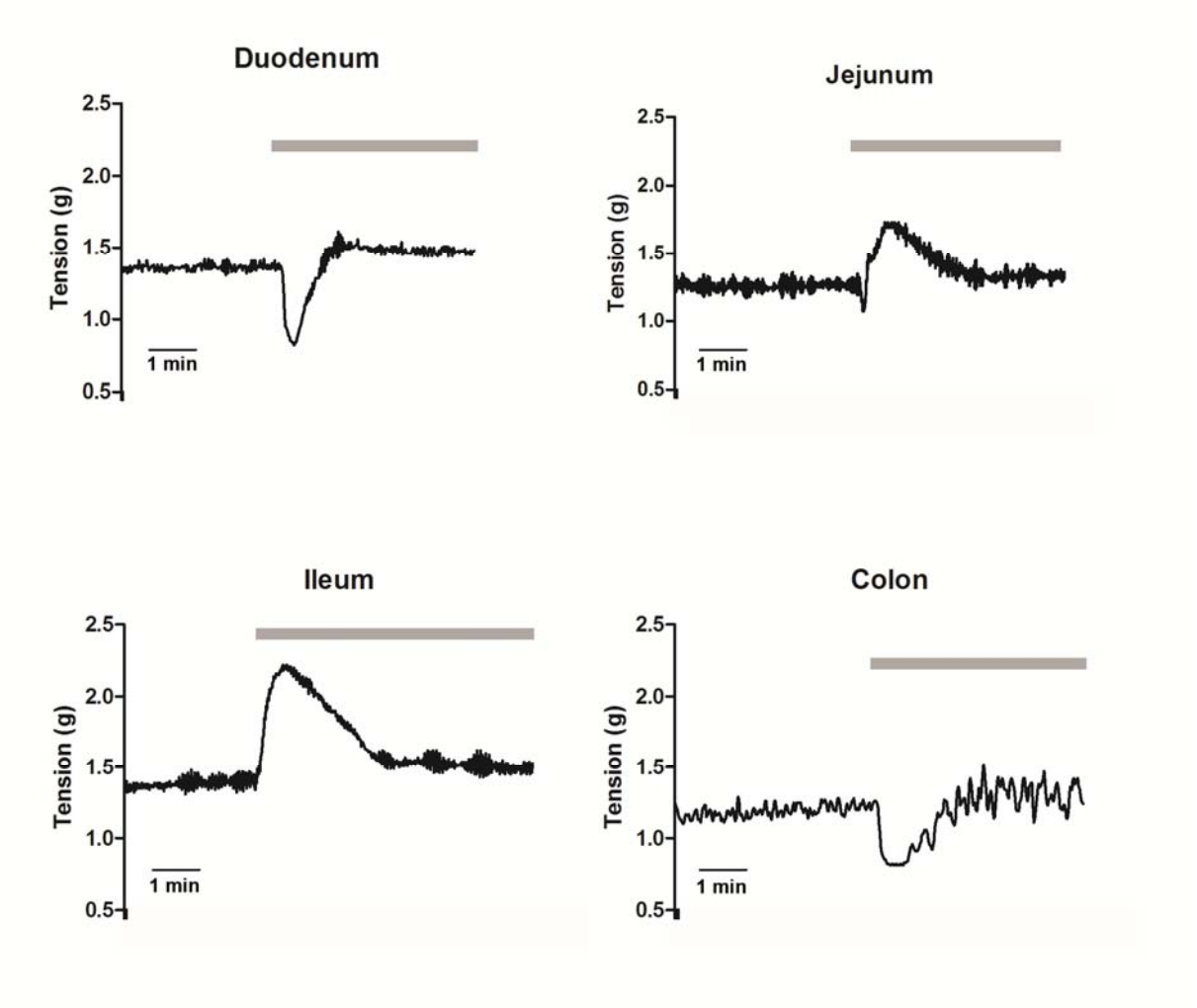

Figure 3.23: Time course of the effect of bradykinin (10^{-7} mol·l $^{-1}$; grey bars) on the contractility of full-thickness preparations from different parts of the intestine.
Typical tracings from 6 to 7 experiments; for statistics, see Table 3.2.

	Duodenum	Jejunum	Ileum	Colon
		Isometric force [g]		
Δ Minimum	-0.47 ± 0.04[a]	-0.13 ± 0.02[b]	-0.15 ± 0.06[b]	-0.50 ± 0.09[a]
Δ Maximum	0.31 ± 0.04[c]	0.50 ± 0.04[d]	1.04 ± 0.32[d]	0.27 ± 0.05[c]

Table 3.2: Effect of bradykinin (10^{-7} mol·l^{-1}) on the contractility of full thickness preparations from different parts of rat intestine.
Given is the maximal relaxation (Δ minimum) or maximal contraction (Δ maximum) measured under isometric conditions as difference to the baseline just prior administration of the kinin. Values are means ± SEM; n = 6 - 7. The Δ Minimum values and the Δ Maximum values for the intestinal segments were compared separately; statistically homogenous groups are marked with the same letter (a,b for the Δ Minimum and c,d for the Δ Maximum;). $P < 0.05$ (one-way analysis of variances followed by linear contrast analysis via Tukey test).

The contraction in a smooth muscle cell is Ca^{2+}-dependent, since Ca^{2+} forms a complex with calmodulin and thus enables the interaction of myosin with actin being essential for a contraction (see 1.5.1). In order to investigate whether differences in the bradykinin-induced changes in cytosolic Ca^{2+}-concentration are responsible for the segment-dependent responses (Figure 3.23), imaging-experiments were performed, in which the effect of bradykinin on dissociated muscle cells was compared between cells obtained from the colon and cells originating from the small intestine. In concentration response experiments performed with dissociated muscle cells from the small intestine, bradykinin turned out to be most effective at a concentration of 10^{-8} mol·l^{-1} (data not shown).

In the colon, 70 out of 71 cells (all of them proved to be viable in the viability control performed with carbachol ($5 \cdot 10^{-5}$ mol·l^{-1})) responded to bradykinin (10^{-8} mol·l^{-1}) with a change in the cytosolic Ca^{2+} concentration (see Methods for description of the threshold for acceptance of a response), which differed, however, in time course and direction (Figure 3.24). A minority of cells (23 %, i.e. 16/71 cells) responded with a decrease in the fura-2 ratio, which in average amounted to -0.04 ± 0.01 (n = 16). In 10 of these cells this was followed by a secondary increase. The majority of cells (n = 54) responded to bradykinin with a monophasic rise of the fura-2 signal (Figure 3.24). Overall, the increase of the fura-2 signal reached an average value of 0.29 ± 0.04 (n = 64)

In the small intestine, 67 out of 118 cells (here a total of 193 cells were tested, from which, however, only 118 fulfilled the viability criteria) responded to bradykinin (10^{-8} mol·l^{-1}) with a change in cytosolic Ca^{2+} concentration. Only three out of 118 cells responded with a decrease in fura-2 ratio, which reached an average of -0.01 ± 0.002 (n = 3), with a secondary increase in one of these cells. The majority of cells (n = 64) responded with a monophasic increase in the fura-2 ratio. Overall, in the small intestine, this peak amounted to an average of 0.3 ± 0.01 (n = 65).

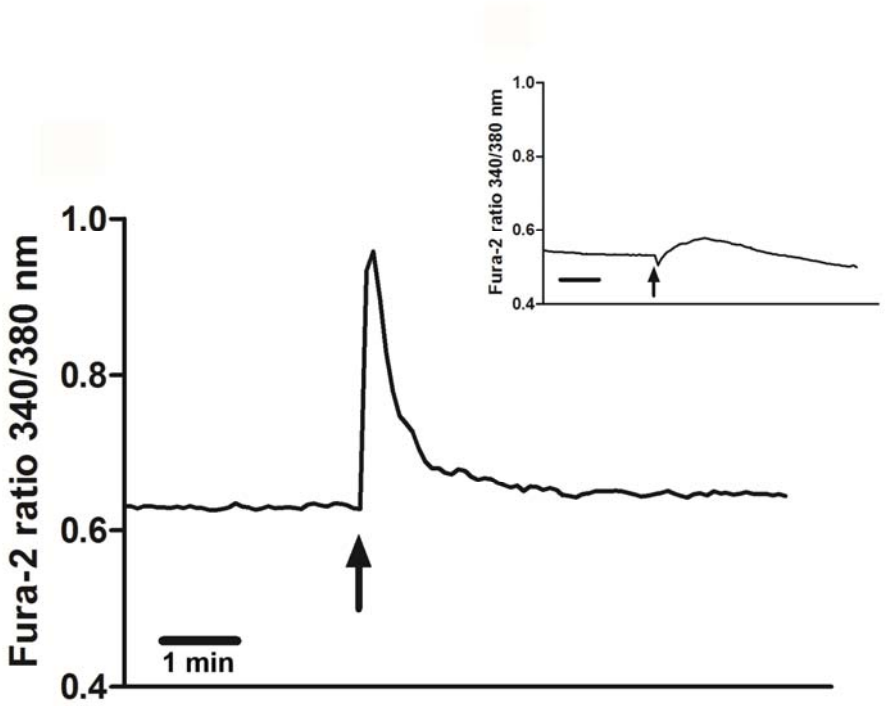

Figure 3.24: Changes of the fura-2 ratio reflecting changes in the cytosolic Ca^{2+} concentration induced by bradykinin ($2 \cdot 10^{-8}$ mol·l^{-1}; arrow) in dissociated smooth muscle cells from rat colon.
In the majority of cells, bradykinin evoked an increase in the fura-2 ratio signal. The inset shows a transient tiny decrease in the fura-2 ratio signal, which was observed in a smaller group of cells. This decrease could either occur alone or was followed by a secondary increase in the fura-2 signal as depicted here.
Exemplary tracings from n = 70. For statistics, see text. Scale bar: 1 min.

As isolated smooth muscle cells from small and large intestine exhibited essentially the same changes in cytosolic Ca^{2+} concentration when exposed to bradykinin, other reasons must underlie the segment-dependency in the bradykinin-induced effect, since the average amplitude of the fura-2 signal is comparable in both intestinal parts. The frequent occurrence of a small decrease in the fura-2 signal in the colonic muscle cells induced by

bradykinin was much too short to explain the relaxation of the intact muscle and was not further investigated.

In the immunocytological analysis of cells obtained from the colon with cells originating from the small intestine, no differences in the bradykinin receptor expression could be revealed (data not shown). Therefore, the difference in the effect of bradykinin on the contractile response in both segments is unlikely to be caused by a different receptor distribution and must have other reasons.

3.5.2 The involvement of the bradykinin receptors in the contractility of the colon

It was hypothesised that in rat duodenum the activation of the B_2 receptor by bradykinin induced a relaxation, whereas the activation of the B_1 receptor results in a contraction. (Boschcov *et al.* 1984; Paiva *et al.* 1989). In order to find out whether this might also hold true for the colon, selective agonists for the two bradykinin receptors were used.

Since the B_1 receptor is known to be absent in native tissue, but to be inducible by in vitro incubation (Bouthillier *et al.* 1987; Teather & Cuthbert 1997), two preparations were compared, both originating from the colon: Freshly prepared full-thickness preparation and full-thickness preparation after in vitro preincubation of five hours. Using freshly prepared full-thickness preparations, only the bradykinin B_2 receptor agonist, hyp^3-bradykinin (10^{-7} mol·l^{-1}), mimicked the effect of bradykinin, i.e. it evoked a transient relaxation (maximal fall in isometric force: -0.62 ± 0.11 g), followed by secondary contraction (maximal increase in force: 0.25 ± 0.04 g, n = 13; Figure 3.25, Table 3.3). The B_1 agonist (des-arg^9-bradykinin; 10^{-7} mol·l^{-1}) was completely ineffective under these conditions. However, after the in vitro preincubation, the B_1 receptor agonist induced a pronounced contraction, whereas the initial, relaxing response evoked by the B_2 receptor agonist was reduced 10-fold (Figure 3.25, Table 3.3).

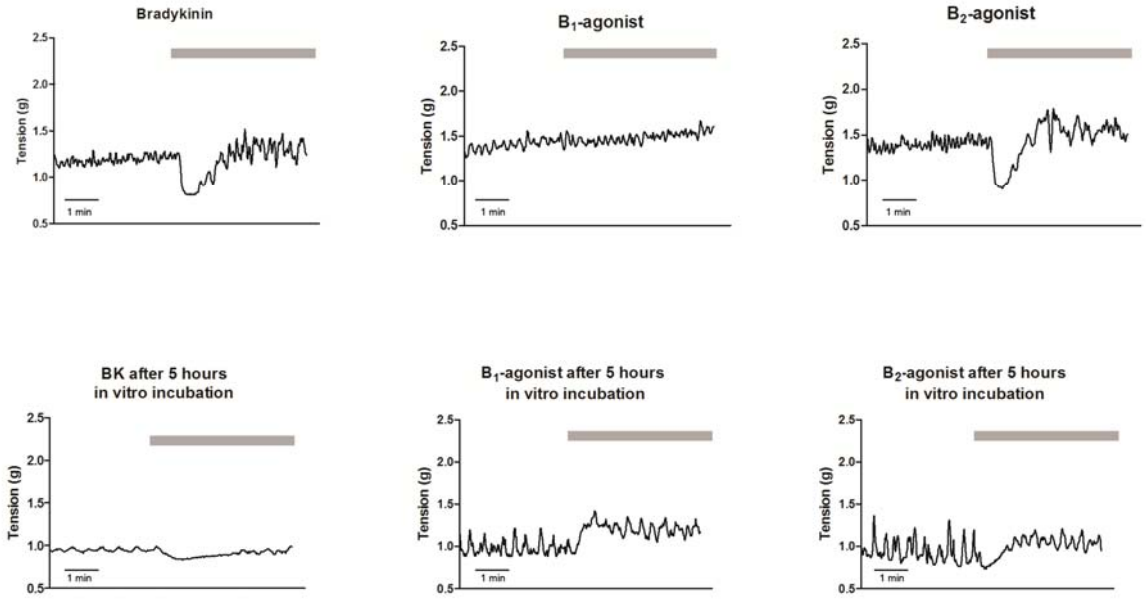

Figure 3.25: The effect of bradykinin (10^{-7} mol·l^{-1}), the B_1 agonist des-arg^9-bradykinin (10^{-7} mol·l^{-1}), and the B_2 agonist hyp^3-bradykinin (10^{-7} mol·l^{-1}) on the contractility of full-thickness preparations from rat colon.

First row: native colon wall; second row: colon wall incubated for 5 hours. Grey bar: presence of the respective substance. Whereas bradykinin and hyp^3-bradykinin induced a relaxation in the native colon tissue, des-arg^9-bradykinin caused no response. After five hours of incubation, the effect of bradykinin and hyp^3-bradykinin was diminished and des-arg^9-bradykinin induced a contraction. Typical tracings from 5 to 6 experiments; for statistics, see Table 3.3.

	Native colon		After incubation	
	Δ Minimum	**Δ Maximum**	**Δ Minimum**	**Δ Maximum**
	Isometric force [g]			
Bradykinin	-0.50 ± 0.09	0.27 ± 0.05	-0.18 ± 0.09*	0.17 ± 0.06
B_1 agonist	ineffective	ineffective	-0.05 ± 0.03*	0.54 ± 0.23*
B_2 agonist	-0.62 ± 0.11	0.25 ± 0.04	-0.06 ± 0.01*	0.32 ± 0.08

Table 3.3: The effect of bradykinin (10^{-7} mol·l^{-1}), the B_1 agonist des-arg^9-bradykinin (10^{-7} mol·l^{-1}), and the B_2 agonist hyp^3-bradykinin (10^{-7} mol·l^{-1}) on the contractility of full-thickness preparations from rat colon under native and incubated conditions.
Given is the maximal relaxation (Δ minimum) or maximal contraction (Δ maximum) measured under isometric conditions as difference to the baseline just prior to the administration of the respective peptide. Values are means ± SEM; n = 5 - 6. *: P < 0.05 versus response to the respective peptide in native tissue.

In order to investigate changes in cytosolic Ca^{2+} concentration underlying the responses of the intestinal muscle to bradykinin and the receptor agonists, the effect of bradykinin, the B_1 agonist des-arg^9-bradykinin, and the B_2 agonist hyp^3-bradykinin on the change in cytosolic Ca^{2+} concentration in the colon was investigated.

Overall, 118 out of 124 viable cells (investigated were 124 colonic smooth muscle cells, from which all fulfilled the viability criteria) responded to des-arg^9-bradykinin (10^{-7} mol·l^{-1}). This response followed different time patterns. About 43 % (53 out of 124 cells) showed only a decrease in the fura-2 signal, amounting to an average of -0.03 ± 0.01 (n = 53). In 31 % of the cells (38 out of 124 cells) this initial fall in the fura-2 signal was followed by a secondary increase in the fura-2 ratio. The largest fraction of cells (52 %, i.e. 65 out of 124 cells) responded only with an increase in the fura-2 signal. Overall, the rise in the fura-2 signal reached an average peak of 0.47 ± 0.06 (n = 103; Figure 3.27; Figure 3.26).

Hyp^3-bradykinin (10^{-7} mol·l^{-1}) induced similar changes in the fura-2 signal in 119 out of 119 viable cells (tested were 119 cells which all proved to be viable). This could consist in a fall of the fura-2 ratio signal (18 %, i.e. 22 out of 119 cells), which was followed by a secondary increase in most of these cells (i.e. 19 out of 22 cells). Other cells (n = 97) responded with a monophasic increase of the fura-2 ratio (Figure 3.27). Overall, the rise in the fura-2 ratio amounted in average to 0.86 ± 0.12 (n = 116).

Native bradykinin (10^{-8} mol·l^{-1}) induced a change in the fura-2 signal in 55 out of 55 viable cells (tested were in total 56 cells, from which one did not fulfil the viability criteria) with seven out of 55 cells showing an initial decrease in the signal amounting to -0.02 ± 0.005, all of them being followed by a secondary increase. 48 out of 55 cells responded with a monophasic increase in the fura-2 signal. Overall, the rise in the fura-2 signal reached in average 0.78 ± 0.07 (n = 55, Figure 3.27).

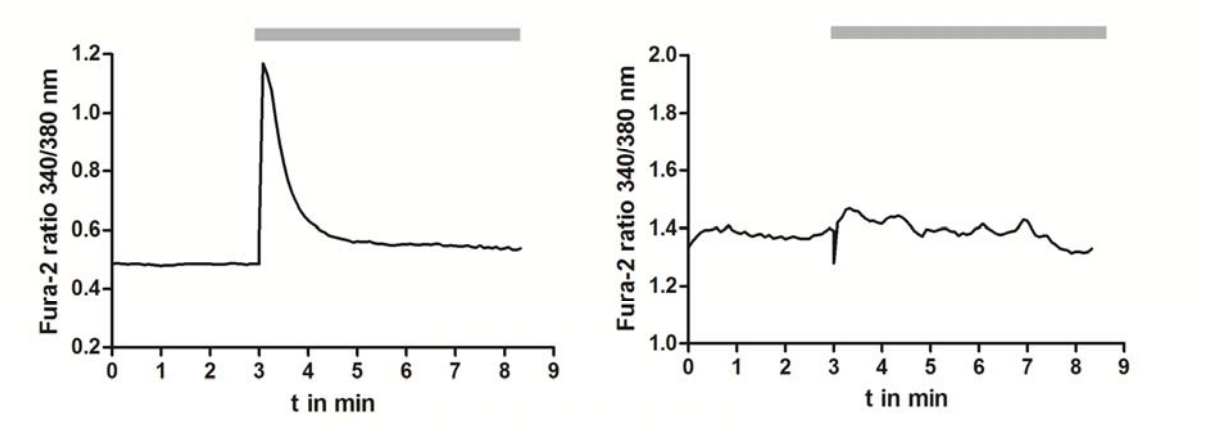

Figure 3.26: Changes of the fura-2 ratio reflecting changes in the cytosolic Ca^{2+} concentration induced by the B_1 agonist des-arg^9-bradykinin (10^{-7} mol·l^{-1}; grey bar) in dissociated smooth muscle cells from rat colon.

Two typical tracings from 124 measured cells. For statistics, see text.

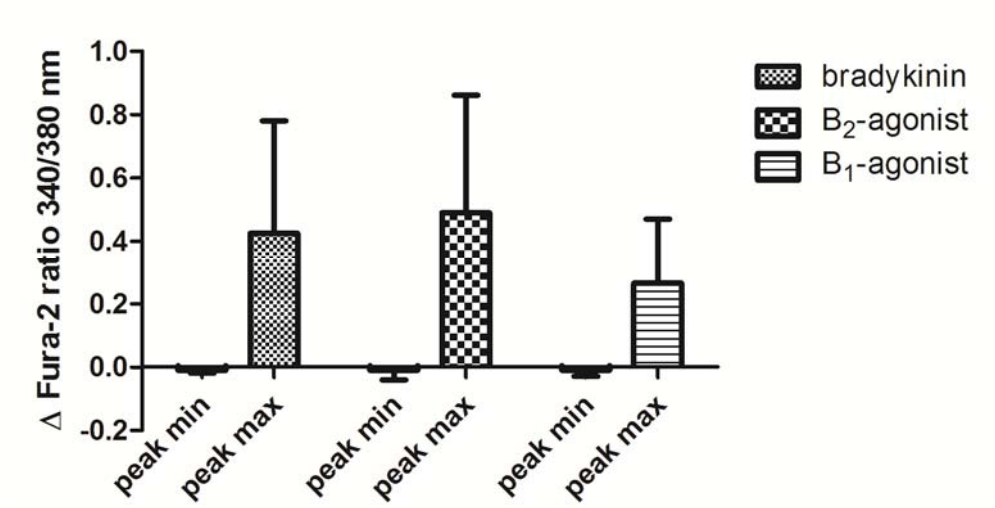

Figure 3.27: The effect of bradykinin ($2 \cdot 10^{-8}$ mol·l^{-1}), the B_1 agonist des-arg^9-bradykinin (10^{-7} mol·l^{-1}), and the B_2 agonist hyp^3-bradykinin (10^{-7} mol·l^{-1}) on the fura-2 ratio (i.e. the cytocolic Ca^{2+}-concentration) of muscle cells obtained from the colon.
Given is the change in the fura-2 ratio compared to the baseline (Δ fura-2 ratio) after administration of the respective test substance for peak min (the minimum reached within 15 s after administration) and peak max (the maximum reached later than 15 s after administration). Values are means ± SEM; n = 55 – 124.

These results demonstrate that differences in the cytosolic Ca^{2+} concentration induced after the respective receptor activation cannot explain the divergent effects of the agonist on the colonic contractility, as both bradykinin B_1 and B_2 receptor stimulation evoked essentially the same changes in the cytosolic Ca^{2+} concentration. The frequently observed tiny fall in the cytosolic Ca^{2+} level after administration of the B_1 agonist (Figure 3.27) does not fit to the purely contractile response measured in the isometric contraction measurement (Figure 3.25), since a decrease of cytosolic Ca^{2+} concentration would rather lead to a relaxation, than a contraction.

In order to investigate the expression and localisation of bradykinin B_1 and B_2 receptors in the colonic wall, immunocytochemical and immunohistochemical stainings were performed. As shown in Figure 3.28A, in native rat tissue the B_2 receptor was expressed throughout the colonic wall including the muscularis propria. The B_1 receptor, however, could not be detected in the muscularis propria, but was expressed by a distinct population of epithelial cells.

In contrast, if smooth muscle cells from the colon were dissociated and cultivated for 16 h, an immunocytochemical signal for the B_1 receptor was clearly recognised. As expected, the B_2 receptor was expressed as well (Figure 3.28B).

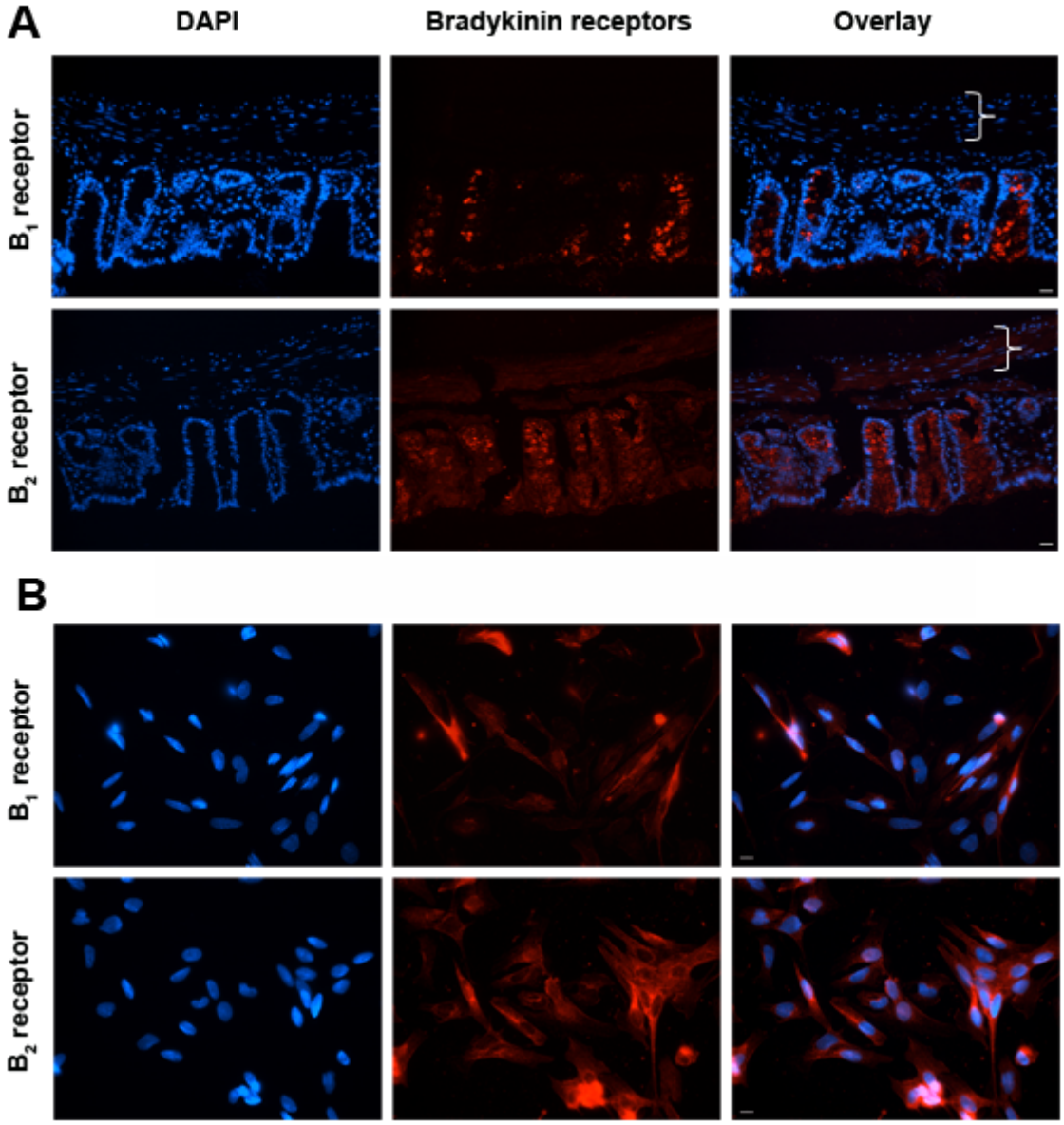

Figure 3.28: Immunohistochemical staining of the colonic wall for the nuclear marker DAPI (left column) combined the bradykinin B_1 receptor (first row) or the B_2 receptor (second row).
The curly bracket shows the location of the muscularis propria. Typical results from three independent experiments. Scale bars: 20 µm.
B: Immunocytochemical staining of intestinal muscle cells isolated from rat colon.
Shown are double stainings of the nuclear marker DAPI (left column) and the B_1 (first row) or the B_2 receptor (second row). Typical results from three independent experiments. Scale bars: 10 µm.

These findings obtained in the immunofluorescence analysis were partly confirmed in the RT-PCR experiments. When mRNA was isolated from the colonic muscularis propria, a signal for both bradykinin B_1 and B_2 receptors was found (Figure 3.29). This differs from the immunohistochemical staining and might be caused either by the higher sensitivity of the detection method or indicate that the gene for the bradykinin B_1 receptor was transcribed, but did not undergo translation.

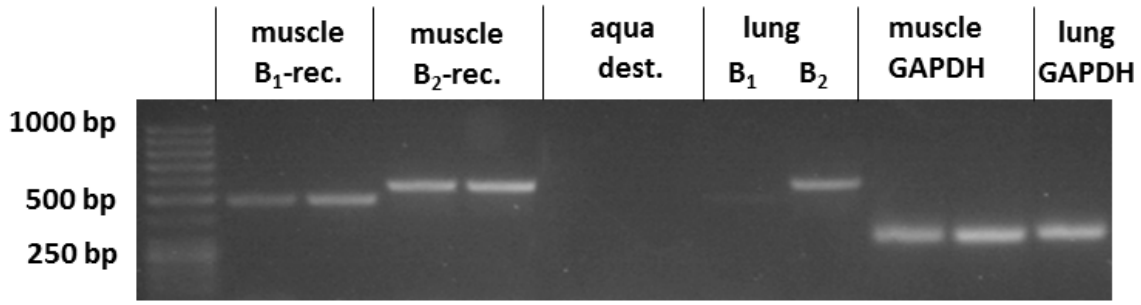

Figure 3.29: RT-PCR detection of the mRNA expression of bradykinin B_1 and B_2 receptor in the muscularis propria of the rat colon.
Shown are bands of cDNA amplified using primer pairs for the B_1 receptor (fragment size of 481 bp) and the B_2 receptor (fragment size of 553 bp). For proving the efficiency of the reaction, transcripts of the lung were used as a control. The amplification of GAPDH (fragment size of 303 bp) in muscle and lung served as a further control for testing the quality of the PCR reaction. Water control without template cDNA as well as a RT^- control, in which the reverse transcription had been performed without the reverse transcriptase, showed no amplificates. Each reaction was performed as a duplicate (apart from lung). Shown is a representative result from three independent PCR-reactions.

3.5.3 The mediation of the bradykinin-induced changes in contractility

In order to distinguish whether the changes in intestinal motility evoked by bradykinin are caused by stimulation of bradykinin receptors on enteric neurons or by receptors on smooth muscle cells, it was tested if the changes in isometric force induced by the kinin were sensitive to tetrodotoxin (10^{-6} mol·l^{-1}), a neurotoxin blocking voltage-dependent Na^+ channels in neurons (Catterall 1980). However, in none of the intestinal segments investigated, this neurotoxin had any significant effect on the contractile response evoked by bradykinin (Table 3.4).

As bradykinin is known to induce the release of prostaglandins in different tissues (Baird *et al.* 2008; Liu *et al.* 2012), the effect of the kinin was tested in the absence or presence of indomethacin (10^{-6} mol·l^{-1}), an inhibitor of cyclooxygenase(s) (Kato *et al.* 2001). However, in no intestinal segment the response to the kinin was altered in the presence of this inhibitor. Also a release of nitric oxide, which is well known to induced intestinal relaxation, is obviously not involved, as neither blockade of NO synthases with L-NAME (10^{-5} mol·l^{-1}), a potent blocker of NO synthases (Rees *et al.* 1990), nor methylene blue (10^{-5} mol·l^{-1}), an inhibitor of the main cellular target enzyme of NO, i.e. the guanylate cyclase (Mayer *et al.* 1993; Ragy & Elbassuoni 2012), had any effect on the response to bradykinin (Table 3.4).

The relaxation induced by bradykinin in rat duodenum has been shown to be caused by the activation of Ca^{2+}-dependent K^+ channels (Feres *et al.* 1992). In order to investigate the involvement of these channels in the biphasic effect of bradykinin in the different rat intestinal segments, the response to bradykinin was tested in the absence and the presence of tetrapentylammonium (10^{-4} mol·l^{-1}), a K^+ channel blocker preferentially inhibiting Ca^{2+}-dependent K^+ channels (McNamara *et al.* 1999).

In the presence of tetrapentylammonium, the relaxation induced by bradykinin was significantly inhibited in the colon, whereas the apparent reduction in the duodenum and ileum did not reach statistical significance (Table 3.4). However, also the contraction induced by the kinin during the late phase of the bradykinin response was reduced in the duodenum and ileum in the presence of this channel blocker (Table 3.4). The response to the viability control carbachol ($5 \cdot 10^{-5}$ mol·l^{-1}) was slightly reduced as well.

	Δ Minimum	Δ Maximum	Δ Minimum	Δ Maximum
	- Inhibitor		+ Inhibitor	
Duodenum: isometric force [g]				
Tetrodotoxin	-0.41 ± 0.10	0.40 ± 0.07	-0.24 ± 0.09	0.23 ± 0.02
Indomethacin	-0.37 ± 0.10	0.32 ± 0.04	-0.45 ± 0.03	0.22 ± 0.04
L-NAME	-0.89 ± 0.32	0.17 ± 0.47	-0.86 ± 0.32	0.24 ± 0.06
Methylene blue	-0.62 ± 0.05	0.34 ± 0.07	-0.83 ± 0.14	0.35 ± 0.08
Tetrapentylammonium	-0.51 ± 0.02	0.43 ± 0.13	-0.17 ± 0.04	0.02 ± 0.02*
Ileum: isometric force [g]				
Tetrodotoxin	-0.11 ± 0.03	1.33 ± 0.25	-0.18 ± 0.04	0.96 ± 0.24
Indomethacin	-0.04 ± 0.14	1.42 ± 0.37	-0.15 ± 0.02	1.07 ± 0.24
L-NAME	-0.69 ± 0.32	0.71 ± 0.26	-0.75 ± 0.35	0.80 ± 0.31
Methylene blue	-0.38 ± 0.11	1.14 ± 0.27	-0.23 ± 0.11	0.84 ± 0.17
Tetrapentylammonium	-0.20 ± 0.12	1.36 ± 0.29	-0.06 ± 0.03	0.26 ± 0.19*
Colon: isometric force [g]				
Tetrodotoxin	-0.67 ± 0.20	0.34 ± 0.09	-0.66 ± 0.17	0.31 ± 0.09
Indomethacin	-0.72 ± 0.19	0.27 ± 0.06	-0.69 ± 0.19	0.20 ± 0.05
L-NAME	-0.99 ± 0.33	0.33 ± 0.08	-0.82 ± 0.45	0.30 ± 0.06
Methylene blue	-0.43 ± 0.17	0.21 ± 0.11	-0.47 ± 0.17	0.35 ± 0.19
Tetrapentylammonium	-0.39 ± 0.15	0.54 ± 0.17	-0.07 ± 0.04*	0.42 ± 0.15

Table 3.4: Effect of bradykinin (10^{-7} mol·l^{-1}) on full thickness preparations from different parts of rat intestine under isometric conditions in the absence (- inhibitor) and presence (+ inhibitor) of different inhibitors.

Inhibitor concentrations were: tetrodotoxin (10^{-6} mol·l^{-1}), indomethacin (10^{-6} mol·l^{-1}), L-NAME (10^{-5} mol·l^{-1}), methylene blue (10^{-5} mol·l^{-1}), and tetrapentylammonium (10^{-4} mol·l^{-1}). Given is the maximal relaxation (Δ minimum) or maximal contraction (Δ maximum) measured under isometric conditions as difference to the baseline just prior administration of bradykinin. Values are means ± SEM; n = 5 - 12. * $P < 0.05$ versus the corresponding values in the group without the respective inhibitor.

As described above (Figure 3.24), the B_1 agonist des-arg^9-bradykinin caused a contraction in the rat colon after prolonged in vitro incubation. For investigating a possible involvement of paracrine mediators in this contractile effect, inhibitor experiments were performed. However, neither the neurotoxin, tetrodotoxin (10^{-6} mol·l^{-1}), nor the cyclooxygenase(s) inhibitor, indomethacin (10^{-6} mol·l^{-1}), nor BW A4C (10^{-5} mol·l^{-1}), a lipoxygenase inhibitor (Tateson *et al.* 1988), did affect any of the two phases of the response evoked by des-arg^9-bradykinin (10^{-7} mol·l^{-1}) (Table 3.5). In the presence of tetrodotoxin, the response evoked by the B_1 receptor agonist even seemed to be enhanced (Figure 3.30). This suggests that also after induction of B_1 receptors, direct effects at smooth muscle cells dominate the functional response evoked by the kinin.

	Δ Minimum	Δ Maximum
Alone	-0.05 ± 0.03	0.54 ± 0.23
Tetrodotoxin	-0.14 ± 0.11	0.80 ± 0.15
Indomethacin	-0.06 ± 0.04	0.71 ± 0.25
BW 4AC	-0.02 ± 0.01	0.39 ± 0.08

Table 3.5: Effect of the B_1 agonist des-arg^9-bradykinin (10^{-7} mol·l^{-1}) on the contractility of full-thickness preparations from rat colon after 5 h in vitro incubation.
Isometric contractions were measured in the absence ('alone') and presence of different inhibitors. Inhibitor concentrations were tetrodotoxin (10^{-6} mol·l^{-1}), indomethacin (10^{-5} mol·l^{-1}), BW 4AC (10^{-5} mol·l^{-1}). Given is the maximal relaxation (Δ minimum) or maximal contraction (Δ maximum) measured under isometric conditions as difference to the baseline just prior administration of the B_1 agonist. Values are means ± SEM; n = 4 - 9.

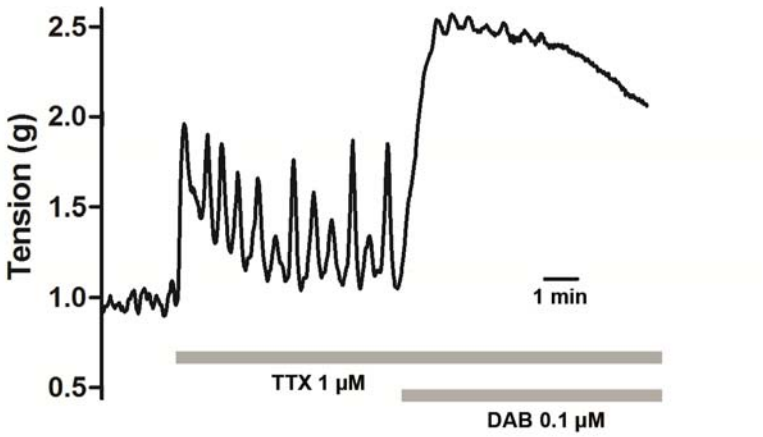

Figure 3.30: Effect of tetrodotoxin (TTX; 10^{-6} mol·l^{-1}) and the B_1 agonist des-arg^9-bradykinin (DAB; 10^{-7} mol·l^{-1}) on isometric force generated by full-thickness colonic preparations preincubated in vitro for 5 h.

Tetrodotoxin induced a strong increase in spontaneous contractions and enhanced the contraction induced by the B_1-agonist. Typical tracing from n = 9; for statistic see Table 3.5.

3.5.4 The influence of the different layers of the rat colonic wall on the bradykinin-induced changes in contractility

Wassdal et al. (Wassdal *et al.* 1999b) assumed that the relaxation induced by bradykinin in rat duodenum was not a direct effect on the muscle cells, but mediated through adjacent non-muscle cells. In order to test this hypothesis, experiments with different preparations of the colonic wall were performed, in which individual layers of the wall were manually dissected (Figure 2.1). In order to exclude potential damage of the tissue due to the preparation, the effect of bradykinin was compared to the force generated by the viability control (carbachol, $5 \cdot 10^{-5}$ mol·l^{-1}) in the respective preparation and given as % maximal force (see Figure 3.31 for quantification). These experiments were restricted to the colon, as only in this part of the gut a manual dissection was possible due to the thicker intestinal wall.

The full-thickness preparation of the colon responded to bradykinin (10^{-7} mol·l^{-1}) with a relaxation, which reached an average of -22 % compared to the maximal carbachol response (Figure 3.31). The following contraction amounted to 61 % of the maximal carbachol response (n = 3). In the muscularis-submucosa-lamina propria preparation, bradykinin induced an average relaxation of -18 % and contraction of 37 % compared to the maximal carbachol effect (n = 9). The muscularis-submucosa preparation responded to bradykinin with a relaxation having an average of -8 % and a contraction with an average of 18 % of the maximal carbachol response (n = 7). The muscularis preparation showed in response to bradykinin a relaxation of -3 % and a contraction of 7 % of the maximal carbachol effect (n = 7). In other words, removal of adjacent tissue layers nearly abolished the response to the kinin, although the contractile effect evoked by carbachol was only slightly reduced excluding a rough damage of the muscle. Neighbouring cells obviously sensitise the smooth muscle to the stimulation of these receptors.

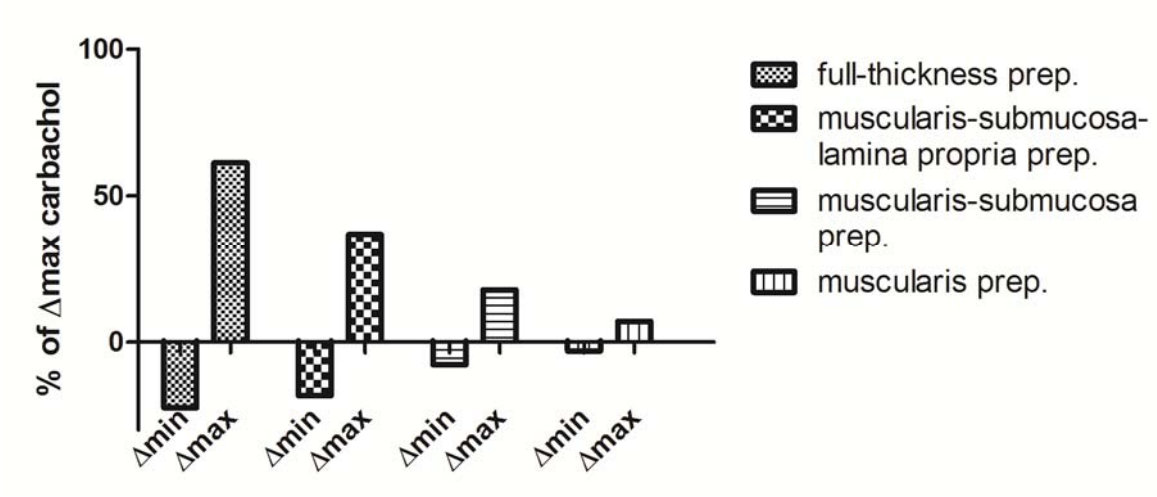

Figure 3.31: The effect of bradykinin (10^{-7} mol·l^{-1}) on the different layers of the colon, i.e. full-thickness preparations, muscularis-submucosa-lamina propria preparations, muscularis-submucosa preparations and muscularis preparations.

Given is the maximal relaxation (Δ min) or maximal contraction (Δ max) measured under isometric conditions. Data are normalised in comparison to the maximal force induced by carbachol ($5 \cdot 10^{-5}$ mol·l^{-1}), which was set to 100 %. The cholinergic agonist caused a contraction of 1.10 ± 0.14 g in full thickness preparations, 0.91 ± 0.16 g in muscularis-submucosa-lamina propria-preparations, 0.76 ± 0.42 g in muscularis-submucosa-preparations and 0.60 ± 0.15 g in muscularis-preparations.

4 Discussion

4.1 The effect of bradykinin on myenteric neurons

4.1.1 The biphasic effect of bradykinin

The effect of the inflammatory mediator bradykinin was investigated with microelectrode arrays. The intriguing feature of this technique is that the ganglionic cells are cultured directly on the electronic chip. This entails the following advantages compared to the classical electrophysiological techniques, such as patch-clamping or intracellular microelectrodes: Firstly, the cell culture allows the cells to rebuild their cellular contacts and to create new synapses and signal pathways, as described by other groups (Jessen *et al.* 1983; Nishi & Willard 1985). Secondly, in microelectrode arrays the measurement can be performed from multiple electrodes and therefore the properties and reactions of many neurons to a certain stimuli, in this case bradykinin, can be investigated simultaneously. Thirdly, repeated measurements with one set of cells are possible, an instance reducing the number of laboratory animals needed to be sacrificed, as well as material and time for the preparation. All in all, the method of microelectrode arrays enables the investigator to gain insight into the electrical behaviour of neurons that is closer to the in vivo situation than other electrophysiological methods.

However, there are also disadvantages: The microelectrode array technique does not allow to exactly investigating the ion currents involved in a certain effect, as it can be performed with e.g. patch-clamping. Furthermore, the high amount of cells giving signals can be impedimental, since the myenteric plexus contains different types of neurons and it is not possible to match a certain signal with the morphology of a certain neuron (although it is possible to optically examine the group of cells being located closely to the respective electrode). Also the fact that one group of neurons might respond in a different way to a stimulus than another group is difficult to evaluate, although the waveform-analysis (see 2.5.7) can be a tool for this. Additionally, due to the heterogeneity of the neurons, the results often exhibit a quite large variability, which makes it necessary to increase the number of repetitions for an experiment.

However, since the technique of microelectrode arrays enables to shed a different light on the properties and reactions of myenteric neurons, it was used in the present study to investigate the effect of bradykinin on these neurons. The results were controlled and further elaborated by Ca^{2+} imaging, immunocytochemistry and real time PCR.

There is only one publication using microelectrode arrays for the investigation of myenteric neurons (Medert *et al.* 2013); therefore, the first step was to establish the method in the lab, especially in regard to the best preparational technique, the procedure of the measurement and the elaboration of the obtained data (see 3.1).

The main experiments focused on the effect of bradykinin on myenteric neurons. Bradykinin induced a biphasic change in excitability with a rapid 1^{st} peak and a delayed 2^{nd} peak (Figure 3.6, Figure 3.7). In the BSA control, no 2^{nd} peak, but a 1^{st} peak was detected. It could be assumed that the first peak was due to the stimulation of mechanosensitive neurons (Mazzuoli & Schemann 2009) by the administration procedure. These neurons play an important role in the registration of bowel movements and filling of the intestinal tract. The assumption that these neurons are the elicitors of the 1^{st} peak was supported by my finding that Gd^{3+}, a blocker of mechanogated ion channels (Hamill & McBride 1996), reduced the 1^{st} peak induced by bradykinin (data not shown). However, if the bradykinin receptors were blocked by receptor antagonists, the 1^{st} peak was reduced as well (Table 3.1). Therefore, I assume that the 1^{st} peak is partly due to a stimulation of mechanosensitive neurons and partly represents a 'true' effect of bradykinin on the myenteric neurons.

This response pattern of rat myenteric neurons was confirmed in Ca^{2+} imaging experiments, in which bradykinin induced a biphasic rise in the cytosolic Ca^{2+} concentration as well (Figure 3.9). However, the time course differed: whereas in the microelectrode array measurements the 2^{nd} peak appeared in a time frame of 1.5 to 12 minutes, in the Ca^{2+} imaging experiments the 2^{nd} peak could be detected between 10 min and 20 min after administration of the kinin. I assume that this is due to the different experimental conditions: The microelectrode measurements were performed at 37 °C, whereas the fura-2 experiments were carried out at room temperature.

Not all neurons responded in a biphasic way: the waveform analysis of the microelectrode array data (Figure 3.8) as well as the evaluation of the percentage of the responding neurons in the fura-2 experiments (Figure 3.10) showed that approximately 40 % of the neurons

responded to bradykinin and some of these neurons displayed only the early (1st) or only the late (2nd) peak. This might be due to the heterogeneity of the myenteric neurons: they contain different types of neurons, on a morphological (Dogiel I – III) as well as on an electrophysiological (AH/S neurons) and functional (sensory, inter, motor neurons) basis (see 1.1.2.1).

The percentage of the overall responding neurons in the present study is consistent with the fura-2 results of Murakami et al. (Murakami *et al.* 2007) at the given bradykinin concentration. However, Murakami et al. detected solely a monophasic effect of bradykinin. Also other investigations of the effect of bradykinin on myenteric or submucosal neurons of rat and guinea pig (Gelperin *et al.* 1994; Hu *et al.* 2003; Hu *et al.* 2004a; Avemary & Diener 2010a) did not reveal a biphasic response pattern. This may be due to the length of their measurements. Since the second peak occurs in fura-2 measurements between the 10th and the 20th minute after administration of bradykinin, it might have been missed in these studies, in which the response to the kinin was not investigated over longer experimental periods.

4.1.2 The bradykinin receptors involved

As described in 1.2.2, bradykinin binds to two different receptors: the constitutively expressed B_2 receptor and the B_1 receptor, which is upregulated during tissue injury or inflammation.

Several studies at myenteric and submucosal neurons of the rat and guinea pig (Gelperin *et al.* 1994; Hu *et al.* 2003; Hu *et al.* 2004a; Murakami *et al.* 2007; Avemary & Diener 2010b) found that the effect of bradykinin is mediated solely by the B_2 receptor. In contrary to this, the effect of bradykinin on the cytosolic Ca^{2+} concentration of myenteric neurons in the present study was mimicked by both selective B_1 and B_2 receptor agonists (Figure 3.10). Furthermore, in microelectrode array measurements the combined presence of receptor antagonists of both receptors did inhibit the bradykinin response (Table 3.1), whereas the blockers applied singularly only partially reduced the response (data not shown). Immunocytochemical stainings revealed that the B_2 receptor was, as expected, constitutively expressed in the myenteric neurons (Figure 3.12A), in contrast to the B_1 receptor, which, however, was upregulated after one day of culturing (Figure 3.12B). This upregulation was confirmed by real time PCR, revealing that already after 3 hours of cultivation, there was an

increase of mRNA expression relatively to the amount of mRNA originating from freshly prepared myenteric neurons (Figure 3.13).

An upregulation of the B_1 receptor by short-term culture has been shown in different tissues, including rabbit isolated aorta, rabbit isolated mesenteric vein, rat colonic epithelium and rat ileum (Regoli *et al.* 1978; Bouthillier *et al.* 1987; Teather & Cuthbert 1997; Ueno *et al.* 2002) and occurs within three to four hours after tissue preparation (Regoli *et al.* 1978). It has been shown that this effect can be blocked by cycloheximide and actinomycin D, indicating a de-novo protein synthesis (Regoli *et al.* 1978).

The upregulation of the B_1 receptor under cell culture conditions is probably a result of a cytokine release. When tissue undergoes injury, an inflammatory response is stimulated. The damage-associated molecular pattern (DAMP) molecules are released by injured cells. Usually DAMPs are intracellular molecules, such as ATP (Boeynaems & Communi 2006; Bours *et al.* 2006) or uric acids (Shi *et al.* 2003), but there also exist other sources for DAMPs such as the extracellular matrix (heparan, hyaluronan) (Scheibner *et al.* 2006). In addition active pro-inflammatory cytokines and chemokines, such as interleukin (IL)-1α (Eigenbrod *et al.* 2008) and IL-33 (Moussion *et al.* 2008) are released by the injured cells. During the preparation and cultivation of the myenteric ganglia, DAMPs might have been released in the same manner as in vivo. This was demonstrated in rabbit aorta, where a preparation-induced release of IL-1ß was described (Clinton *et al.* 1991). Furthermore, Sardi and co-workers (Sardi 2002; Sardi *et al.* 1998; Sardi *et al.* 1999) showed that pro-inflammatory cytokines, such as IL-1β, tumor necrosis factor-α (TNFα) or IL-6 led to a leftward shift of the concentration-dependent contractile response to the B_1 agonist des-arg^9-bradykinin in human umbilical vein preparation, whereas anti-inflammatory cytokines resulted in the opposite effect. And also in rat myenteric neurons the exposure to IL-1ß led to an upregulation of the B_1 receptor on glia cells (Murakami *et al.* 2008). So it can be speculated that a release of DAMPs due to the tissue damage caused by the preparation with a following cytokine release provoked the upregulation of the B_1 receptor in the present study.

The immunocytochemical stainings also revealed that both receptors are located on neurons as well as glia cells (Figure 3.12A+B). This is consistent with findings of Murakami et al. (Murakami *et al.* 2007), who, however, could only find the B_2 receptor on both glia and

neurons, since they did not detect a signal for the B_1 receptor, even after cell culture. The reason for this divergent observation is unclear, but could be due to the culture conditions.

Murakami et al. (Murakami *et al.* 2007) proposed that two mechanisms were involved in the response of myenteric neurons to bradykinin: Firstly, there was a direct stimulation of the neurons resulting in a depolarisation. Secondly, they found that bradykinin, by binding to the glial bradykinin receptors, induced a prostaglandin release, which then stimulated the neurons via EP_1 receptor activation (Murakami *et al.* 2007). This was confirmed for the guinea pig submucosal plexus by Hu et al. (Hu *et al.* 2004a), but rejected for the rat submucosal neurons, where prostaglandins apparently played no role in the mediation of the bradykinin-induced effect (Avemary & Diener 2010b).

My results obtained from measurements with microelectrode arrays partly confirmed this theory. Prostaglandins are produced in two steps: Firstly, arachidonic acid is produced by the Ca^{2+}-dependent enzyme phospholipase A_2. Arachidonic acid is the substrate for the cyclooxygenases (I and II), which produce prostaglandins (Rainsford 1975). In the presence of the cyclooxygenase inhibitor piroxicam, the bradykinin-induced increase in action potential frequency was reduced (although this inhibition did not reach statistical significance) suggesting an at least partial involvement of prostaglandins (Figure 3.14). However, when the cells were cultured in the presence of a mitosis inhibitor suppressing the glial growth, the effect of bradykinin was not diminished (Figure 3.15), indicating that the glia cells do not play a role in the effect of bradykinin on the neurons. The reason for this discrepancy to the findings of Murakami et al. (Murakami *et al.* 2007) remains unclear.

4.1.3 The signal transduction of the bradykinin receptors

Bradykinin receptors are classical G_q-protein-coupled receptors (Leeb-Lundberg 2005). After receptor binding, phospholipase C is activated which forms inositol-1,4,5-trisphosphate (IP_3). This second messenger binds to IP_3 receptors, which are located on intracellular Ca^{2+} stores and cause a release of Ca^{2+} into the cytosol. However, there are also several studies demonstrating that extracellular Ca^{2+} is additionally or exclusively involved. Whereas Hu et al. (Hu *et al.* 2004a) found that bradykinin causes a release of intracellular Ca^{2+} via the IP_3 pathway in the guinea pig submucosal plexus, Avemary et al. (Avemary & Diener 2010a) demonstrated at rat submucosal neurons that an influx of Ca^{2+} from the extracellular space via voltage-dependent Ca^{2+} channels is essential for the response to the kinin. In rat myenteric neurons it was found by Gelperin et al. (Gelperin *et al.* 1994) that bradykinin induces both a release of Ca^{2+} from intracellular stores and an influx of Ca^{2+} from the extracellular space. Whereas the first effect was independent from prostaglandins, the latter turned out to be prostaglandin-dependent. This is in contrast to the findings of Murakami et al. (Murakami *et al.* 2007), as they demonstrated solely an influx of extracellular Ca^{2+}, partly via voltage-dependent Ca^{2+} channels, partly via non-selective cation channels; this influx was apparently prostaglandin-dependent. These contradictory findings make it clear that the signal transduction of bradykinin exhibits large variation throughout different tissues and species.

In this study, I demonstrated that bradykinin receptors in myenteric neurons act via G_q-proteins, as a blocker of this protein did inhibit the bradykinin response significantly (Figure 3.16). However, in consistency with Murakami et al. (Murakami *et al.* 2007), I found that the IP_3 pathway was not involved in this response, since a blocker of the IP_3 receptors did not affect the increased electrical activity caused by bradykinin (Figure 3.17A). The removal of Ca^{2+} from the buffer solution inhibited the bradykinin effect on cytosolic Ca^{2+} concentration significantly (Figure 3.17B), strongly suggesting that an influx of extracellular Ca^{2+} forms the basis for the bradykinin response. In the presence of a blocker of voltage-dependent Ca^{2+} channels, the response to bradykinin was reduced, although this inhibition did not reach statistical significance (Figure 3.17C). The hypothesis of an influx of Ca^{2+} from the extracellular space is supported by the manganese quenching experiments showing that bradykinin accelerated the decline in the fluorescence, which indicated that Mn^{2+} from

extracellular moves into the cell due to the opening of Ca^{2+} channels in the plasma membrane. The experiments suggest furthermore that the phase between the first and the second peak, in which the electrical activity (microelectrode array measurements) and the fura-2 ratio (Ca^{2+}-imaging), respectively, is reduced, is due to a closure of Ca^{2+} channels in the plasma membrane.

Based on these findings, I hypothesise that bradykinin, by binding to its G_q-protein-coupled receptor, induces an influx of extracellular Ca^{2+} via voltage-dependent Ca^{2+} channels and perhaps additionally via non-selective cation channels, as described by Murakami et al. (Murakami *et al.* 2007). The mechanisms of activation of these Ca^{2+} channels remain unknown.

4.2 The effect of bradykinin on the ion and mucus secretion in rat and human colon

4.2.1 Bradykinin-induced changes of the short-circuit currents in the rat colon

As described in the introduction (see 1.3.5), there is evidence from several species that bradykinin causes a chloride secretion. All of these investigations (Musch *et al.* 1983; Cuthbert *et al.* 1984a, 1984b; Perkins *et al.* 1988; Phillips & Hoult 1988; Baird *et al.* 2008) demonstrate that the effect of bradykinin is sensitive to a cyclooxygenase inhibitor, indicating an involvement of prostaglandins, as it has been described for several tissues throughout the body (Regoli & Barabe 1980; Baird *et al.* 2008; Liu *et al.* 2012).

Another mediating factor is neurons: Diener et al. (Diener *et al.* 1988) and Perkins et al. (Perkins *et al.* 1988) demonstrated that the effect of bradykinin is, besides a direct stimulation of the epithelial cells, partly induced by the activation of submucosal neurons. However, the involvement of the myenteric plexus, which has also been described to influence the intestinal secretion (Jodal *et al.* 1993; See & Bass 1993), in the effect of bradykinin has not been investigated so far. Therefore, I aimed to find out if the myenteric plexus plays a role in the effect of bradykinin on the chloride secretion.

In Ussing chamber experiments I compared three different preparations, a full-thickness preparation containing both the submucosal plexus and the myenteric plexus, a mucosa-submucosa preparation containing only the submucosal plexus, and a mucosa preparation, in which neither the submucosal nor the myenteric plexus were present (Figure 2.1). As described previously (Diener *et al.* 1988), in the present study bradykinin causes a concentration-dependent increase in short-circuit current (I_{sc}) in the rat colon (Figure 3.19A). In the present study, the mucosa-submucosa preparation and the mucosa preparation responded in a similar manner. However, the change in I_{sc} in the full-thickness preparation caused by bradykinin was decreased (Figure 3.19A).

Measurements with agonists of both receptors revealed that the effect of bradykinin on the I_{sc} is mediated merely by the constitutively expressed B_2 receptor (Figure 3.18B); the inducible B_1 receptor is not involved (Figure 3.19C). This was also confirmed in immunohistochemical stainings, where the B_2 receptor was found to be expressed almost

throughout the whole intestinal wall, including the epithelium, whereas the B_1 receptor could only marginally be detected at the apical regions of the epithelial cells (Figure 3.28A).

Since there is a functional dominance of inhibitory motor neurons in the myenteric plexus, as the overall action of the enteric nervous system on gastrointestinal motility is an inhibitory one (Hansen 2003b), demonstrated e.g. by the increase in intestinal motility after blockade of neuronal activity with the neurotoxin tetrodotoxin (Diener & Gabato 1994 and Figure 3.30), I hypothesised that the reduced response of the full-thickness preparation to bradykinin might be due to inhibitory actions of the myenteric neurons, which I proved to be stimulated by bradykinin in microelectrode array and fura-2 measurements (Figure 3.6, Figure 3.9). I performed Ussing chamber experiments in the presence of the neurotoxin tetrodotoxin, which inhibits the propagation of action potentials by blocking voltage-dependent Na^+ channels in cells (Catterall 1980). In the full-thickness preparations the effects of bradykinin and the B_2 agonist hyp^3-bradykinin were abolished when tetrodotoxin was present (Figure 3.20A). However, in the mucosa-submucosa preparation, the B_2 agonist induced a concentration-dependent increase in I_{sc} despite of the presence of tetrodotoxin (bradykinin itself was not tested; Figure 3.20B).

These findings reject the hypothesis that the myenteric plexus is involved in the effect of bradykinin on the chloride secretion. Although the reduced effect of bradykinin in full-thickness preparations could indicate an inhibitory involvement of myenteric neurons stimulated by bradykinin, the absent bradykinin-induced response in the full-thickness preparation if tetrodotoxin was present is clearly contradictory to this theory, since an abolition of the inhibitory effect of the myenteric plexus by tetrodotoxin should lead to an increase of the bradykinin-induced secretion. As this is not the case and because of the finding that the B_2 agonist shows an effect on the I_{sc} in mucosa-submucosa preparation even in the presence of tetrodotoxin, it is most likely that the missing response of the full-thickness preparation is due to the muscle layer building a diffusion barrier for bradykinin. Bradykinin does not reach the epithelium in the same concentration as in the preparations devoid of the muscle layer.

Therefore, I confirm the findings of other researchers (Diener *et al.* 1988; Phillips & Hoult 1988) that bradykinin induces a change in short-circuit current via direct stimulation of epithelial cells, as well as activation of – most likely submucosal - neurons. Based on previous

investigations, it can be assumed that this change in I_{sc} is due to a chloride secretion. The hypothesis that myenteric neurons might be involved in this effect has to be rejected.

4.2.2 The comparison of the effect of bradykinin on the ion and mucus secretion between ulcerative colitis patients and control patients

After demonstrating that bradykinin increases the short-circuit current concentration-dependently in the rat colon (see 3.3, Figure 3.19), I aimed to investigate whether these findings can be transferred to the human colon, especially in regard to the pathogenesis of inflammatory bowel diseases (see 1.4).

In human tissue there is already evidence that bradykinin induces a chloride secretion (Baird *et al.* 2008). However, functional studies investigating the effect of bradykinin comparing tissue from patients suffering from inflammatory bowel diseases (IBD) with control patients have not been performed so far. As described in the introduction (see 1.4.2), bradykinin is assumed to be involved in the genesis of Crohn´s disease and ulcerative colitis. This has been concluded from rat enterocolitis models and also from human tissue obtained from patients suffering from inflammatory bowel diseases (Stadnicki *et al.* 1998a; Stadnicki *et al.* 1998b; Stadnicki *et al.* 2003a; Devani *et al.* 2005). All parts of the kallikrein-kinin system – the substrate kininogen, the enzyme kallikrein and the receptors for the product bradykinin - seem to be present in the inflamed intestine, which makes it very likely that this system is involved.

Due to these promising findings, I aimed to find out whether bradykinin has an impact on the ion and mucus secretion in human colon, especially in regard to the comparison of tissue obtained from control patients to tissue from patients suffering from ulcerative colitis. Since these experiments have been performed at the Department of Medical Biochemistry and Cell Biology at the University of Gothenburg (Sweden) under the kind supervision of Henrik Sjövall and Jenny Gustafsson, this study was limited in time and the results have to be considered as preliminary.

Some comments have to be done on the tissue samples. The ulcerative colitis patients in this study were patients undergoing colonoscopy in the course of the regular check-up. Theoretically these patients can be considered as ‘in remission’. However, it is known from remissional patients that many of them still suffer from gastrointestinal symptoms, such as diarrhoea and abdominal pain, despite an inconspicuous mucosa (Isgar *et al.* 1983; Simren *et*

al. 2002). During colonoscopy, the grade of inflammation was evaluated by the gastroenterologist by applying the 'Mayo score' (see 2.2). It turned out that two patients were not in a classic remissional state (Mayo score 0), but exhibited inflammatory alterations (Mayo score 1 and 2, see Table 2.3). However, all patients were, independently from their scoring, included into the study.

Another comment has to be made concerning the control patients. These patients were not healthy subjects, but underwent colonoscopy because of other reasons than intestinal inflammation (see Table 2.4) and can therefore be seen as 'disease controls'. The advantage of using this material is that the group of patients is very heterogeneous, which reduces the risk for error due to a common disease denominator. But it has to be taken into account that this heterogeneity requires a higher number of patients, which could not be provided here due to the time limitations.

Bradykinin induced an increase of the short-circuit current (I_{sc}) in control and ulcerative colitis patients, but without any significant difference (Figure 3.21A). Since the B_1 agonist turned out to be ineffective in both groups (data not shown) and the B_2 agonist caused a quite strong response (Figure 3.21A), this effect is most likely mediated by B_2 receptors. Interestingly, the response of control patients to hyp^3-bradykinin was significantly higher than the response of the same patient group to bradykinin. Since the B_1 receptor obviously does not play a role in this effect, the most plausible explanation is that the concentration used for hyp^3-bradykinin turned out to be more effective than the concentration used for bradykinin. In ulcerative colitis patients this increased response to the B_2 agonist cannot be found: here the response is significantly smaller compared to the B_2 induced response in control patients (Figure 3.21A). This might indicate that the epithelium in ulcerative colitis patients has a reduced sensitivity to the B_2 agonist. In a mouse model of colitis it was found that the bradykinin-induced increase in I_{sc} in Ussing chamber measurements was reduced in the colitis mice compared to the control mice (Kachur *et al.* 1995). Maybe, there is a similar effect in the epithelium of ulcerative colitis patients, possibly due to desensitisation of the receptor, which has been described in several tissues (Leeb-Lundberg 2005). But the number of measured tissues in the present study is too small to draw definite conclusions.

A similar effect can be seen on the mucus secretion. Bradykinin induces a small mucus secretion in both control and ulcerative colitis patients (Figure 3.21B). Hyp^3-bradykinin, however, induced a significantly stronger response in control patients compared to

ulcerative colitis samples, in which the response was almost abolished. It can also be speculated that this effect is due to receptor desensitisation in the diseased patients. The finding that bradykinin induces a mucus-release from the goblet cells is especially interesting in regard to the finding of Stadnicki et al., showing that goblet cells release kallikrein (Stadnicki *et al.* 2003a), the enzyme producing bradykinin. It might be speculated that there exists a positive feedback-mechanisms, but this has to be investigated further before drawing definite conclusions.

I also evaluated the involvement of enteric neurons in the bradykinin-induced response. In control as well as ulcerative colitis patients the response of the short-circuit current to bradykinin in the presence of the neurotoxin tetrodotoxin was reduced (Figure 3.22A). A similar effect was observed concerning the capacitance: Although it did not reach statistical significance, a tendency towards reduction of the bradykinin-induced response on the mucus-secretion in the presence of tetrodotoxin can be seen (Figure 3.22B). This is an interesting finding, since the biopsies used for these experiments are purely mucosal biopsies and should be devoid of the submucosal plexus, which is known to regulate the secretion in the colon and also has been demonstrated to change its activity in response to bradykinin (Diener *et al.* 1988; Avemary & Diener 2010b). Due to the small number of patients and the limited time of the present study, we can only speculate on this effect: One explanation could be that the mucosal plexus (see 1.1.1), which was shown to be existent in human tissue on a morphological basis (Kramer *et al.* 2011) and also seems to be involved in the regulation of intestinal secretion (Bridges *et al.* 1986), could mediate these effects. Another possible explanation could be the stimulation of sensory nerves, which then activate a reflex circuitry leading to secretion. A similar process has been shown in rat duodenum, where bradykinin stimulated capsaicin-sensitive afferent nerves, which then resulted in a thickening of the mucus-layer (Akiba *et al.* 2001).

However, to draw conclusions from these findings more experiments have to be performed. But these results give a first hint that bradykinin has an impact on the secretory pathways in patients suffering from inflammatory bowel diseases, which is certainly worthwhile investigating further, especially in regard to possible treatments. In a mice model of colitis the application of the B_2 antagonist icatibant exhibited preventive effects on the severity of intestinal inflammation (Arai *et al.* 1999). Another group demonstrated that a non-peptide

B_1 receptor antagonist improved the histopathological effects in a murine model of colitis (Hara *et al.* 2008).

This indicates that the bradykinin-related research in inflammatory bowel diseases might be relevant for future treatment of this high-prevalence disease.

4.3 The effect of bradykinin on the contractility of rat intestine

4.3.1 The segment-dependent effect of bradykinin on the contractility of the rat intestine

The main function of the gastrointestinal tract is to mix and transport the ingesta in order to allow an efficient digestion of food and the absorption of nutrients, water and electrolytes. These different tasks are fulfilled in different parts of the intestine; therefore, it is comprehensible that each intestinal segment exhibits different motility patterns.

I was interested in the comparison of the effect of bradykinin on the intestinal motility in full-thickness preparations in regard to the different segments of the gut (duodenum, jejunum, ileum, and colon). In the rat, most studies have been performed at the duodenum (Altinkurt & Ozturk 1990; Feres *et al.* 1992; Ozturk *et al.* 1993; Wassdal *et al.* 1999a; Wassdal *et al.* 1999b). To our knowledge, there is only one rudimentary description of the effect of bradykinin at the rat colon (Elliott *et al.* 1960) and none at the other intestinal segments. In the guinea pig, however, a wider variety of segments has been investigated, including the duodenum, the ileum and the colon and also the circular muscle layer of the colon (Hall & Bonta 1973; Ozturk *et al.* 1993; Calixto 1995; Zagorodnyuk *et al.* 1998).

In this study, we performed isometric contraction measurements, meaning that the force generated by the intestinal muscle was measured under conditions that prevent the muscle from altering its length. Due to the orientation of the intestinal muscle in the chamber, only the contraction of the longitudinal muscle was detected. The results clearly show a segment-dependency in the effect of bradykinin on the contractility (Figure 3.23, Table 3.2). As described in literature (Altinkurt & Ozturk 1990; Feres *et al.* 1992; Ozturk *et al.* 1993; Wassdal *et al.* 1999a; Wassdal *et al.* 1999b), the duodenum responded in a biphasic manner, with a relaxation followed by a contraction. Although the jejunum and the ileum followed a similar pattern – a biphasic response – the emphasis shifted towards a contractile response in these parts of the intestinal tract. The ileum even exhibited only a minimal relaxation and a quite strong contraction. The colon responded similarly as the duodenum. These results show that the different segments of the gut respond in a specific manner to the kinin. Considering the different functions and also the sheer length of the intestinal tract - in the human it has a length of approximately eight meters – this is comprehensible. Whereas the duodenum is the principal segment for cleavage of the nutrients, the jejunum functions as

the main absorber of these nutrients, which explains the immense length of this part of the intestinal tract. The ileum is additionally responsible for the immune defence, whereas the colon is crucial for the final absorption of water and ions as well as for hosting bacteria fermenting structure carbohydrates, for which mammals do not express digestive enzymes. Obviously, this specialisation in function of the individual intestinal segments is linked with different responses evoked by bradykinin.

Bradykinin is produced after inflammation, which is a basic defence mechanism initiated by any kind of tissue damage (Regoli & Barabe 1980). Therefore, one might speculate that the motor response evoked by this mediator of inflammation, bradykinin, aims to eliminate potentially hazardous agents as fast as possible. On the other hand, this quick transport could induce severe diarrhoea due to the reduced transit time diminishing the time for the absorption of nutrients, which will harm the organism as well. Thus, the reason for the segment-dependency in the bradykinin-induced effect might be part of a sensitive regulatory system for transporting the agent out of the body with as little side effects as possible.

Based on these findings, two questions evolved:

1) Which receptors are involved in this effect on intestinal contractility?

2) Which are the mechanisms underlying the response to bradykinin, regarding the biphasic pattern as well as the segment-dependency?

4.3.2 The involvement of the bradykinin receptors in the contractility of the colon

Bradykinin binds to two receptors, the constitutively expressed B_2 receptor and the B_1 receptor, which is inducible by tissue injury and inflammation. It has been proposed that the relaxative component of the bradykinin response was mediated by the B_2 receptor, whereas the contractile part was caused by the activation of the B_1 receptor (Boschcov *et al.* 1984; Paiva *et al.* 1989). Paiva et al. (Paiva *et al.* 1989) observed that the B_1 agonist des-arg^9-bradykinin induced a contraction and a bradykinin analogue with a higher affinity to the B_2 receptor (a specific B_2 agonist was not developed yet) evoked a stronger relaxative response than bradykinin itself. However, in my study the B_2 agonist induced an effect with a similar time course as native bradykinin in the full-thickness preparation of the colon (Figure 3.25, Table 3.2). In addition, the isometric contraction measurements as well as immunohistochemistry of freshly prepared colonic wall (Figure 3.28) clearly showed that the B_1 receptor is not expressed in native muscle tissue and therefore cannot be involved in the

biphasic effect induced by bradykinin. The B_2 receptor was, as expected, found to be expressed in the intestinal muscle. This was confirmed by RT-PCR of the colonic muscularis propria (Figure 3.29)

Similar as I have described for the myenteric neurons (see 4.1.2), it was possible to upregulate the B_1 receptor in the muscle tissue by prolonged in vitro incubation. After five hours, the full-thickness preparations responded to the B_1 agonist des-arg^9-bradykinin with a contraction (Figure 3.25). The RT-PCR showed a band for the B_1 receptor already in native tissue (Figure 3.29), but it has to be taken into account that this detection method has a higher sensitivity and/or that the gene for the B_1 receptor might have been transcribed without having undergone translation. The upregulation was further confirmed by an immunocytochemistry of dissociated colonic muscle cells (Figure 3.28B), showing that the B_1 receptor, in contrary to native muscle tissue, was expressed, most probably due to the culture period, as observed in the myenteric ganglionic cells (Figure 3.12B).

An involvement of the B_1 receptor in the mediation of the effect of kinins has been described in several studies of the intestinal muscle, all of them showing the induction of a purely contractile response in native intestinal preparation by a B_1 agonist (Paiva *et al.* 1989; Feres *et al.* 1992; Ozturk *et al.* 1993). Contrarily, other studies could not detect an effect of a B_1 agonist (Hall & Morton 1991) or – similar to our findings – only after prolonged in vitro incubation (Boschcov *et al.* 1984). The reason for these oppositional results is unclear, but could be related to e.g. holding conditions of the animals. However, our findings as well as the observations of another group (Boschcov *et al.* 1984) clearly show an upregulation of the B_1 receptor in vitro, which should be taken into account when interpreting the effect of a B_1 agonist. Depending on the preparation time and the equilibration period, the B_1 receptor expression might be progressed far enough to induce a contractile response to a B_1 agonist.

Another finding of this experiment is that the relaxation induced by bradykinin or the B_2 agonist hyp^3-bradykinin was reduced 10 fold after 5 h in vitro incubation (Figure 3.25, Table 3.3). Taking into consideration that bradykinin binds to both B_1 and B_2 receptors, it is tempting to draw the conclusion that the contractile response caused by the B_1 agonist is superimposing the relaxation induced by the B_2 receptor stimulated by bradykinin. However, the reason why the response to the B_2 agonist alone is reduced as well remains unclear, but it can be speculated that the desensitisation of this receptor, which has been described in various tissues (Pizard *et al.* 1998; Prado *et al.* 2002), could play a role.

4.3.3 The mediation of the bradykinin-induced changes in contractility

The second part of the isometric force studies focused on the mediation of the bradykinin-induced changes in contractility. The enteric nervous system, especially the myenteric plexus, plays an important role in the regulation of intestinal motility (see 1.1.2). Since I observed that bradykinin has stimulating effects on myenteric neurons (Figure 3.6, Figure 3.7), I aimed to know if this stimulation might influence the motility of the intestinal muscle or whether the effect observed in the contraction measurements arouse from a direct activation of the muscle cells. Therefore, I measured the changes in isometric force in the presence of tetrodotoxin. However, this inhibitor of voltage-dependent Na^+ channels (Catterall 1980) did not affect the response to bradykinin in any of the segments tested (Table 3.4). This suggests that the expression of bradykinin receptors on myenteric neurons and the stimulation caused by activation of these receptors might have effects that are beyond the possible detection by this system or might induce effects other than changes in motility.

Bradykinin is well known to induce the release of eicosanoids from many tissues and cells. Baird et al. (Baird *et al.* 2008) showed that bradykinin caused a release of prostaglandins in human colonic tissue and Bramley et al. (Bramley *et al.* 1990) demonstrated that the guinea pig isolated trachea produced prostaglandins in response to bradykinin, which then influenced the contractility of the tracheal smooth muscle. Prostaglandins are produced in two steps: Firstly, arachidonic acid is cleaved from membrane phospholipids by the Ca^{2+}-dependent enzyme phospholipase A_2. Arachidonic acid is the substrate for the cyclooxygenases (I and II), which produce prostaglandins (Rainsford 1975).

In order to test the involvement of prostaglandins in the bradykinin-induced effect, we tested the response of the intestinal muscle to bradykinin in the presence of the cyclooxygenase inhibitor indomethacin. However, this blocker did not alter the response caused by bradykinin in the different intestinal segments (Table 3.4). Therefore, it is unlikely that bradykinin mediates its effects via a release of prostaglandins in the intestinal smooth muscle of the rat.

Other eicosanoids known to be released due to the receptor activation by bradykinin are leukotrienes. Rehn & Diener (Rehn & Diener 2012) showed that the blockade of the 5-lipoxygenase, an enzyme metabolizing arachidonic acid to leukotrienes, blocked the

bradykinin-induced change in cytosolic Ca^{2+} concentration in rat submucosal neurons. However, in my experiments the blockade of the synthesis of leukotrienes with BWA4C did not alter the response to bradykinin (Table 3.4), suggesting that none of the metabolites of arachidonic acids, neither prostaglandins nor leukotrienes, can be considered as mediators in any of the intestinal segments.

Schlemper & Calixto (Schlemper & Calixto 1994) demonstrated a bradykinin-induced release of nitric oxide from tracheal epithelium causing a relaxation of the tracheal smooth muscle. Nitric oxide is produced from L-arginine by the enzyme nitric oxide synthase (Pouokam *et al.* 2011). As nitric oxide is a gaseous substance, it diffuses freely across the membrane of the target cell and activates the soluble guanylyl cyclase, which converts guanosine triphosphate to cyclic guanosine monophosphate (Morgado *et al.* 2012). This molecule influences the conductance of Ca^{2+} channels as well as the sensitivity of the contractile apparatus to Ca^{2+}, leading to a relaxation of the muscle cell (Nishimura 2006). In my experiments I used two blockers to find out if nitric oxide is involved in the relaxative response in the different segments evoked by bradykinin: L-NAME, a blocker of the nitric oxide synthase(s) (Rees *et al.* 1990), and methylene blue, which inhibits the soluble guanylate cyclase (Mayer *et al.* 1993; Ragy & Elbassuoni 2012). However, both blockers did not affect the bradykinin induced effect in the rat colon (Table 3.4), which is consistent with findings in the rat duodenum (Rhaleb & Carretero 1994).

Several studies at the rat duodenum showed that the relaxation caused by bradykinin is inhibited by blockers of Ca^{2+}-activated K^+ channels (Hall & Morton 1991; Griesbacher 1992; Zagorodnyuk *et al.* 1998; Wassdal *et al.* 1999b). Therefore, we tested the involvement of these channels in the bradykinin response in the different parts of the intestine. We found that tetrapentylammonium, an inhibitor of K^+ channels preferentially blocking Ca^{2+}-activated K^+ channels (Maguire 1999), significantly reduced the relaxation in the colon and also caused a reduction of the relaxation in the duodenum (Table 3.4), which, however, was not significant, but has been proven by the studies listed above.

Since these K^+ channels are activated by Ca^{2+}, we investigated the changes in cytosolic Ca^{2+} concentration induced by bradykinin with fura-2 measurements. Dissociated and cultured muscle cells from the small intestine and from the colon were measured. Independently from the origin of the cells, bradykinin induced an increase in cytosolic Ca^{2+} concentration (see 3.5.1).

There are three different types of Ca^{2+} activated K^+ channels: BK (big conductance), IK (intermediate conductance) and SK (small conductance) K^+ channels based on their single channel conductance (for review, see Berkefeld *et al.* 2010). After activation of these channels by Ca^{2+}, they allow an efflux of K^+, subsequently hyperpolarising the cell and regulating the cytosolic Ca^{2+} concentration by deactivation of voltage-dependent Ca^{2+} channels or by a reduction of the transport activity of the Na^+/Ca^{2+} exchanger.

It is assumed that the activation of these channels is either caused by an influx of Ca^{2+} via L-type voltage-dependent Ca^{2+} channels, or, more importantly, due to a local Ca^{2+} release from the endoplasmic reticulum, which is called – dependently on the receptors releasing the ion - Ca^{2+} sparks and puffs (Wray *et al.* 2005). This often occurs in regions of the cell, where the endoplasmic reticulum is located in close proximity to the plasma membrane; an instance limiting the diffusion of the released Ca^{2+} and allowing the Ca^{2+} to reach the Ca^{2+}-activated K^+ channels in the plasma membrane. As the gap between the endoplasmic reticulum and the plasma membrane is only 30 – 100 nm (Wray *et al.* 2005), the Ca^{2+} sparks and puffs are difficult to investigate, especially with the method used in this study, the fura-2 measurements.

Therefore, a possible explanation for the relaxing component of the bradykinin response (Figure 3.23, Table 3.2), which is observed despite of the increase in the cytosolic Ca^{2+} concentration (Figure 3.24), might be caused by the activation of Ca^{2+}-dependent K^+ channels in the plasma membrane. I clearly demonstrated that Ca^{2+}-activated K^+ channels are not only involved in the bradykinin-induced relaxation in the duodenum as described before (Hall & Morton 1991; Griesbacher 1992; Zagorodnyuk *et al.* 1998; Wassdal *et al.* 1999b), but also in the relaxative response in the colon. Since the resulting hyperpolarisation leads to an inactivation of voltage-dependent Ca^{2+} channels, the contractile responses in the segments are partly blocked by tetrapentylammonium as well. Perhaps a differential distribution of Ca^{2+}-activated K^+ channels might be responsible for the observation that some parts of the small intestine such as the ileum do not show a relaxing response when exposed to bradykinin (Figure 3.23, Table 3.2).

After investigating the mediators involved in the biphasic response of bradykinin in the different intestinal segments, we focused on the question why B_1 receptor activation and B_2 receptor activation differed in the final motor response evoked at rat colonic smooth muscle. Both receptors use similar intracellular transduction pathways (Regoli & Barabe

1980). Therefore, we hypothesised that paracrine mediators might be involved in the divergent motor responses. However, blockade of the synthesis of eicosanoids with either indomethacin or BWA4C did not affect the contraction induced by des-arg^9-bradykinin in the colon, in which B_1 receptor expression had been forced by prolonged in vitro incubation (Table 3.5). Also the blockade of the propagation of action potentials with tetrodotoxin did not alter the response; quite to the contrary, in the presence of tetrodotoxin the spontaneous activity of the intestinal muscle was increased and the muscle reacted with phasic contractions (Figure 3.30). Des-arg^9-bradykinin evoked an even stronger contraction in the presence of tetrodotoxin than without. This effect is probably explained by the functional dominance of inhibitory motor neurons in the myenteric plexus, as the overall, predominant action of the enteric nervous system on gastrointestinal motility is an inhibitory one (Hansen 2003b), demonstrated e.g. by the increase in intestinal motility after blockade of neuronal activity with tetrodotoxin (see e.g. Diener and Gabato 1994 or Figure 3.30). By blocking the propagation of action potentials in this plexus, tetrodotoxin abolished the inhibiting effect of the myenteric motor neurons on the intestinal muscle (Lyster *et al.* 1995).

Ca^{2+} imaging experiments with bradykinin, the B_1 agonist des-arg^9-bradykinin and the B_2 agonist hyp^3-bradykinin did not show obvious differences as well: all three substances induced an increase in the cytosolic Ca^{2+} concentration (Figure 3.27), similar as it has been described by Wassdal et al. for rat duodenum (Wassdal *et al.* 1999a). Therefore it remains unclear how the B_1 receptor can induce a purely contractile response, whereas the B_2 receptor causes a biphasic reaction. It might be a different signal transduction of the receptors involved, but the investigation of this hypothesis was beyond the scope of this study.

4.3.4 The influence of the different layers of the rat colonic wall on the bradykinin-induced change in contractility

The observation that bradykinin induces the release of mediators influencing neighbouring cells in a paracrine manner has been described at several organs (Warhurst *et al.* 1987; Bramley *et al.* 1990). The most popular example for such a paracrine transduction pathway (but in relation to another substance) is that of Furchgott and his colleagues, who showed that the ablation of the endothelium abolished the relaxing effect of acetylcholine on the

muscle cells in blood vessels (Furchgott & Zawadzki 1980). They proved that the endothelium released nitric oxide in response to acetylcholine and demonstrated for the first time that the gas nitric oxide plays a crucial role in the regulation of the blood pressure. An analogous observation has been made with bradykinin at the isolated guinea pig trachea (Bramley *et al.* 1990). Here it was shown that bradykinin induced a release of prostaglandins from the epithelial cells, which in turn caused a relaxation of the smooth muscle cells. Interestingly, if the epithelium was removed, bradykinin induced merely a contraction due to the direct stimulation of the smooth muscle cells by bradykinin.

In order to test the possible involvement of adjacent tissues/cells in the motor response evoked by bradykinin, I performed isometric contraction measurements with preparations, in which distinct layers of the intestinal wall had been removed (Figure 2.1). These experiments were restricted to the colon as only there a differential ablation of individual layers was possible due to the sufficient thickness of the colonic wall. The results clearly show that, for unfolding its full effect, bradykinin needs the presence of all layer of the colonic wall (Figure 3.31). Since the effect of bradykinin increases with every additional layer being present, it is likely that not only one layer is essential to induce the maximal effect. Because the relaxation as well as the contraction was affected by the ablation of the layers, this communication between adjacent cells seems to be involved in both phases of the motor response evoked by the kinin. A possible damage of the tissue due to the preparation, which might cause the decrease in intensity of the bradykinin response, can be excluded, since the response to the cholinergic agonist carbachol was only slightly reduced after each ablation step excluding a gross damage of the smooth muscle cells.

I hypothesise that the activation of bradykinin receptors located in other parts of the gut such as intestinal epithelium (Figure 3.28A) or enteric neurons (Figure 3.12) or others induces the release of one or several paracrine mediators. Since bradykinin can induce a (small) biphasic motor response at the colonic muscularis propria devoid of other parts of the colonic wall (Figure 3.31), which is consistent with the expression of bradykinin receptors directly on the smooth muscle cells (Figure 3.28B), it seems likely that these substances released by bradykinin do not mediate the effect of the kinin, but rather sensitise the intestinal muscle towards bradykinin.

As described in 1.4.2, this sensitisation might occur via a change in the activity of the myosin light kinase phosphatase, but has not been further investigated in this study. The nature of

this sensitising mediator remains in the dark as well, although we excluded prostaglandins, leukotrienes, nitric oxide and the involvement of the enteric nervous system.

This finding demonstrates that the effect of bradykinin on the intestinal motility goes beyond a classic receptor activation of the target cell, but uses a complex mechanism involving other parts of the intestine as well.

5 Summary

Bradykinin is a peptide, which is responsible for inflammatory processes throughout the body. In the intestine it is assumed to be involved in the development of diarrhea by altering gastrointestinal motility and ion secretion. My PhD-thesis focused on these effects of bradykinin on intestinal functions and on the question, how the different systems influenced by the kinin, i.e. enteric nervous system, motility and secretion, interact with each other.
Therefore, I investigated the effect of bradykinin on rat myenteric neurons, rat intestinal muscle and rat and human colonic epithelium by applying microelectrode arrays, Ca^{2+} imaging, immunofluorescence analysis, isometric contraction measurements as well as standard and real time reverse transcription PCR.

Bradykinin stimulated rat myenteric neurons in a biphasic manner, which was shown on an action potential level measured with microelectrode arrays as well as on a cytosolic Ca^{2+} level, as demonstrated by Ca^{2+} imaging experiments. This effect was mediated by both the B_1 and the B_2 receptor, with the B_1 receptor being upregulated due to the cell culture. This upregulation was confirmed by immunocytochemistry as well as real time PCR. The stimulation of myenteric neurons by bradykinin was based on an influx of Ca^{2+} from the extracellular space, since a removal of extracellular Ca^{2+} significantly reduced the bradykinin-induced peak in the fura-2 ratio.

In the rat intestinal muscle bradykinin induced biphasic responses with a relaxation followed by a contraction. This effect exhibited a strong segment-dependency. Since the neurotoxin tetrodotoxin did not alter the bradykinin-induced effect, the enteric nervous system was most likely not involved in the change of contractility. Tetrapentylammonium, a K^+ channel blocker preferentially inhibiting Ca^{2+}-activated K^+ channels, reduced the relaxant component of the response. In dissociated intestinal muscle cells bradykinin induced an increase of the cytosolic Ca^{2+} level as detected in Ca^{2+} imaging experiments. In native tissue bradykinin acts via B_2 receptors, whereas in vitro incubation induced the expression of B_1 receptors, which then caused a purely contractile response after stimulation with a B_1 agonist.

Immunofluorescence analysis of the colonic wall and of dissociated intestinal muscle cells, as well as RT-PCR confirmed this finding. The consecutive ablation of adherent layers of the intestinal wall strongly reduced the response to bradykinin in comparison to a control stimulus, i.e carbachol, suggesting a contribution of non-muscle cells in the mediation of this response.

In Ussing chamber experiments with human and rat colonic tissue I demonstrated a bradykinin-induced ion secretion. Measurements with rat full-thickness preparations showed reduced effects of bradykinin and the B_2 receptor agonist on the change in short-circuit current compared to preparations devoid of the muscle layer. In the presence of tetrodotoxin, the effect of bradykinin was abolished in full-thickness preparations, whereas in preparations devoid of the muscle layer, the response was unaltered. This demonstrates that the reduction of the bradykinin-response in full-thickness preparations is not due to inhibiting influences of the myenteric plexus, but to the muscle layer forming a diffusion barrier for the kinin.
In human mucosa biopsies bradykinin as well as the B_2 agonist (but not the B_1 agonist) induced an ion and mucus secretion. This response was reduced in ulcerative colitis patients compared to control patients, showing that the bradykinin-system is most likely involved in ulcerative colitis. Tetrodotoxin partially inhibited the bradykinin-effect on both the ion and the mucus secretion, demonstrating a neuronal component of the bradykinin-response in the human mucosal biopsies.

These results demonstrate an involvement of bradykinin in the regulatory systems of the intestine, influencing the enteric nervous system, the intestinal muscle layer, as well as the ion and mucus secreting epithelium, which might, especially on the basis of an interaction of these systems, lead to the beneficial as well as hazardous effects of the inflammatory mediator bradykinin on intestinal functions.

6 Zusammenfassung

Bradykinin ist wichtiger Entzündungsmediator. Es wird angenommen, dass Bradykinin an der Entstehung von Durchfällen bei entzündlichen Darmerkrankungen beteiligt ist, indem es die gastrointestinale Motilität und die epitheliale Sekretion beeinflusst. In meiner PhD-Arbeit beschäftigte ich mich mit dem Einfluss dieses Kinins auf intestinale Funktionen und mit der Frage, inwiefern die unterschiedlichen durch Bradykinin beeinflussten Systeme, d.h. das enterische Nervensytem, die Motilität und die Sekretion, miteinander interagieren.
Daher untersuchte ich die Wirkung von Bradykinin auf myenterische Neurone und die intestinale Muskulatur der Ratte sowie auf das Colonepithel von Ratte und Mensch. Dazu wurden Microelectrode arrays, Ca^{2+}-Imaging, Immunfluoreszenztechniken, isometrische Kontraktionsmessungen und molekularbiologische Methoden eingesetzt.

Bradykinin induzierte eine biphasische Stimulation der myenterischen Neurone, die als Anstieg der Frequenz von Aktionspotentialen (gemessen mit Microelectrode arrays) oder als Anstieg der cytosolischen Ca^{2+}-Konzentration (gemessen mit Ca^{2+}-Imaging) erfasst wurde. Diese Wirkung wurde sowohl durch B_1- als auch B_2-Rezeptoren vermittelt, wobei der induzierbare B_1-Rezeptor unter Zellkulturbedingungen an den myenterischen Neuronen hochreguliert wurde. Diese Hochregulation wurde mittels Immunzytochemie und real time PCR bestätigt. Die Wirkung von Bradykinin war komplett von der Anwesenheit von Ca^{2+} im Nährmedium abhängig und beruht daher auf einem Einstrom von Ca^{2+} in die Zellen.

In intestinalen Längsmuskelpräparaten aus der Ratte induzierte Bradyinin eine biphasische Reaktion, bestehend aus einer Relaxation und einer darauffolgenden Kontraktion. Der Zeitverlauf dieser Antwort war stark vom jeweiligen intestinalen Segment abhängig. Das Neurotoxin Tetrodotoxin hatte keinerlei Einfluss auf die Bradykininantwort; daher erscheint es unwahrscheinlich, dass das enterische Nervensystem an diesem Effekt beteiligt ist. Die initiale Relaxation wurde durch Tetrapentylammonium, einen Blocker von Ca^{2+}-abhängigen K^+-Kanälen, gehemmt. In dissoziierten Muskelzellen induzierte Bradykinin einen Anstieg der cytosolischen Ca^{2+}-Konzentration. An frisch präparierten Muskelgeweben wurde die Antwort auf Bradykinin durch B_2-Rezeptoren vermittelt. Lediglich nach mehreren Stunden in vitro

Vorinkubation löste ein B_1-Agonist eine kontraktile Antwort aus. Diese Hochregulation des muskulären B_1-Rezeptors wurde sowohl mittels Immunfluoreszenz-Analyse der intakten Darmwand und von dissoziierten Muskelzellen als auch durch RT-PCR bestätigt. Nach konsekutiver Abtragung der verschiedenen Schichten der intestinalen Wand war die Wirkung von Bradykinin stark reduziert. Dies weist auf eine Beteiligung nicht-muskulärer Zellen bei der Vermittlung der Antwort auf diesen Entzündungsmediator hin.

In Ussingkammer-Versuchen mit Colongewebe von Mensch und Ratte induzierte Bradykinin eine Anionensekretion. Messungen, welche an der intakten Darmwand durchgeführt wurden, zeigten eine reduzierte Wirkung des B_2-Agonisten auf den Kurzschlussstrom im Vergleich zu Präparationen, in denen die Lamina muscularis entfernt worden war. In Anwesenheit von Tetrodotoxin war die Wirkung von Bradykinin an der intakten Darmwand unterdrückt. Diese starke Hemmung durch das Neurotoxin war nicht zu beobachten in Präparaten, in denen die Lamina muscularis entfernt worden war. Diese Beobachtung zeigt, dass die reduzierte Wirkung von Bradykinin an der intakten Darmwand kein Resultat von inhibierenden Einflüssen des myenterischen Plexus ist, sondern dass die Muskelschicht eine Diffusionsbarriere darstellt, die Bradykinin daran hindert, in ausreichender Konzentration die Epithelschicht zu erreichen, um dort eine Sekretion auszulösen.
In humanen Mucosabiopsien löste Bradykinin oder ein B_2-Rezeptor-Agonist (aber nicht ein B_1-Rezeptor-Agonist) eine Ionen- und Mukussekretion aus. Diese Reaktion war bei Patienten, die an Colitis ulcerosa erkrankt waren, stark vermindert, was auf eine Beteiligung des Kinin-Systems an dieser Erkrankung hinweist. Tetrodotoxin führte zu einer teilweisen Hemmung der Bradykinin-induzierten Ionen- und Mukussekretion, was nahelegt, dass der Wirkung des Kinins eine neuronale Komponente unterliegt.

Die Ergebnisse meiner PhD-Arbeit demonstrieren multiple Angriffsorte von Bradykinin in den regulatorischen Systemen des Gastrointestinaltrakts. Das Kinin beeinflusst sowohl das enterische Nervensystem als auch die intestinale Muskelschicht und das ionen- und mukussezernierende Epithel. Vor allem in Hinblick auf eine Interaktion dieser Systeme scheint der Entzündungsmediator Bradykinin eine zentrale Rolle beim Zustandekommen von Entzündungsreaktionen an diesem Organsystem zu spielen.

7 References

Abdel-Latif, A.A. 1986. Calcium-mobilizing receptors, polyphosphoinositides, and the generation of second messengers. *Pharmacol Rev* **38**, 227–272.

Akiba, Y., Furukawa, O., Guth, P.H., Engel, E., Nastaskin, I. & Kaunitz, J.D. 2001. Sensory pathways and cyclooxygenase regulate mucus gel thickness in rat duodenum. *Am J Physiol Gastrointest Liver Physiol* **280**, G470-G474.

Altinkurt, O. & Ozturk, Y. 1990. Bradykinin receptors in isolated rat duodenum. *Peptides* **11**, 39–44.

Andres, H., Rock, R., Bridges, R.J., Rummel, W., Schreiner, J. 1985. Submucosal plexus and electrolyte transport across rat colonic mucosa. *J Physiol* **364**, 301-312.

Arai, Y., Takanashi, H., Kitagawa, H., Wirth, K.J. & Okayasu, I. 1999. Effect of icatibant, a bradykinin B_2 receptor antagonist, on the development of experimental ulcerative colitis in mice. *Dig Dis Sci* **44**, 845–851.

Auerbach, L. 1864. Fernere vorläufige Mittheilung über den Nervenapparat des Darmes. *Virchows Arch. path. Anat. Physiol*. **30**, 457-460.

Avemary, J. & Diener, M. 2010a. Bradykinin-induced depolarisation and Ca^{2+} influx through voltage-gated Ca^{2+} channels in rat submucosal neurons. *Eur J Pharmacol* ***635***, 87–95.

Avemary, J. & Diener, M. 2010b. Effects of bradykinin B_2 receptor stimulation at submucosal ganglia from rat distal colon. *Eur J Pharmacol* ***627***, 295–303.

Baird, A.W., Skelly, M.M., O'Donoghue, D.P., Barrett, K.E. & Keely, S.J. 2008. Bradykinin regulates human colonic ion transport in vitro. *Br J Pharmacol* **155**, 558–566.

Barrett, K.E. & Keely, S.J. 2000. Chloride secretion by the intestinal epithelium: molecular basis and regulatory aspects. *Annu Rev Physiol* **62**, 535–572.

Bayliss, W.M. & Starling, E.H. 1899. The movements and innervation of the small intestine. *J Physiol* **24**, 99–143.

Berkefeld, H., Fakler, B. & Schulte, U. 2010. Ca^{2+}-activated K^+ channels: from protein complexes to function. *Physiol Rev* **90**, 1437–1459.

Bertrand, C.A., Durand, D.M., Saidel, G.M., Laboisse, C. & Hopfer, U. 1998. System for dynamic measurements of membrane capacitance in intact epithelial monolayers. *Biophys J* **75**, 2743–2756.

Bertrand, C.A., Laboisse, C.L. & Hopfer, U. 1999. Purinergic and cholinergic agonists induce exocytosis from the same granule pool in HT29-Cl.16E monolayers. *Am J Physiol* **276**, C907-C914.

Binder, H.J., Sandle, G.J., Rajendran, V.M. 1991. Colonic fluid and electrolyte transport in health and disease. The large intestine: physiology, pathophysiology and disease. Ed.: S.F. Phillips, J.D. Hermberton, R.G. Shorter, Raven Press, New York, 141 – 168.

Binder, H.J., Sandle, G.J. 1994. Electrolyte transport in the mammalian colon, The large intestine: physiology, pathophysiology and disease. Ed.: S.F. Phillips, J.D. Hermberton, R.G. Shorter, Raven Press, New York, 2133 – 2171.

Boeynaems, J.-M. & Communi, D. 2006. Modulation of inflammation by extracellular nucleotides. *J Invest Dermatol* **126**, 943–944.

Boschcov, P., Paiva, A.C., Paiva, T.B. & Shimuta, S.I. 1984. Further evidence for the existence of two receptor sites for bradykinin responsible for the diphasic effect in the rat isolated duodenum. *Br J Pharmacol* **83**, 591–600.

Bours, M.J.L., Swennen, E.L.R., Di Virgilio, F., Cronstein, B.N. & Dagnelie, P.C. 2006. Adenosine 5'-triphosphate and adenosine as endogenous signaling molecules in immunity and inflammation. *Pharmacol Ther* **112**, 358–404.

Bouthillier, J., Deblois, D. & Marceau, F. 1987. Studies on the induction of pharmacological responses to des-Arg^9-bradykinin in vitro and in vivo. *Br J Pharmacol* **92**, 257–264.

Bowen, R. 1996. Electrophysiology of gastrointestinal smooth muscle. http://www.vivo.colostate.edu/hbooks/pathphys/digestion/basics/slowwaves.html

Bramley, A.M., Samhoun, M.N. & Piper, P.J. 1990. The role of the epithelium in modulating the responses of guinea-pig trachea induced by bradykinin in vitro. *Br J Pharmacol* **99**, 762–766.

Bridges, R.J., Rack, M., Rummel, W. & Schreiner, J. 1986. Mucosal plexus and electrolyte transport across the rat colonic mucosa. *J Physiol* **376**, 531–542.

Cajal, S.R.Y. 1911. Histologie du système nerveux de l'homme et des vertébrés. Maloine, Paris.

Calixto, J.B. 1995. Multiple mechanisms of bradykinin-induced contraction in rat and guinea pig smooth muscles in vitro. *Eur J Pharmacol* **281**, 279–288.

Calixto, J.B., Medeiros, R., Fernandes, E.S., Ferreira, J., Cabrini, D.A. & Campos, M.M. 2004. Kinin B_1 receptors: key G-protein-coupled receptors and their role in inflammatory and painful processes. *Br J Pharmacol* **143**, 803–818.

Carty, T.J., Eskra, J.D., Lombardino, J.G. & Hoffman, W.W. 1980. Piroxicam, a potent inhibitor of prostaglandin production in cell culture. Structure-activity study. *Prostaglandins* **19**, 51–59.

Catterall, W.A. 1980. Neurotoxins that act on voltage-sensitive sodium channels in excitable membranes. *Annu Rev Pharmacol Toxicol* **20**, 15–43.

Catterall, W.A., Perez-Reyes, E., Snutch, T.P., Striessnig, J., 2005. International Union of Pharmacology. XLVIII. Nomenclature and structure-function relationships of voltage-gated calcium channels. *Pharmacol Rev* **57**, 411-425.

Chien, C.B. & Pine, J. 1991. An apparatus for recording synaptic potentials from neuronal cultures using voltage-sensitive fluorescent dyes. *J Neurosci Methods* **38**, 93–105.

Clinton, S.K., Fleet, J.C., Loppnow, H., Salomon, R.N., Clark, B.D., Cannon, J.G., Shaw, A.R., Dinarello, C.A. & Libby, P. 1991. Interleukin-1 gene expression in rabbit vascular tissue in vivo. *Am J Pathol* **138**, 1005–1014.

Cooke, H.J. 1991. Regulation of the colonic transport by the autonomic nervous system. The large intestine: physiology, pathophysiology and disease. Ed.: S.F. Phillips, J.D. Hermberton, R.G. Shorter, Raven Press, New York, 169 – 179.

Coons, A.H. 1958. Fluorescent antibody methods. *Gen Cytochem Methods* **1**, 399–422.

Cuthbert, A.W., Halushka, P.V., Margolius, H.S. & Spayne, J.A. 1984a. Mediators of the secretory response to kinins. *Br J Pharmacol* **82**, 597–607.

Cuthbert, A.W., Halushka, P.V., Margolius, H.S. & Spayne, J.A. 1984b. Role of calcium ions in kinin-induced chloride secretion. *Br J Pharmacol* **82**, 587–595.

Cuthbert, A.W. & Margolius, H.S. 1982. Kinins stimulate net chloride secretion by the rat colon. *Br J Pharmacol* **75**, 587–598.

Devani, M., Vecchi, M., Ferrero, S., Contessini Avesani, E., Arizzi, C., Chao, L., Colman, R.W. & Cugno, M. 2005. Kallikrein-kinin system in inflammatory bowel diseases: Intestinal involvement and correletion with the degree of tissue inflammation. *Dig Liver Dis **37**,* 665–673.

Diener, M., Bridges, R.J., Knobloch, S.F. & Rummel, W. 1988. Indirect effects of bradykinin on ion transport in rat colon descendens: mediated by prostaglandins and enteric neurons. *Naunyn Schmiedebergs Arch Pharmacol* **337**, 69–73.

Diener, M. & Gabato, D. 1994. Thromboxane-like actions of prostaglandin D_2 on the contractility of the rat colon in vitro. *Acta Physiol Scand* **150**, 95–101.

Diener, M., Knobloch, S.F., Bridges, R.J., Keilmann, T. & Rummel, W. 1989. Cholinergic-mediated secretion in the rat colon: neuronal and epithelial muscarinic responses. *Eur J Pharmacol* **168**, 219–229.

Diener, M., Nobles, M. & Rummel, W. 1992. Activation of basolateral Cl^- channels in the rat colonic epithelium during regulatory volume decrease. *Pflugers Arch* **421**, 530–538.

Dogiel, A.S. 1899. Über den Bau der Ganglien in den Geflechten des Darmes und der Gallenblase des Menschen und der Säugetiere. *Arch Anat Physiol Anat Abt*, 130–158.

Droge, M.H., Gross, G.W., Hightower, M.H. & Czisny, L.E. 1986. Multielectrode analysis of coordinated, multisite, rhythmic bursting in cultured CNS monolayer networks. *J Neurosci* **6**, 1583–1592.

Ehrlein, H. 2010. Motorik des Dünndarms, In: Physiologie der Haustiere. 3. Edition, Ed.: Engelhardt W. von, Breves G., Enke im Hippokrates Verlag, Stuttgart, 365 – 372.

Eigenbrod, T., Park, J.-H., Harder, J., Iwakura, Y. & Nunez, G. 2008. Cutting edge: critical role for mesothelial cells in necrosis-induced inflammation through the recognition of IL-1 alpha released from dying cells. *J Immunol* **181**, 8194–8198.

Elliott, D.F., Horton, E.W. & Lewis, G.P. 1960. Actions of pure bradykinin. *J Physiol* **153**, 473–480.

Farmer, S.G. & Burch, R.M. 1992. Biochemical and molecular pharmacology of kinin receptors. *Annu Rev Pharmacol Toxicol* **32**, 511–536.

Feres, T., Paiva, A.C. & Paiva, T.B. 1992. BK_1 and BK_2 bradykinin receptors in the rat duodenum smooth muscle. *Br J Pharmacol* **107**, 991–995.

Field, M. & Semrad, C.E. 1993. Toxigenic diarrheas, congenital diarrheas, and cystic fibrosis: disorders of intestinal ion transport. *Annu Rev Physiol* **55**, 631–655.

Furchgott, R.F. & Zawadzki, J.V. 1980. The obligatory role of endothelial cells in the relaxation of arterial smooth muscle by acetylcholine. *Nature* **288**, 373–376.

Furness, J.B. 2006. In: The Enteric Nervous System. Blackwell Publishing, Oxford.

Garcia, M.A.S., Yang, N. & Quinton, P.M. 2009. Normal mouse intestinal mucus release requires cystic fibrosis transmembrane regulator-dependent bicarbonate secretion. *J Clin Invest* **119**, 2613–2622.

Gelperin, D., Mann, D., Del Valle, J. & Wiley, J.W. 1994. Bradykinin (Bk) increases cytosolic calcium in cultured rat myenteric neurons via Bk-2 receptors coupled to mobilization of extracellular and intracellular sources of calcium: evidence that calcium influx is prostaglandin dependent. *J Pharmacol Exp Ther* **271**, 507–514.

Green, B.T., Calvin, A., O'Grady, S.M. & Brown, D.R. 2003. Kinin-induced anion-dependent secretion in porcine ileum: characterization and involvement of opioid- and cannabinoid-sensitive enteric neural circuits. *J Pharmacol Exp Ther* **305**, 733–739.

Griesbacher, T. 1992. Kinin-induced relaxations of the rat duodenum. *Naunyn Schmiedebergs Arch Pharmacol* **346**, 102–107.

Gross, G.W. & Schwalm, F.U. 1994. A closed flow chamber for long-term multichannel recording and optical monitoring. *J Neurosci Methods* **52**, 73–85.

Grubb, B.R. & Gabriel, S.E. 1997. Intestinal physiology and pathology in gene-targeted mouse models of cystic fibrosis. *Am J Physiol* **273**, G258-G266.

Gustafsson, J.K., Hansson, G.C. & Sjövall, H. 2012. Ulcerative colitis patients in remission have an altered secretory capacity in the proximal colon despite macroscopically normal mucosa. *Neurogastroenterol Motil* **24**, 381-391.

Hall, D.W. & Bonta, I.L. 1973. The biphasic response of the isolated guinea-pig ileum by bradykinin. *Eur J Pharmacol* **21**, 147–154.

Hall, J.M. & Morton, I.K. 1991. Bradykinin B_2 receptor evoked K^+ permeability increase mediates relaxation in the rat duodenum. *Eur J Pharmaco* **193**, 231–238.

Hallam, T.J., Jacob, R., Merritt, J.E. 1988. Evidence that agonists stimulate bivalent cation influx into human endothelial cells. *Biochem J* **255**, 179-184.

Halm, D.R. & Halm, S.T. 2000. Secretagogue response of goblet cells and columnar cells in human colonic crypts. *Am J Physiol Cell Physiol* **278**, C212-C233.

Halm, D.R., Halm, S.T., DiBona, D.R., Frizzell, R.A. & Johnson, R.D. 1995. Selective stimulation of epithelial cells in colonic crypts: relation to active chloride secretion. *Am J Physiol* **269**, C929-C942.

Hamill, O.P. & McBride Jr. D. W. 1996. Pharmacology of mechanogated membrane ion channels. *Pharmcol Rev **48***, 231–252.

Hansen, M.B. 2003a. The Enteric Nervous System I: Organisation and Classification. *Pharmacol Toxicol **92***, 105–113.

Hansen, M.B. 2003b. The Enteric Nervous System II: Gastrointestinal Functions. *Pharmacol Toxicol* ***92***, 249–257.

Hara, D.B., Leite, D.F., Fernandes, E.S., Passos, G.F., Guimaraes, A.O., Pesquero, J.B., Campos, M.M. & Calixto, J.B. 2008. The relevance of kinin B_1 receptor upregulation in a mouse model of colitis. *Br J Pharmacol* **154**, 1276–1286.

Hara, D., Fernandes, E., Campos, M. & Calixto, J. 2007. Pharmacological and biochemical characterization of bradykinin B_2 receptors in the mouse colon: influence of the TNBS-induced colitis. *Regul Pept* **141**, 25–34.

Harlow, E., Lane, D. 1988. Antibodies – A labatory manual. Cold Spring Harbour Laboratory Press, Cold Spring Harbour, New York.

Hemlin, M., Jodal, M., Lundgren, O., Sjövall, H. & Stage, L. 1988. The importance of the subepithelial resistance for the electrical properties of the rat jejunum in vitro. *Acta Physiol Scand* **134**, 79–88.

Hirst, G.D. & McKirdy, H.C. 1974. A nervous mechanism for descending inhibition in guinea-pig small intestine. *J Physiol* **238**, 129–143.

Hsieh, H.-L., Wang, H.-H., Wu, C.-Y., Jou, M.-J., Yen, M.-H., Parker, P. & Yang, C.-M. 2007. BK-induced COX-2 expression via PKC-delta-dependent activation of p42/p44 MAPK and NF-kappaB in astrocytes. *Cell Signal* **19**, 330–340.

Hu, H.-Z., Gao, N., Liu, S., Ren, J., Wang, X., Xia, Y. & Wood, J.D. 2004a. Action of bradykinin in the submucosal plexus of guinea pig small intestine. P*harmacol Exp Ther* ***309***, 320–327.

Hu, H.-Z., Gao, N., Liu, S., Ren, J., Xia, Y. & Wood, J.D. 2004b. Metabotropic signal transduction for bradykinin in submucosal neurons of guinea pig small intestine. *J Pharmacol Exp Ther* **309**, 310–319.

Hu, H.-Z., Liu, S., Gao, N., Xia, Y., Mostafa, R., Ren, J., Zafirov, D.H. & Wood, J.D. 2003. Actions of bradykinin on electrical and synaptic behavior of neurones in the myenteric plexus of guinea-pig small intestine. *Br J Pharmacol* ***138***, 1221–1232.

Huber, K. 2010. Muskulatur. Physiologie der Haustiere. 3. Edition, Ed.: Engelhardt W. von, Breves G., Enke im Hippokrates Verlag, Stuttgart, 118 – 140.

Ikuma, M., Geibel, J., Binder, H.J. & Rajendran, V.M. 2003. Characterization of Cl-HCO_3 exchange in basolateral membrane of rat distal colon. *Am J Physiol Cell Physiol* **285**, C912-C921.

Isgar, B., Harman, M., Kaye, M.D. & Whorwell, P.J. 1983. Symptoms of irritable bowel syndrome in ulcerative colitis in remission. *Gut* **24**, 190–192.

Ishimoto, H., Matsuoka, I., Nakanishi, H. & Nakahata, N. 1996. A comparative study of arachidonic acid metabolism in rabbit cultured astrocytes and human astrocytoma cells (1321N1). *Gen Pharmacol* **27**, 313–317.

Isordia-Salas, I., Pixley, R.A., Li, F., Sainz, I., Sartor, R.B., Adam, A. & Colman, R.W. 2002. Kininogen deficiency modulates chronic intestinal inflammation in genetically susceptible rats. *Am J Physiol Gastrointest Liver Physiol* **283**, G180-G186.

Jessen, K.R., Saffrey, M.J. & Burnstock, G. 1983. The enteric nervous system in tissue culture. I. Cell types and their interactions in explants of the myenteric and submucous plexuses from guinea pig, rabbit and rat. *Brain Res* **262**, 17–35.

Jobling, D.T., Smith, J.G. & Wheal, H.V. 1981. Active microelectrode array to record from the mammalian central nervous system in vitro. *Med Biol Eng Comput* **19**, 553–560.

Jodal, M., Holmgren, S., Lundgren, O. & Sjoqvist, A. 1993. Involvement of the myenteric plexus in the cholera toxin-induced net fluid secretion in the rat small intestine. *Gastroenterology* **105**, 1286–1293.

Kachur, J.F., Keshavarzian, A., Sundaresan, R., Doria, M., Walsh, R., las Alas, M.M. de & Gaginella, T.S. 1995. Colitis reduces short-circuit current response to inflammatory mediators in rat colonic mucosa. *Inflammation* **19**, 245–259.

Kamat, K., Hayashi, I., Mizuguchi, Y., Arai, K., Saeki, T., Ohno, T., Saigenji, K. & Majima, M. 2002. Suppression of dextran sulfate sodium-induced colitis in kininogen-deficient rats and non-peptide B_2 receptor antagonist-treated rats. *Jpn J Pharmacol* **90**, 59–66.

Kato, M., Nishida, S., Kitasato, H., Sakata, N. & Kawai, S. 2001. Cyclooxygenase-1 and cyclooxygenase-2 selectivity of non-steroidal anti-inflammatory drugs: investigation using human peripheral monocytes. *J Pharm Pharmacol* **53**, 1679–1685.

Kockerling, A. & Fromm, M. 1993. Origin of cAMP-dependent Cl^- secretion from both crypts and surface epithelia of rat intestine. *Am J Physiol* **264**, C1294-C1301.

Koh, S.D., Ward, S.M. & Sanders, K.M. 2012. Ionic conductances regulating the excitability of colonic smooth muscles. *Neurogastroenterol Motil* **24**, 705–718.

Kramer, K., da Silveira, A.B.M., Jabari, S., Kressel, M., Raab, M. & Brehmer, A. 2011. Quantitative evaluation of neurons in the mucosal plexus of adult human intestines. *Histochem Cell Biol* **136**, 1–9.

Kunzelmann, K. & Mall, M. 2002. Electrolyte transport in the mammalian colon: mechanisms and implications for disease. *Physiol Rev* **82**, 245–289.

Kunze, W.A. & Furness, J.B. 1999. The enteric nervous system and regulation of intestinal motility. *Annu Rev Physiol* **61**, 117–142.

Lacinova, L. 2005. Voltage-dependent calcium channels. *Gen Physiol Biophys* **24**, 1–78.

Leeb-Lundberg, L.M.F. 2005. International Union of Pharmacology. XLV. Classification of the kinin receptor family: from molecular mechanisms to pathophysiological consequences. *Pharmacol Rev* **57**, 27–77.

Leibig et al., in: Proceedings of the 8th International Meeting on Substrate-Integrated Micro Electrode Arrays, 2012, Reutlingen, Germany, 236-237.

Lewis, J.D., Chuai, S., Nessel, L., Lichtenstein, G.R., Aberra, F.N. & Ellenberg, J.H. 2008. Use of the noninvasive components of the Mayo score to assess clinical response in ulcerative colitis. *Inflamm Bowel Dis* **14**, 1660–1666.

Lindqvist, S.M., Sharp, P., Johnson, I.T., Satoh, Y. & Williams, M.R. 1998. Acetylcholine-induced calcium signaling along the rat colonic crypt axis. *Gastroenterology* **115**, 1131–1143.

Lister, J. 1858. Preliminary account of an inquiry into the functions of the visceral nerves, with special reference to the socalled 'inhibitory system'. *Proc. R. Soc. Lond.* **9**: 367–380.

Liu, B., Luo, W., Zhang, Y., Li, H., Zhu, N., Huang, D. & Zhou, Y. 2012. Role of cyclooxygenase-1-mediated prostacyclin synthesis in endothelium-dependent vasoconstrictor activity of porcine interlobular renal arteries. *Am J Physiol Renal Physiol* **302**, F1133-F1140.

Lomax, A.E. & Furness, J.B. 2000. Neurochemical classification of enteric neurons in the guinea-pig distal colon. *Cell Tissue Res* **302**, 59–72.

Lyster, D.J., Bywater, R.A. & Taylor, G.S. 1995. Neurogenic control of myoelectric complexes in the mouse isolated colon. *Gastroenterology* **108**, 1371–1378.

Maguire, D., MacNamara, B., Cuffe, J.E., Winter, D., Doolan, C.M., Urbach, V., O' Sullivan, G.C., Harvey, B.J. 1999. Rapid responses to aldosterone in human distal colon. Steroids **64**, 51-63.

Maher, M.P., Pine, J., Wright, J. & Tai, Y.C. 1999. The neurochip: a new multielectrode device for stimulating and recording from cultured neurons. *J Neurosci Meth **87***, 45–56.

Marconi, E., Nieus, T., Maccione, A., Valente, P., Simi, A., Messa, M., Dante, S., Baldelli, P., Berdondini, L. & Benfenati, F. 2012. Emergent functional properties of neuronal networks with controlled topology. *PLoS One* **7**, e34648.

Maroto, R., Raso, A., Wood, T.G., Kurosky, A., Martinac, B. & Hamill, O.P. 2005. TRPC1 forms the stretch-activated cation channel in vertebrate cells. *Nature cell biology*, 179–185.

Maruyama, T., Kanaji, T., Nakade, S., Kanno, T., and Mikoshiba, M 1997. 2-APB, 2-aminoethoxydiphenyl borate, a membrane-penetrable modulator of Ins(1,4,5)P_3-induced Ca^{2+} release. *J Biochem* **122**: 498-505.

Mayer, B., Brunner, F. & Schmidt, K. 1993. Inhibition of nitric oxide synthesis by methylene blue. *Biochem Pharmacol* **45**, 367–374.

Mazzuoli, G. & Schemann, M. 2009. Multifunctional rapidly adapting mechanosensitive enteric neurons (RAMEN) in the myenteric plexus of the guinea pig ileum. *J Physiol* **587**, 4681–4694.

McNamara, B., Winter, D.C., Cuffe, J.E., O'Sullivan, G.C. & Harvey, B.J. 1999. Basolateral K^+ channel involvement in forskolin-activated chloride secretion in human colon. *J Physiol* **519**, 251–260.

Medert, R., Schuster, A., Schwarz, L.K., Schwab, T., Schaefer, K.H. 2013. Spiking rate of myenteric neurons recorded from multi-electrode arrays depending on local microenvironment. *Phys. Status Solidi,* in press.

Mestres, P., Diener, M. & Rummel, W. 1992a. Electron microscopy of the mucosal plexus of the rat colon. *Acta Anat* **143**, 275–282.

Mestres, P., Diener, M. & Rummel, W. 1992b. Histo- and immunocytochemical characterization of the neurons of the mucosal plexus in the rat colon. *Acta Anat* **143**, 268–274.

Michel, K., Reiche, D. & Schemann, M. 2000. Projections and neurochemical coding of motor neurones to the circular and longitudinal muscle of the guinea pig gastric corpus. *Pflugers Arch* **440**, 393–408.

Morgado, M., Cairrao, E., Santos-Silva, A.J. & Verde, I. 2012. Cyclic nucleotide-dependent relaxation pathways in vascular smooth muscle. Cell Mol Life Sci **69**, 247-266.

Morin, F.O., Takamura, Y. & Tamiya, E. 2005. Investigating neuronal activity with planar microelectrode arrays: achievements and new perspectives. *J Biosci Bioeng* **100**, 131–143.

Mostafa, R.-M., Moustafa, Y. & Hamdy, H. 2010. Interstitial cells of Cajal, the Maestro in health and disease. *World J Gastroenterol* **16**, 3239–3248.

Moussion, C., Ortega, N. & Girard, J.-P. 2008. The IL-1-like cytokine IL-33 is constitutively expressed in the nucleus of endothelial cells and epithelial cells in vivo: a novel 'alarmin'? *PLoS One* **3**, e3331.

Müller, L.R. 1920. Das vegetative Nervensystem. Springer, Berlin.

Murakami, M., Ohta, T. & Ito, S. 2008. Interleukin-1beta enhances the action of bradykinin in rat myenteric neurons through up-regulation of glial B_1 receptor expression. *Neuroscience* **151**, 222–231.

Murakami, M., Ohta, T. & Ito, S. 2009. Lipopolysaccharides enhance the action of bradykinin in enteric neurons via secretion of interleukin-1beta from enteric glial cells. *J Neurosci Res* **87**, 2095–2104.

Murakami, M., Ohta, T., Otsuguro, K.-I. & Ito, S. 2007. Involvement of prostaglandin E_2 derived from enteric glial cells in the action of bradykinin in cultured rat myenteric neurons. *Neuroscience* **145**, 642–653.

Musch, M.W., Kachur, J.F., Miller, R.J., Field, M. & Stoff, J.S. 1983. Bradykinin-stimulated electrolyte secretion in rabbit and guinea pig intestine. Involvement of arachidonic acid metabolites. *J Clin Invest* **71**, 1073–1083.

Nagaki, M., Shimura, S., Irokawa, T., Sasaki, T., Oshiro, T., Nara, M., Kakuta, Y. & Shirato, K. 1996. Bradykinin regulation of airway submucosal gland secretion: role of bradykinin receptor subtype. *Am J Physiol* **270**, L907-L913.

Negishi, T., Ishii, Y., Kyuwa, S., Kuroda, Y. & Yoshikawa, Y. 2003. Primary culture of cortical neurons, type-1 astrocytes, and microglial cells from cynomolgus monkey (Macaca fascicularis) fetuses. *J Neurosci Methods* **131**, 133–140.

Nishi, R. & Willard, A.L. 1985. Neurons dissociated from rat myenteric plexus retain differentiated properties when grown in cell culture. I. Morphological properties and immunocytochemical localization of transmitter candidates. *Neuroscience* **16**, 187–199.

Nishimura, J. 2006. Topics on the Na^+/Ca^{2+} exchanger: Involvement of Na^+/Ca^{2+} exchanger in the vasodilator-induced vasorelaxation. J Pharmacol Sci **102**, 27-31.

Ozturk, Y., Altan, V.M., Yidizoglu-Ari, N. & Altinkurt, O. 1993. Bradykinin receptors in intestinal smooth muscles and their post-receptor events related to calcium. *Mediators Inflamm* **2**, 309–315.

Paiva, A.C., Paiva, T.B., Pereira, C.C. & Shimuta, S.I. 1989. Selectivity of bradykinin analogues for receptors mediating contraction and relaxation of the rat duodenum. *Br J Pharmacol* **98**, 206–210.

Paton, W.D. & Zar M.A. 1968. The origin of acetylcholine released from guinea-pig intestine and longitudinal muscle strips. *J Physiol* **194**, 13–33.

Perkins, M.N., Forster, P.L. & Dray, A. 1988. The involvement of afferent nerve terminals in the stimulation of ion transport by bradykinin in rat isolated colon. *Br J Pharmacol* **94**, 47–54.

Pfannkuche, H., Reiche, D., Firzlaff, U., Sann, H. & Schemann, M. 1998. Enkephalin-immunoreactive subpopulations in the myenteric plexus of the guinea-pig fundus project primarily to the muscle and not to the mucosa. *Cell Tissue Res* **294**, 45–55.

Phillips, J.A. & Hoult, J.R. 1988. Secretory effects of kinins on colonic epithelium in relation to prostaglandins released from cells of the lamina propria. *Br J Pharmacol* **95**, 701–712.

Pine, J. 1980. Recording action potentials from cultured neurons with extracellular microcircuit electrodes. *J Neurosci Methods* **2**, 19–31.

Pine, J. 2006. A history of MEA development, In: Advances in network electrophysiology, Ed.: Taketani, M., Baudry, M., Springer Science and Buisiness Media, New York, 3-23.

Pizard, A., Marchetti, J., Allegrini, J., Alhenc-Gelas, F. & Rajerison, R.M. 1998. Negative cooperativity in the human bradykinin B_2 receptor. *J Biol Chem* **273**, 1309–1315.

Potten, C.S., Booth, C. & Pritchard, D.M. 1997. The intestinal epithelial stem cell: the mucosal governor. *Int J Exp Pathol* **78**, 219–243.

Potter, S.M. & DeMarse, T.B. 2001. A new approach to neural cell culture for long-term studies. *J Neurosci Methods* **110**, 17–24.

Poulsen, J.H., Fischer, H., Illek, B. & Machen, T.E. 1994. Bicarbonate conductance and pH regulatory capability of cystic fibrosis transmembrane conductance regulator. *Proc Natl Acad Sci USA* **91**, 5340–5344.

Prado GN, Taylor L, Zhou X, Ricupero, D., Mierke, D.F. & Polgar P 2002. Mechanisms regulating the expression, self-maintenance, and signaling-function of the bradykinin B_2 and B_1 receptors. *J Cell Physiol* **193**, 275–286.

Ragy, M. & Elbassuoni, E. 2012. The role of nitric oxide and L-type calcium channel blocker in the contractility of rabbit ileum in vitro. *J Physiol Biochem* **68**, 521–528.

Rainsford K.D., 1975. Inhibitors of eicosanoid metabolism. In: Prostaglandins: Biology and chemistry of prostaglandins and related eicosanoids, Ed.: Curtis-Prior PB, Churchill Livingstone, Edinburg, 52-68.

Rees, D.D., Palmer, R.M., Schulz, R., Hodson, H.F. & Moncada, S. 1990. Characterization of three inhibitors of endothelial nitric oxide synthase in vitro and in vivo. *Br J Pharmacol* **101**, 746–752.

Regoli, D. & Barabe, J. 1980. Pharmacology of bradykinin and related kinins. *Pharmacol Rev* **32**, 1–46.

Regoli, D., Marceau, F. & Barabe, J. 1978. De novo formation of vascular receptors for bradykinin. *Can J Physiol Pharmacol* **56**, 674–677.

Rehn, M. & Diener, M. 2012. Cysteinyl leukotrienes mediate the response of submucosal ganglia from rat colon to bradykinin. *Eur J Pharmacol* **681**, 100–106.

Rescigno, M. 2008. Don't forget to have a second brain. *Muc Immunol* **1**, 328–329.

Rhaleb, N.E. & Carretero, O.A. 1994. Role of B_1 and B_2 receptors and of nitric oxide in bradykinin-induced relaxation and contraction of isolated rat duodenum. *Life Sci* **55**, 1351–1363.

Sanders, K.M. 2008. Regulation of smooth muscle excitation and contraction. *Neurogastroenterol Motil* **20**, 39–53.

Sardi, S.P. 2002. Further pharmacological evidence of nuclear factor-kappa B pathway involvement in bradykinin B_1 receptor-sensitized responses in human umbilical vein. *J Pharmacol Exp Ther* **301**, 975–980.

Sardi, S.P., Ares, V.R., Errasti, A.E. & Rothlin, R.P. 1998. Bradykinin B_1 receptors in human umbilical vein: pharmacological evidence of up-regulation, and induction by interleukin-1 beta. *Eur J Pharmacol* **358**, 221–227.

Sardi, S.P., Daray, F.M., Errasti, A.E., Pelorosso, F.G., Pujol-Lereis, V.A., Rey-Ares, V., Rogines-Velo, M.P. & Rothlin, R.P. 1999. Further pharmacological characterization of bradykinin B_1 receptor up-regulation in human umbilical vein. *J Pharmacol Exp Ther* **290**, 1019–1025.

Sartor, R.B., DeLa Cadena, R.A., Green, K.D., Stadnicki, A., Davis, S.W., Schwab, J.H., Adam, A.A., Raymond, P. & Colman, R.W. 1996. Selective kallikrein-kinin system activation in inbred rats differentially susceptible to granulomatous enterocolitis. *Gastroenterology* **110**, 1467–1481.

Schäfer, K.H., Hänsgen, A. & Mestres, P. 1999. Morphological changes of the myenteric plexus during early postnatal development of the rat. *Anat Rec* **256**, 20–28.

Schäfer, K.H., Saffrey, M.J., Burnstock, G. & Mestres-Ventura, P. 1997. A new method for the isolation of myenteric plexus from the newborn rat gastrointestinal tract. *Brain Res Brain Res Protoc* **1**, 109–113.

Scheibner, K.A., Lutz, M.A., Boodoo, S., Fenton, M.J., Powell, J.D. & Horton, M.R. 2006. Hyaluronan fragments act as an endogenous danger signal by engaging TLR2. *J Immunol* **177**, 1272–1281.

Schemann, M., Schaaf, C. & Mader, M. 1995. Neurochemical coding of enteric neurons in the guinea pig stomach. *J Comp Neurol* **353**, 161–178.

Schemann, M. 2000: Enterisches Nervensystem und Innervation des Magen-Darm-Traktes, In: Physiologie der Haustiere. 3. Edition, Ed.: Engelhardt W. von, Breves G., Enke im Hippokrates Verlag, Stuttgart.

Schlemper, V. & Calixto, J.B. 1994. Nitric oxide pathway-mediated relaxant effect of bradykinin in the guinea-pig isolated trachea. *Br J Pharmacol* **111**, 83–88.

Schultheiss, G., Lan Kocks, S. & Diener, M. 2002a. Methods for the study of ionic currents and Ca^{2+}-signals in isolated colonic crypts. *Biol Proced Online* **3**, 70–78.

Schultheiss, G., Seip, G., Kocks, S.L. & Diener, M. 2002b. Ca^{2+}-dependent and -independent Cl^- secretion stimulated by the nitric oxide donor, GEA 3162, in rat colonic epithelium. *Eur J Pharmacol* **444**, 21–30.

See, N.A. & Bass, P. 1993. Glucose-induced ion secretion in rat jejunum: a mucosal reflex that requires integration by the myenteric plexus. *J Auton Nerv Syst* **42**, 33–40.

Shi, Y., Evans, J.E. & Rock, K.L. 2003. Molecular identification of a danger signal that alerts the immune system to dying cells. *Nature* **425**, 516–521.

Simren, M., Axelsson, J., Gillberg, R., Abrahamsson, H., Svedlund, J. & Bjornsson, E.S. 2002. Quality of life in inflammatory bowel disease in remission: the impact of IBS-like symptoms and associated psychological factors. *Am J Gastroenterol* **97**, 389–396.

Sjövall, H. 1984. Evidence for separate sympathetic regulation of fluid absorption and blood flow in the feline jejunum. *Am J Physiol* **247**, G510-4.

Spassova, M.A., Soboloff, J., He, L.-P., Hewavitharana, T., Xu, W., Venkatachalam, K., van Rossum, D.B., Patterson, R.L. & Gill, D.L. 2004. Calcium entry mediated by SOCs and TRP channels: variations and enigma. *Biochim Biophys Acta* **1742**, 9–20.

Specht, W. 1977. Morphology of the intestinal wall, Intestinal permeation, Ed.: F. Lauterbach, Amsterdam, Oxford: Excerpta medica, 4 – 40.

Specian, R.D. & Oliver, M.G. 1991. Functional biology of intestinal goblet cells. *Am J Physiol* **260**, C183-C193.

Stadnicki, A., Chao, J., Stadnicka, I., van Tol, E., Lin, K.F., Li, F., Sartor, R.B. & Colman, R.W. 1998a. Localization and secretion of tissue kallikrein in peptidoglycan-induced enterocolitis in Lewis rats. *Am J Physiol* **275**, G854-G861.

Stadnicki, A., DeLa Cadena, R.A., Sartor, R.B., Bender, D., Kettner, C.A., Rath, H.C., Adam, A. & Colman, R.W. 1996. Selective plasma kallikrein inhibitor attenuates acute intestinal inflammation in Lewis rat. *Dig Dis Sci* **41**, 912–920.

Stadnicki, A., Mazurek, U., Gonciarz, M., Plewka, D., Nowaczyk, G., Orchel, J., Pastucha, E., Plewka, A., Wilczok, T. & Colman, R.W. 2003a. Immunolocalization and expression of kallistatin and tissue kallikrein in human inflammatory bowel disease. *Dig Dis Sci* **48**, 615–623.

Stadnicki, A., Mazurek, U., Plewka, D. & Wilczok, T. 2003b. Intestinal tissue kallikrein-kallistatin profile in inflammatory bowel disease. *Int Immunopharmacol* **3**, 939–944.

Stadnicki, A., Pastucha, E., Nowaczyk, G., Mazurek, U., Plewka, D., Machnik, G., Wilczok, T. & Colman, R.W. 2005. Immunolocalization and expression of kinin B_1R and B_2R receptors in human inflammatory bowel disease. *Am J Physiol Gastrointest Liver Physiol* **289**, G361-G366.

Stadnicki, A., Sartor, R.B., Janardham, R., Stadnicka, I., Adam, A.A., Blais, C. & Colman, R.W. 1998b. Kallikrein-kininogen system activation and bradykinin B_2 receptors in indomethacin induced enterocolitis in genetically susceptible Lewis rats. *Gut* **43**, 365–374.

Stanley, C.M. & Phillips, T.E. 1994. Bradykinin modulates mucin secretion but not synthesis from an intestinal goblet cell line. *Agents Act* **42**, 141–145.

Strabel, D., Diener, M. 1995. Evidence against direct activation of chloride secretion by carbachol in the rat distal colon. Eur J Pharmacol **274**, 181-191.

Strober, W., Fuss, I. & Mannon, P. 2007. The fundamental basis of inflammatory bowel disease. *J Clin Invest* **117**, 514–521.

Takasaki, J., Saito, T., Taniguchi, M., Kawasaki, T., Moritani, Y., Hayashi, K. & Kobori, M. 2004. A novel Gαq/11-selective inhibitor. *J Biol Chem* **279**, 47438–47445.

Tanious, F.A., Veal, J.M., Buczak, H., Ratmeyer, L.S. & Wilson, W.D. 1992. DAPI (4',6-diamidino-2-phenylindole) binds differently to DNA and RNA: minor-groove binding at AT sites and intercalation at AU sites. *Biochemistry* **31**, 3103–3112.

Tateson, J.E., Randall, R.W., Reynolds, C.H., Jackson, W.P., Bhattacherjee, P., Salmon, J.A. & Garland, L.G. 1988. Selective inhibition of arachidonate 5-lipoxygenase by novel acetohydroxamic acids: biochemical assessment in vitro and ex vivo. *Br J Pharmacol* **94**, 528–539.

Teather, S. & Cuthbert, A.W. 1997. Induction of bradykinin B_1 receptors in rat colonic epithelium. *Br J Pharmacol* **121**, 1005–1011.

Thiebaud, P., Rooij, N.F. de, Koudelka-Hep, M. & Stoppini, L. 1997. Microelectrode arrays for electrophysiological monitoring of hippocampal organotypic slice cultures. *IEEE Trans Biomed Eng* **44**, 1159–1163.

Thomas, C.A., JR, Springer, P.A., Loeb, G.E., Berwald-Netter, Y. & Okun, L.M. 1972. A miniature microelectrode array to monitor the bioelectric activity of cultured cells. *Exp Cell Res* **74**, 61–66.

Tooker, A., Meng, E., Erickson, J., Tai, Y.-C. & Pine, J. 2004. Development of biocompatible parylene neurocages. *Conf Proc IEEE Eng Med Biol Soc* **4**, 2542–2545.

Tsien, R.Y., Poenie, M. 1986. Fluorescence ratio imaging: a new window into intracellular ionic signaling. *Trends Biochem Sci* **11**, 450-455.

Turnberg, L.A. 1984. Mechanisms of control of intestinal transport: a review. *J R Soc Med* **77**, 501–505.

Ueno, A., Dekura, E., Kosugi, Y., Yoshimura, M., Naraba, H., Kojima, F. & Oh-ishi, S. 2002. Effects of dexamethasone and protein kinase C inhibitors on the induction of bradykinin B_1 mRNA and the bradykinin B_1 receptor-mediated contractile response in isolated rat ileum. *Biochem Pharmacol* **63**, 2043–2053.

Ussing, H.H., Zerahn, K. 1951. Active transport of sodium as the source of electric current in the short-circuited isolated frog skin. *Acta Physiol Scand* **23**, 110-127.

Warhurst, G., Lees, M., Higgs, N.B. & Turnberg, L.A. 1987. Site and mechanisms of action of kinins in rat ileal mucosa. *Am J Physiol* **252**, G293-G300.

Wassdal, I., Larsen, K. & Iversen, J.G. 1999a. Bradykinin elevates cytosolic Ca^{2+} concentration in smooth muscle cells isolated from rat duodenum. *Acta Physiol Scand* **165**, 259–264.

Wassdal, I., Nicolaysen, G. & Iversen, J.G. 1999b. Mechanisms of the relaxant and contractile responses to bradykinin in rat duodenum. *Acta Physiol Scand* **165**, 271–276.

Welsh, D.K., Logothetis, D.E., Meister, M. & Reppert, S.M. 1995. Individual neurons dissociated from rat suprachiasmatic nucleus express independently phased circadian firing rhythms. *Neuron* **14**, 697–706.

Wheeler, B.C. & Novak, J.L. 1986. Current source density estimation using microelectrode array data from the hippocampal slice preparation. *IEEE Trans Biomed Eng* **33**, 1204–1212.

Wood, J.D. 1994. Physiology of the enteric nervous system. In: Physiology of the gastrointestinal tract. Volume 1, 2nd edition, Ed.: L.R. Johnson, Raven press, New York, 423-482.

Wotherspoon, G. & Winter, J. 2000. Bradykinin B_1 receptor is constitutively expressed in the rat sensory nervous system. *Neurosci Lett* **294**, 175–178.

Wray, S., Burdyga, T. & Noble, K. 2005. Calcium signalling in smooth muscle. *Cell Calcium* **38**, 397–407.

Wright R.D., Jennings M.A., Florey H.W., Lium R. 1940. The influence of nerves and drugs on secretion by the small intestine, and an investigation of the enzymes in the intestinal juice. *Q J Exp Physiol* **30**, 73–120.

Zagorodnyuk, V., Santicioli, P. & Maggi, C.A. 1998. Evidence for the involvement of multiple mechanisms in the excitatory action of bradykinin in the circular muscle of guinea-pig colon. *Naunyn Schmiedebergs Arch Pharmacol* **357**, 197–204.

Zamponi, G.W., Bourinet, E. & Snutch, T.P. 1996. Nickel block of a family of neuronal calcium channels: subtype- and subunit-dependent action at multiple sites. *J Membr Biol* **151**, 77–90.

Zeitlin, I.J. & Smith, A.N. 1973. Mobilization of tissue kallikrein in inflammatory disease of the colon. *Gut* **14**, 133–138.

8 Declaration

I declare that I have completed this dissertation single-handedly without the unauthorized help of a second party and only with the assistance acknowledged therein. I have appropriately acknowledged and referenced all text passages that are derived literally from or are based on the content of published and unpublished work of others, and all information that relates to verbal communications. I have abided by the principles of good scientific conduct laid down in the charter of the Justus Liebig University Giessen in carrying out the investigations described in the dissertation.

9 Acknowledgements/Danksagung

Ich möchte allen Menschen danken, die mich während der Zeit meiner Promotion so tatkräftig unterstützt haben.

An erster Stelle gilt mein Dank meinem Betreuer Prof. Dr. Martin Diener, der immer ein offenes Ohr für Fragen hatte und Probleme tatkräftig anging. Des Weiteren danke ich Bärbel Schmidt, Brigitta Brück, Eva Haas und Alice Stockinger, die nicht nur im Labor immer hilfreich zur Stelle waren, sondern auch für eine offene, vertrauensvolle und fröhliche Atmosphäre sorgten, welche sehr einzigartig in unserer Arbeitsgruppe ist. Eure „Hexe“ wird Euch vermissen! Michael Haas danke ich für die gewissenhafte Betreuung unserer Tiere und die große Hilfsbereitschaft. Auch dem Team der Werkstatt gilt mein Dank für die Lösung aller technischen Hindernisse. Auch unverwechselbar waren meine „Mit-Doktorandinnen“ Sandra Bader und Anna Bell, die für mich viel mehr als nur Kolleginnen sind und deren Fröhlichkeit, Gemeinschaftssinn und Hilfsbereitschaft im Beruflichen wie im Privaten ihresgleichen sucht! Vielen Dank dafür, ihr seid wunderbar! Mein ganz besonderer Dank gilt Dr. Julia Steidle, ohne die die letzten drei Jahre nur halb so schön gewesen wären und die durch ihre Integrität und bedingungslose Freundschaft ein Vorbild für mich geworden ist.

Ich möchte mich weiterhin bei Daniela Ott bedanken, die zu jeder Zeit ein offenes Ohr für jegliche Art von Sorgen hatte. Auch allen anderen Mitarbeiten der AG Gerstberger danke ich für die tollen letzten 3 Jahre.

Außerdem möchte ich meinen besten Freundinnen Anne Völpel, Anja Hucke und Mona Schommer danken, die immer an mich und den Weg, den ich einschlug, geglaubt haben und deren Freundschaft und Treue mich tief geprägt haben. Ich möchte Euch nie wieder missen, Mädels!

Mein tiefer Dank gilt Tobias Wiesner dafür, dass es ihn gibt, dass er ist, wie er ist und dass er immer zu mir gehalten hat. Du bist ein ganz besonderer Mensch für mich und wirst das immer bleiben, Tobi!

Mein größter Dank gilt meinen Eltern, die mir immer alle Wege geöffnet haben, die ich beschreiten wollte, auf die ich mich jederzeit hundertprozentig verlassen konnte und die mir immer das Gefühl gaben, dass sie vorbehaltslos an mich glauben. Daher möchte ich diese Arbeit meinen Eltern widmen.

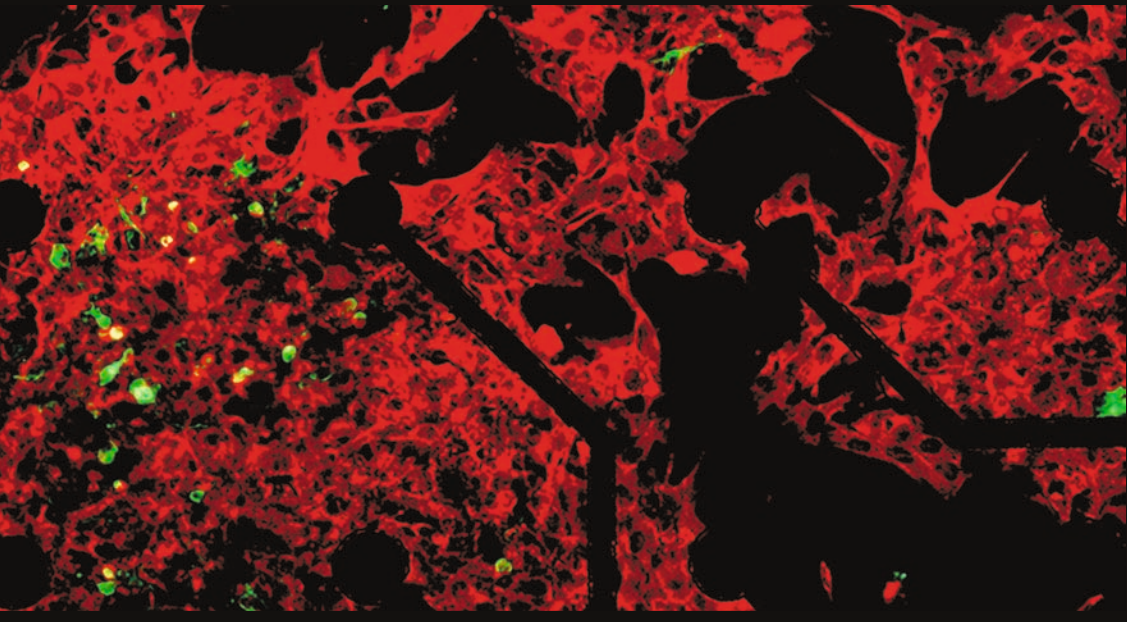

édition scientifique
VVB LAUFERSWEILER VERLAG

VVB LAUFERSWEILER VERLAG
STAUFENBERGRING 15
D-35396 GIESSEN

Tel: 0641-5599888 Fax: -5599890
redaktion@doktorverlag.de
www.doktorverlag.de

ISBN: 978-3-8359-6076-3